MAGNETOHYDRODYNAMIC WAVES IN DYNAMIC PLASMAS WITH SOLAR APPLICATIONS: EFFECT OF THERMAL CONDUCTION

Khalil Salim Ahmed Al-Ghafri

Solar Physics & Space Plasma Research Centre
School of Mathematics and Statistics
University of Sheffield

A thesis submitted for the degree of
Doctor of Philosophy
January 2013

Supervisors: R. von Fáy-Siebenbürgen, M. S. Ruderman

Dedication

To the memory of my father, dear mother, loving wife "Noura" and sweet sons "Basel and Ahmed"

To my brothers, sisters and all members of my family

Acknowledgements

First and foremost, my great thanks goes to Almighty Allah who enabled me to complete this thesis. I would like to express my sincere thanks to my supervisor Prof. Robertus von Fáy-Siebenbürgen for his advice, useful guidance and encouragement throughout my project. Without his assistance and valuable comments, this project would not have completed.

I would like to take this opportunity to thank Prof. Michael Ruderman for his constant assistance, inspiring guidance and useful suggestions during this study.

I am also grateful to Dr. Richard Morton who supported me in all stages of my project. I would also thank all members (staff and colleagues) of the School of Mathematics and Statistics for their great help through the period of my study.

My deepest and special thanks to my beloved mother, stepmother, my wife 'Noura', my sons for their patient and continuous encouragement; brothers, sisters and all members of my family for their support and emotional sense.

Finally, I would like to thank the Ministry of Higher Education, Oman for the financial support.

Abstract

The highly magnetised coronal loops have been confirmed to support a variety of MHD waves and oscillations which are observed widely in the solar atmosphere and most of them are seen to be rapidly damped. One of these oscillations are interpreted as longitudinal slow (propagating or standing) MHD waves. In the last decade, the slow MHD waves have been subject to many observational and theoretical studies to investigate the dominant damping mechanisms. Thermal conduction is the main dissipation mechanism that is suggested to be the essential cause of the damping when compared to the other mechanisms. Therefore, we concentrate here on the damping of both propagating and standing slow magneto-acoustic waves due to thermal conduction.

In the present thesis we examine the effect of the cooling background coronal plasma on damping coronal oscillations. Most of the previous studies have assumed models with a time-independent equilibrium. Here we avoid this restriction and allow the equilibrium to develop as a function of time. The background plasma is assumed to be cooling because of thermal conduction. Moreover, the cooling of the background temperature is assumed to have an exponential profile with characteristic cooling times typical for solar coronal loops.

We have investigated the propagating slow magneto-acoustic waves in a homogeneous magnetised plasma embedded in a hot coronal loop. The background plasma is assumed to be cooling due to thermal conduction in a weakly stratified atmosphere. The influence of cooling of the background plasma on the properties of magneto-acoustic waves is examined. The background temperature is found to decrease exponentially with time by solving the background plasma equations.

On the other hand, we have considered the influence of a cooling background plasma on the longitudinal standing (slow) magneto-acoustic waves generated in a loop of hot corona. The cooling of the background plasma is dominated by a physically unspecified thermodynamic source. A dominance of the cooling in the absence of any dissipative mechanisms is found to amplify the oscillation amplitude. Thermal conduction, which is presumed to be a weak, is only present in the perturbations, causing a damping for the hot-loop oscillations.

The previous study is expanded on investigating the effect of *strong* thermal conduction on the hot coronal oscillations. The competition between the cooling of plasma and the damping of oscillations can be captured from the behaviour of MHD waves. The hot-loop oscillations undergo strong damping due to thermal conduction, although the cooling coronal plasma exerts resistive role on the damping method by decreasing the rate of decaying for cool coronal oscillations.

Contrary to cool loops, the amplitude of very hot loops that undergoes a high amount of cooling experiences faster damping than others. However, the damping of the standing slow (acoustic) waves, because of strong thermal conduction, is brought to an end at a certain time instant and then the rate of damping decreases gradually beyond this limit.

In our analytic work for the models assumed above, we have applied the WKB theory to solve the governing equation which is derived and non-dimensionalised. The WKB estimates are used here since they provide good approximations to the properties of MHD waves. Further to this, we have exploited the method of characteristics and the properties of Sturm-Liouville problems to obtain the solution of the temporally evolving amplitude for the propagating and standing slow MHD waves. Numerical evaluations are employed to give clear view into the behaviour of slow acoustic waves, where the variable background plasma comprising the wave amplitude is measured using typical coronal values. In additions to this, the obtained results are compared to observations.

Contents

List of Figures

List of Tables

Chapter 1

Introduction

1.1 Background: The Structure of the Sun

Our bright star known as the Sun, which controls the solar system, has been under study since ancient times because of different beliefs and purposes. Along the time, scientists became aware of the importance of the Sun and its role on creating the energy for our plant, the Earth. The discovery by high-resolution imaging space telescopes and spectrometers in the modern age led to detection of various dynamic phenomena in the solar interior and in its atmosphere. These phenomena have been a focus for numerous, observational and theoretical, studies during the last fifty years to understand the unknown processes that dominate the energy release from the Sun into space. In general, the structure of the Sun, which is essentially a sphere of plasma, is divided into two regions: the interior and the exterior (the atmosphere).

1.1.1 Solar Interior

The radius of the Sun, $R_{\odot}$, is around 6.96×10^8 m. In contrast to the surface (photosphere), the interior of the Sun is not directly invisible. The Sun comprises of around 90% hydrogen, $\sim 10\%$ helium, and small amount of other elements such as carbon, nitrogen and oxygen. The solar interior can be split into three layers: the (nuclear) core, the (intermediate) radiative zone and the (outer) convection zone.

The core extends to a quarter-radius of the Sun, beginning from the centre.

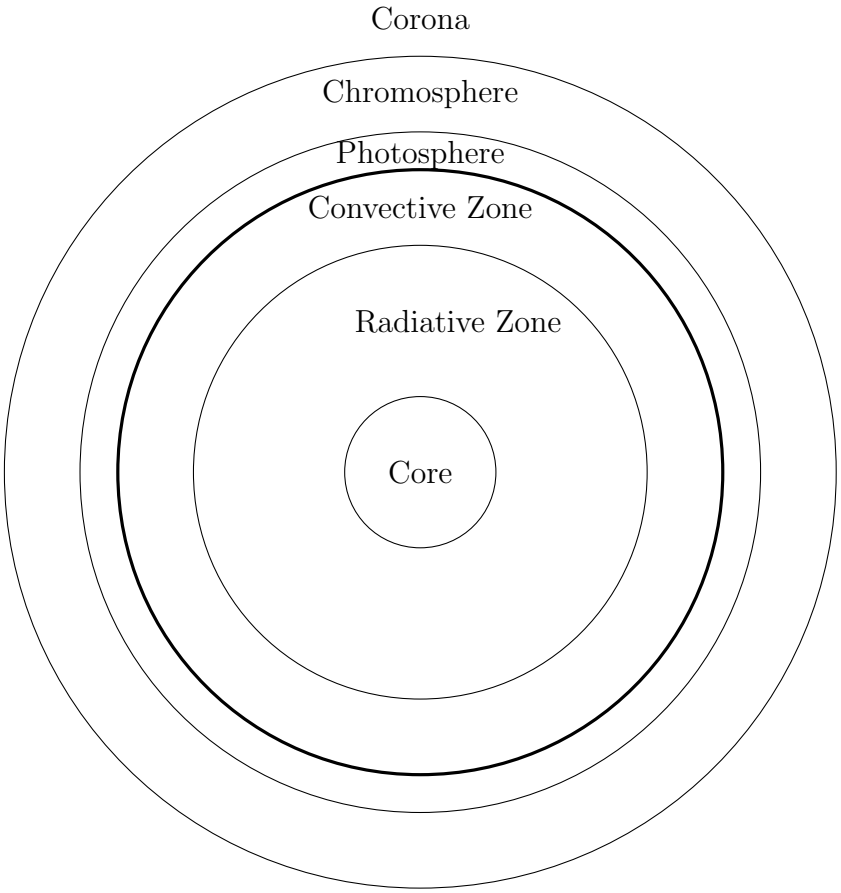

Figure 1.1: Solar Structure

This region embodies half of the solar mass where the bulk of the energy is produced. The high temperature and density in the core reach of the order of 10^7 K and 10^5 kg m^{-3}, respectively. These are sufficiently high to support the nuclear fusion reactions through which hydrogen is converted into helium and eventually generates the energy.

The radiative zone extends from the border of the core up to $0.7R_\odot$. In this layer, the energy is transported by photons that are subject to multiple collisions due to high density of the solar interior. The photons can only move away from the core by the absorption and emission processes. These processes are known as radiative diffusion by which photons spend nearly 10^7 years to reach the surface before the photons can be observed as a light.

The uppermost region in the solar interior is the convection zone, where the energy is transported by convection. This layer covers the volume beyond the

radiative zone, starting from $0.7R_{\odot}$ up to the surface. The high temperature gradient and density change in this region make up an approximately circular convection called convection cells in which the hot plasma rises to the surface and descend again after cooling. It is expected that the dynamic phenomena in the convection zone are responsible for generating the magnetic field where the dominant mechanism is the dynamo.

1.1.2 Solar Atmosphere

The exterior region of the Sun is the visible surface and above, and most observational studies of solar phenomena involve this region. The atmosphere of the Sun is made up of four main regions: the photosphere, chromosphere, transition region and the corona. Some parts of the atmosphere contain dominating magnetic field that leads to formation of numerous magnetic structures that cover the solar atmosphere, such as sunspots, prominences, coronal loops, flares, spicules and solar wind.

The photosphere is the lowest layer of the solar atmosphere. The majority of observed intensity is emitted from this level where the light is recognised by white colour. The temperature of the photosphere varies from 6500 K in the lower part to 4300 K in the upper part. The thickness and density of the photosphere reach around 500 km and 10^{-4} kg m^{-3}, respectively. The photosphere is characterised by the emergence of granules which cover the entire surface of the Sun. The brightness of these granules arises because of hot up-flowing plasma. The presence of magnetic field in the photospheric region leads to magnetic structures such as sunspots, for example, which are overwhelmed with magnetic flux. The Earth is as large as the largest sunspot.

The chromosphere is the next layer in the solar exterior. It has a thickness of nearly 2,000 km. The emissions of the chromospheric region can be observed in *e.g.* the Hα line. The chromospheric temperature rises gradually, ranging from around 6000 K in the lowest part to 20,000 K near the narrow transition region which detaches the chromosphere from the corona. One of the main structures of the chromosphere that is seen on the solar surface are the upwardly emitted huge plasma jets known as spicules.

The transition region, which lies between the chromosphere and the corona, is a thin layer and has a thickness of roughly just a few 100 km. This layer is known to be dynamic and is mainly visible in EUV emission lines. The temperature in the transition region jumps up rapidly so that helium is fully ionised, reaching around 2 MK in the corona.

The corona is the outer part of the solar atmosphere that is clearly seen from the ground at eclipses. The temperature of the corona is much higher than that of the photosphere, extending to over 6 MK. Thus, the heating of the solar corona is a main problem in modern solar physics and astrophysics. As a result, one of the main aims in observing the Sun is to determine the mechanisms that heat the corona (Erdélyi and Ballai, 2007; Taroyan and Erdélyi, 2009). The solar atmosphere is known to be extremely magnetised and dynamic in nature (Vaiana et al., 1973; Schrijver et al., 1999). The highly structured corona consists of numerous features such as coronal loops, open flux tubes, prominences etc. which are caused by the emergence of magnetic fields from inside the Sun (Golub and Pasachoff, 1997). Coronal loops seem to be the fundamental building blocks of the magnetised solar atmosphere.

1.1.3 Coronal Loop Structures

A coronal loop is defined as a magnetic flux tube fixed at both ends in the dense photospheric plasma, and extending into the solar chromosphere and corona. Magnetic loops are considered as a phenomenon of active and quiet regions, and the eminent structures in the solar atmosphere (Nakariakov and Verwichte, 2005; Erdélyi, 2008; De Moortel, 2009; Martínez González and Bellot Rubio, 2009). They have been studied extensively to diagnose the properties of coronal structures and seen to emerge as arch-shaped structures. Space and ground-based observations show that coronal loops can be divided into two distinct categories according to their temperature. One of them is known as hot loops which can be formed at temperatures of more than $1{\times}10^6$ K and observed by the X-ray imagers, *e.g. Yohkoh's Soft X-ray Telescope* (SXT) and *Hinode's X-ray Telescope* (XRT). Cool loops are the other category which exist between $\sim$ 20000 K and $\sim 1{\times}10^6$ K (Bray et al., 1991). Cool loops have been detected in EUV bands which are formed at temperatures below 1 MK. The origin of energy that heats

coronal loops is still a puzzle but, in principle, the potential candidates are nanoflares (DC models) and the dissipation of MHD waves (AC models).

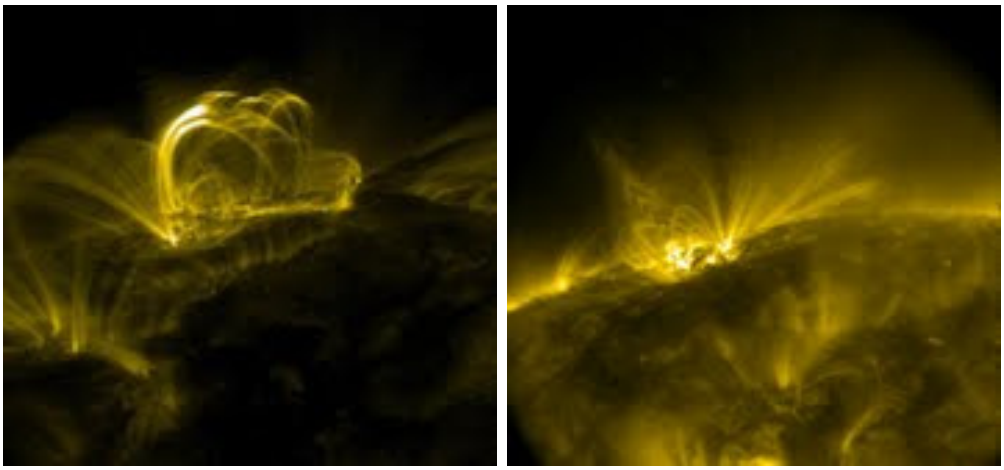

(a) (b)

Figure 1.2: Solar coronal loops as seen by the TRACE satellite telescope in 171 Å: (a) in active region 10808 on 08/09/2005 and (b) in active region 10904 on 09/08/2006.
(http://trace.lmsal.com/POD/TRACEpodoverview.html)

Many studies investigated the properties of solar corona considering different structures of coronal loops, size or expansion of the loop, curvature, loop cross section, temporal behaviour, plasma dynamics, etc, which were seen in observations. For example, Cargill and Priest (1980) have studied the influence of varying flux tube cross-sections and they noticed that the pressure difference at the loop footpoints gives rise to the presence of subsonic and shocked flows. The effect of the loop width on the density scale height was investigated by Petrie (2006) who found that the changes in the stratification depends on the steady flows. Moreover, Dymova and Ruderman (2006) and Erdélyi and Verth (2007) examined the geometry influence on the properties of transverse coronal loop oscillations. They found that the ratios of the period of the fundamental mode of the tube kink oscillations to its first overtone period depend weakly on the loop shape and on the ratio of the loop height to the atmospheric scale height. Further to this, Andries et al. (2005) reported that the observed period ratio can be used as a seismological tool to estimate the density scale height in the solar corona. For example, Ballai et al. (2011) measured the density scale height in

coronal loops observed by TRACE using the ratio of the two periods (see also Orza et al., 2012). Although the traditional model of coronal loop is straight with uniform density and magnetic field, Verth and Erdélyi (2008) and Ruderman et al. (2008) studied the transverse oscillations in an expanding magnetic flux tube under the influence of magnetic and density stratification and found that measuring the plasma density scale height is affected by the coronal loop expansion.

More recently, the effects of density and magnetic stratification on linear longitudinal magnetohydrodynamic (MHD) waves generated in an expanding coronal loop is investigated by Luna-Cardozo et al. (2012). It is found that the frequency ratio of the first overtone and fundamental mode depends on the density profile. In the last decade, the twisted coronal loop embedded in different layers, convective zone, photosphere and chromosphere, has been subject to an extensive attention due to its influence on the plasma dynamics and the behaviour of MHD waves (Linton et al., 2001; Fan and Gibson, 2003; Erdélyi, 2006; Erdélyi and Fedun, 2007b; Ruderman, 2007; Carter and Erdélyi, 2008; Martínez-Sykora et al., 2009; Erdélyi and Fedun, 2010; Luoni et al., 2011). An overview of the effects of curvature on coronal loop kink oscillations has been exhibited by Van Doorsselaere et al. (2009). Morton and Erdélyi (2009*a*) investigated the period ratio of transverse oscillations in a coronal loop of elliptic cross-section considering stages of its emergence from the sub-photosphere into the solar corona. They found that increasing ellipticity leads to increases the value of the period ratio. Further to this, non-axisymmetric oscillations of straight magnetic loops with a constant elliptic cross-section and density have been studied by Ruderman (2003) and with density varying along the loop have been investigated by Morton and Ruderman (2011). There are two kink modes arising in this model, one polarised in the direction of larger axis of the elliptic cross-section, and the other polarised in the direction of smaller axis. The ratio of frequencies of the first overtone and the fundamental mode is found to be the same for both kink mode oscillations.

López Fuentes et al. (2007) looked into the temporal evolution of coronal loops observed by the *Solar X-Ray Imager* (SXI). They found that observed loops can be separated into three phases: rise, main, and decay. Besides, the loop heating during all three evolutionary phases changes slowly (increasing, reaching constant level and decreasing). It is also found that the timescales of the intensity

variations are significantly longer than the cooling time and sound-transit time. The temporal evolution of a highly dynamic loop system observed by the *Transition Region and Coronal Explorer* (TRACE) in the 171 and 195 Å passbands was investigated by Tsiropoula et al. (2007). The measured radiative and conductive cooling times indicate that the examined loop strands are being cooled by radiation. Terra-Homem et al. (2003) studied the properties of propagating MHD waves in flux tube with background flows. In the magnetic cylinder structure, they found that the steady flow can cause changes in the characteristic of wave propagation. It is also found that the the strength of flows may lead to crossing of modes. Contrary to solar coronal conditions, the structure of wave propagation is found to be strongly affected by the background flow under solar photospheric conditions. Gruszecki et al. (2008) studied observed standing fast magneto-acoustic kink oscillations by *Hinode* in the presence of background flow. The results show that uniform and inhomogeneous flows are unable to cause a considerable change in wave period of the mode. In a recent work by Ruderman (2010), the influence of the plasma flow on non-axisymmetric oscillations of a thin magnetic tube was examined. It was found that both the fundamental harmonic of kink oscillations and the ratio of frequencies of the first overtone and fundamental harmonic are weakly affected by the flow (see also Terradas et al., 2010).

1.2 MHD Waves in the Solar Corona

The magnetic structures play an important role in the solar corona since they can support a wide range of magnetohydrodynamic (MHD) waves and oscillations which are natural carriers of energy and may be the key for solving the problem of solar coronal heating (for some recent reviews see Erdélyi, 2008; Taroyan, 2008; Taroyan and Erdélyi, 2009; McLaughlin et al., 2011). Recent observations indicate that waves and oscillations are ubiquitous in the solar atmosphere (Wang et al., 2003b; Tomczyk et al., 2007; De Pontieu et al., 2007; Erdélyi and Fedun, 2007a; Okamoto et al., 2007; Erdélyi and Taroyan, 2008; Van Doorsselaere et al., 2008; Jess et al., 2009). For recent reviews see Nakariakov and Verwichte (2005); Banerjee et al. (2007); De Moortel (2009); Zaqarashvili and Erdélyi (2009); Mathioudakis et al. (2013). Many of the above reports highlight that the observed

waves or oscillations are seen to be strongly damped. The commonly suggested mechanisms for damping are resonant absorption (Sakurai et al., 1991; Ruderman and Roberts, 2002; Goossens et al., 2002; Aschwanden et al., 2003. For a detailed review see Goossens et al., 2011) and thermal conduction (Ofman and Aschwanden, 2002; De Moortel and Hood, 2003, 2004; De Moortel et al., 2004; Mendoza-Briceño et al., 2004a; Erdélyi, 2008) which cause the damping of the fast kink and the (slow or acoustic) longitudinal waves, respectively. More recently, Morton et al. (2010) argued that radiative cooling of the background plasma may be the damping method for coronal oscillations.

Solar coronal waves and oscillations have been observed in the visible light, EUV, X-ray and radio bands and expressed in the form of MHD waves. Oscillations in coronal loops were recently observed by TRACE (*e.g.* Aschwanden et al., 1999; Nakariakov et al., 1999), SUMER (*e.g.* Wang et al., 2002a; Ofman and Wang, 2002) and Hinode (*e.g.* Erdélyi and Taroyan, 2008), and Nobeyama radioheliograph (*e.g.* Asai et al., 2001) where these magnetic loops start to oscillate by a disturbance which is caused by a solar flare or CME. These oscillations were interpreted as fast kink mode MHD standing waves, longitudinal (slow magnetoacoustic) modes and fast sausage mode oscillations, respectively.

1.2.1 Observation of Longitudinal (Propagating and Standing) Oscillations

Propagating plasma disturbances were detected by SOHO/UVCS along coronal plumes at a height of about 1.9 $R_{\odot}$ (Ofman et al., 1997, 1999, 2000a). DeForest and Gurman (1998) observed similar compressive disturbances in polar plumes with SOHO/EIT. The observed compressive disturbances were interpreted as propagating slow magneto-acoustic waves, where the suggested damping mechanism for the waves was compressive viscosity (Ofman et al., 1999, 2000b). Similar intensity disturbances were observed in coronal loops with TRACE and *Yohkoh*/SXT (Schrijver et al., 1999; Nightingale et al., 1999; De Moortel et al., 2000; McEwan and De Moortel, 2006; Berghmans et al., 2001), and SOHO/EIT (Berghmans and Clette, 1999). Nakariakov et al. (2000) and Mendoza-Briceño et al. (2004a) have also interpreted these disturbances as slow magneto-acoustic waves and they found that the wave evolution is affected by dissipation and gravi-

tational stratification. Further to this, Erdélyi and Taroyan (2008) have observed intensity and Doppler-shift oscillations by *Hinode*/EIS on February 19th, 2007. They suggested that these oscillations are longitudinal sausage waves propagating along the loop and appear to be triggered by a footpoint microflare. The maximum amplitude for the Doppler shift is around 4 km s^{-1}. The periodicity of the intensity perturbations in coronal holes is quite larger than that detected in coronal loops.

De Moortel et al. (2002a,b) and McEwan and De Moortel (2006) have analyzed several cases of disturbances observed by TRACE, and McEwan and De Moortel (2006) have summarized their properties (see Table 1.1). The amplitudes are around 4% in the background intensity and the higher amplitudes are observed in transition-region lines. It is suggested that the source of these oscillations is the leakage of the photospheric p modes through the chromosphere and transition region into the corona, *i.e.* a mechanism similar to that put forward to explain spicule formation (De Pontieu et al., 2004; De Pontieu and Erdélyi, 2006), transition-region moss oscillations (De Pontieu et al., 2003), and even coronal oscillations (De Pontieu et al., 2005). The observed examples in TRACE 171 Å ($\sim$ 1 MK) by McEwan and De Moortel (2006) have propagating speeds of the order of 99.7 ± 3.9 km s^{-1} and other propagation speeds with different wavelengths approximated by various authors are given in Table 1.2. In the analyzed examples, the energy flux was found to be of the order of 313 ± 26 ergs cm^{-2} s^{-1}, which is considered too small when comparing with $\sim 10^6$ ergs cm^{-2} s^{-1} that is required to sustain a coronal loop at a temperature of about a million degrees. However, Tsiklauri and Nakariakov (2001) found that wide spectrum slow waves can provide heat deposition rate near the loop footpoints, that is sufficient to heat EUV loops when compared to observations. Only upward propagating disturbances were reported in all cases with nearly constant speeds. The propagating disturbances are quasi-periodic with periods ranging from 145 to 550 seconds with the average equal to 284 ± 10.4 seconds in the examples considered by McEwan and De Moortel (2006). Moreover, De Moortel et al. (2002c) confirmed that loops located above sunspot oscillate with periods of around 3 minutes, while perturbations in non-spot loops have periods of about 5 minutes. Robbrecht et al. (2001) compared the observations done by TRACE 171 Å with observations made by EIT 195 Å and found that propagation speeds vary from 65

to 150 km/s approximately. King et al. (2003) carried out a comparison between TRACE 171 Å and 195 Å wavelength observations.

Parameter	Average	Range
Oscillation Period, P	284.0 ± 10.4 s	$145 - 550$ s
Propagation Speed, v	99.7 ± 3.9 km s^{-1}	$O(45) - O(205)$ km s^{-1}
Relative Amplitude, A	$3.7\% \pm 0.2\%$	$0.7 - 14.6\%$
Detection Length, L_d	8.3 ± 0.6 Mm	$2.9 - 23.2$ Mm
Energy Flux, F	313 ± 26 erg cm^{-2} s^{-1}	$68 - 1560$ erg cm^{-2} s^{-1}

Table 1.1: The average and ranges of the physical properties of the 63 oscillations in coronal loop footpoints analyzed by De Moortel et al. (2002a); McEwan and De Moortel (2006). See De Moortel (2009).

	Speed (km/s)	Wavelength [Å]
Nightingale et al. (1999)	$130 - 190$	171&195
Schrijver et al. (1999)	$70 - 100$	195
Berghmans and Clette (1999)	$75 - 200$	195
De Moortel et al. (2000)	$70 - 165$	171
Robbrecht et al. (2001)	$65 - 150$	171&195
Berghmans et al. (2001)	~ 300	SXT
De Moortel et al. (2002a)	122 ± 43	171
King et al. (2003)	$25 - 40$	171&195
McEwan and De Moortel (2006)	98 ± 6	171
Erdélyi and Taroyan (2008)	~ 170	195, 185&202

Table 1.2: Table of the propagation speeds of propagating slow MHD waves detected in coronal loop. See De Moortel (2009).

Verwichte et al. (2010) have shown that observed coronal spectral signatures of in-phase Doppler velocity and intensity of the observed quasi-periodic perturbations can be explained as propagating slow waves. It is found that slow waves cause line asymmetries when the emission line is averaged over an oscillation period or when a quasi-static plasma component in the line of sight is included. The observed intensity oscillations with a period of ≈ 12 minutes by EUVI instruments on the *STEREO* A and B spacecraft found to propagate outward with phase speed corresponding to the sound speed (Marsh et al., 2009).

These oscillations are explained in terms of the slow magneto-acoustic mode. The three-dimensional geometry of the upward propagation obtained from observations are used to measure phase speed. The calculated phase speed, from *STEREO* A and B, are $132^{+9.9}_{-8.5}$ km s^{-1} and $132^{+13.8}_{-8.4}$ km s^{-1}, respectively; with inferred loop temperature of $0.84^{+0.13}_{-0.11}$ MK and $0.84^{+0.18}_{-0.11}$ MK which is close to the peak of the EUVI 171 Å response functions. Overall, theoretical modelling plays an important role on identifying the observed perturbations of the EUV loops in terms of propagating slow magneto-acoustic waves (De Moortel and Nakariakov, 2012). On the other hand, the interpretation of disturbances as waves or flows is still a controversial issue due to the difficulty in analysing the data of observations.

Oscillations interpreted as longitudinal standing (slow) magneto-acoustic waves have been observed in hot ($T > 6$ MK) active region loops by the Solar Ultraviolet Measurement of Emitted Radiation (SUMER) spectrometer on board SOHO (Wang et al., 2002, 2003b; Taroyan et al., 2007). Wang et al. (2002) analysed two recurring events for SUMER and Yohkoh/SXT observations. Using the measured loop length ($L \approx 140$ Mm) with temperature around 6 MK and oscillation periods ($P = 14 - 18$ min), they found that the estimated phase speed for the fundamental mode, $c_t = 2L/P = 380$ km s^{-1} is close to the sound speed. Therefore, these oscillations were interpreted in terms of the standing fundamental longitudinal slow mode. SUMER oscillations have periods in the range of 8.6 to 32.3 minutes with decay times of $3.1 - 42.3$ minutes and amplitudes between 12 and 353 km s^{-1} (Wang et al., 2005). Moreover, Mariska (2005) has reported Doppler shift oscillations during solar flares with *Yohkoh* in a high temperature region reaching $12 - 14$ MK. These oscillations are interpreted in terms of the standing slow mode MHD waves (Mariska, 2006). The obtained results of observations exhibit average oscillation periods of 5.5 ± 2.7 minutes, decay times of 5.5 ± 2.5 minutes and amplitudes of 17.1 ± 17.0 km s^{-1}.

Evidence for the standing slow mode can be understood from the phase relationship between velocity and intensity where a quarter-period phase difference is a characteristic of the standing waves, while the propagating waves exhibit an in-phase relationship. Therefore, an approximate quarter-period delay of the intensity variations behind the Doppler shift strongly support the assumption that the oscillations observed by SUMER are slow standing modes. The observed

oscillations in coronal loops indicate that the standing slow modes are likely triggered by micro-flares which are produced by impulsive heating (Mendoza-Briceño et al., 2002).

De Moortel and Nakariakov (2012), in a review work, conclude that the model of magnetic flux tube remains the basis of the study of MHD waves and oscillations in the solar corona. A theoretical summary of how the slow mode, under solar coronal conditions, can be derived from the MHD equations has been composed by, *e.g.* Roberts (2006). The magnetic field was assumed straight in the vertical direction in a gravitationally stratified medium. This theory has been applied to the slow waves in coronal loops observed by SUMER and TRACE. Luna-Cardozo et al. (2012) generalised the model to include both magnetic and density stratification, *i.e.* taking into account the expanding nature of loops that support MHD waves.

1.2.2 Damping of Slow (Propagating and Standing) MHD Oscillations

Currently, the damping of slow magneto-acoustic waves has become a subject of remarkable observational and theoretical study due to a possibility of revealing physical processes that dominate energy dissipation in the coronal loops by measuring the wave damping timescales. The majority of theoretical and numerical studies on damping of propagating and standing slow MHD waves show that the understanding of dominant mechanisms of rapid damping can be captured from 1D, linear (Sigalotti et al., 2007) or nonlinear model (Wang, 2011). Since the observation of slow MHD waves many theoretical studies have been focussed on investigating the damping mechanism considering the influence of different mechanisms such as thermal conduction, radiation, gravitational stratification and shock dissipation (Ofman and Wang, 2002; De Moortel and Hood, 2003, 2004; Mendoza-Briceño et al., 2004a; Taroyan et al., 2005; Sigalotti et al., 2007; Bradshaw and Erdélyi, 2008; Verwichte et al., 2008; Erdélyi et al., 2008). For instance, the evolution of the wave amplitudes are found to be affected by dissipation and gravitational stratification (Nakariakov et al., 2000; Mendoza-Briceño et al., 2004a). Furthermore, Tsiklauri and Nakariakov (2001) have studied geometrical effects on the behaviour of slow magneto-acoustic waves by taking into

account the influence of loop plane inclination.

Ibáñez and Escalona (1993) studied the propagation of thermal and magnetosonic waves in an optically thin plasma. They found that thermal waves are always damped whereas the magnetosonic waves are damped in the range of temperature 10^4 K $\leq T < 10^8$ K due to thermal conduction. The dissipation of slow MHD waves travelling in an isothermal medium were studied in detail by De Moortel and Hood (2003, 2004). Thermal conduction, compressive viscosity and optically thin radiation, as well as the effects of gravitational stratification and a diverging magnetic field geometry were investigated. The results of study under coronal conditions (*i.e.* $T \approx 10^6$ K) indicate that thermal conduction is the main cause of decaying wave amplitude comparing with the other mechanisms of either compressive viscosity or optically thin radiation. The thermal mode is found to be purely decaying in the case of standing waves, but is oscillatory and decaying in the case of propagating waves (De Moortel and Hood, 2003). However, it was found that increasing thermal conductivity does not match the damping rate which is detected in observations. In the limit of very large conductivity, the perturbations are only weakly damped and additionally, travel at the slower, isothermal sound speed (De Moortel and Hood, 2003).

Recently, Owen et al. (2009) have confirmed that the existence of thermal conduction leads to a small phase shift between the wave velocity, energy and density. De Moortel and Hood (2004) included also the effect of area divergence, gravitational stratification and thermal conduction. They found that both thermal conduction and area divergence cause the decay of wave amplitude whereas gravitational stratification increases the amplitude. Due to the combination of thermal conduction and area divergence, the perturbations can only be detected in the first $10 - 20$ Mm along the loop, which agrees well with observations. In a non-isothermal medium, the observed perturbation amplitudes decrease very fast as a result of damping by thermal conduction and the effect of the instrument response function (TRACE 171 Å) and this is also in good agreement with observation. In addition, Tsiklauri and Nakariakov (2001) reported that loop curvature, an offset of the loop centre from the base of the corona and inclination with respect to the vertical, will reduce the effect of gravity along the loop and consequently reinforce the damping of perturbations. De Moortel and Hood (2004) studied the coupling of slow and fast MHD waves in a coronal environ-

ment ($\beta < 1$) by using 2D model with a transversal density profile. They found that the coupling to the fast wave is inefficient process to extract energy from the driven slow wave and so is not enough to account for the observed rapid damping. In the same way, Rosenthal et al. (2002) and Bogdan et al. (2003) have shown that the coupling between the slow and fast waves is only propable in a region where the sound and Alfvén speed are comparable (where $\beta \sim 1$).

Fedun et al. (2009, 2011) and Vigeesh et al. (2012) have recently carried out numerical studies to detect the influence of photospheric motion on the solar atmospheric oscillations in three dimensions. They found that high- and low-frequency waves which arise in the photosphere are transmitted through the transition region into the solar corona by the magnetic field. Moreover, it is found that fast and slow waves transport energy from lower atmosphere to the solar corona and the standing waves are supported in the chromospheric region. Overall, the energy leakage is reported to be damping the coronal oscillations. It is also found that the phase mixing of the slow waves due to the transverse density gradient can lead to decaying of the wave amplitude but it is too weak to justify the observed damping. The propagation of slow (acoustic) waves in the solar coronal loop depends on the acoustic cutoff frequency, which is the ratio of the sound speed to twice the density scale height (Lamb, 1932). Further to this, Lamb (1932) and Roberts (2006) have shown that the waves can only propagate if their frequencies are greater than the cutoff frequency. For more details on the effect of cutoff frequency on propagating and standing slow acoustic waves, see Roberts (2006). In a three dimensional model, Marsh et al. (2011) have studied the damping of the slow magneto-acoustic mode observed by *STEREO*/EUVI and *Hinode*/EIS. It is found that thermal conduction is not sufficient to account for the observed short decay length of the waves observed with *STEREO*/EUVI. In comparison with thermal conduction and radiation, magnetic field line divergence alone can be sufficient for the observed damping of coronal loops.

The observed Doppler-shift oscillations in hot flare lines, Fe XIX and Fe XXI, with temperature reaching more than 6 MK by SUMER have been studied by Kliem et al. (2002) and Wang et al. (2003a,b), and it is found that these oscillations suffer a strong damping. Ofman and Wang (2002) and Mendoza-Briceño et al. (2004a) found that the standing MHD waves are strongly damped because of thermal conduction in nonlinear model, whereas, using a linear MHD

model Pandey and Dwivedi (2006) indicated that the individual influence of thermal conduction or viscosity is not enough to account for the observed damping. Mendoza-Briceño et al. (2004a) studied the influence of gravitational stratification on damping of standing MHD waves in hot coronal loops and found that enhanced nonlinear viscous dissipation due to gravity may reduce the damping times by about $10-20\%$ compared to the unstratified loops.

In contrast, Sigalotti et al. (2007) found that thermal conduction can only be accounted as damping mechanism when the compressive viscosity is added to the model. Bradshaw and Erdélyi (2008) reported that the radiation due to a non-equilibrium ionisation balance could cause up to 10% reduction of wave-damping timescale in comparison to the equilibrium case. Verwichte et al. (2008) showed that shock dissipation at large amplitudes gives rise to enhancement of the damping rate which is up to 50% larger than given by thermal conduction alone. In non-isothermal, hot, gravitationally stratified coronal loops, Erdélyi et al. (2008) investigated the damping of standing slow (longitudinal) waves under the effects of various dissipative mechanisms such as thermal conduction, compressive viscosity, radiative cooling, and heating and found that the decay time of waves decreases with the increase of the initial temperature. Further to this, they derived a relation between the damping time and the parameter determining the apex temperature in the form of second-order scaling polynomial.

1.3 Theory of MHD Waves

The theory of MHD waves plays an important role in analysing the observed loop oscillations throughout the study of their properties (speed, wavelength and frequency) that are connected by the dispersion relation. In the study of wave propagation in a magnetised plasma medium, we assume that there is a perturbation about the equilibrium state of the medium and then we see the consequences of this disturbance. Therefore, we write physical parameters in the form $f = f_0 + f_1$, where the subscript '0' represents equilibrium quantities and the subscript '1' indicates perturbed quantities, and substitute them into the MHD equations. Linear equations can be obtained after neglecting the nonlinear terms due to $|f_1| \ll |f_0|$. Then, manipulating algebraically the linearised MHD equations gives the governing equation of the model. Thus, the dispersion relation

describing the nature of wave can be obtained by assuming that the perturbed functions are proportional to $\exp[i(\mathbf{k}\cdot\mathbf{r}-\omega t)]$.

In order to investigate the properties of MHD waves, it is necessary to introduce briefly the basic MHD equations that govern the plasma motion.

1.3.1 MHD Equations

The fundamentals of electricity and magnetism are described by electromagnetic equations in which the combination of Maxwell's equations and Ohm's Law gives the magnetic field induction equation,

$$\frac{\partial \mathbf{B}}{\partial t} = \nabla \times (\mathbf{v} \times \mathbf{B}) + \eta \nabla^2 \mathbf{B}. \tag{1.1}$$

This equation relates the plasma velocity $\mathbf{v}$ to the magnetic field $\mathbf{B}$ that satisfies the condition $\nabla \cdot \mathbf{B} = 0$. In Equation (1.1) η is the magnetic diffusivity (assumed to be constant).

The behaviour of the plasma motion in the solar environment is governed by the fluid equations which consist of equations of continuity, motion and energy.

Equation of Continuity:

The equation of mass continuity is given by

$$\frac{\partial \rho}{\partial t} + \nabla \cdot (\rho \mathbf{v}) = 0, \tag{1.2}$$

where ρ is the plasma density. Continuity equation represents the law of conservation of mass which states that mass cannot be created or destroyed but it is changed into a different form of mass.

Equation of Motion:

The equation of motion, which is derived from Newton's second law of motion, and has the form

$$\rho \frac{\partial \mathbf{v}}{\partial t} + \nabla \cdot (\rho \mathbf{v}) = -\nabla p + \mathbf{j} \times \mathbf{B} + \mathbf{F}, \tag{1.3}$$

where p is the plasma pressure, ∇p is the pressure gradient force exerted by the plasma, $\mathbf{j} \times \mathbf{B}$ is the Lorentz force which is composed of the current density ($\mathbf{j}$) as well as the magnetic field ($\mathbf{B}$), and $\mathbf{F}$ is an external force representing, *e.g.*, the gravitational force ($\rho\mathbf{g}$) and a viscous force ($\rho\nu\nabla^2\mathbf{v}$) for incompressible flow, where $\mathbf{g}$ is the gravity acceleration and ν is the coefficient of kinematic viscosity (assumed to be uniform).

Ideal Gas Law

The ideal gas law is

$$p = \frac{R}{\tilde{\mu}}\rho T, \tag{1.4}$$

where R is the gas constant, $\tilde{\mu}$ is the mean atomic weight, and T is the temperature.

The Energy Equation

The energy equation states the sources and sinks of energy that control the heat rate in the solar environment. In general, the energy equation can be written in several forms and one of them is

$$\frac{\rho^\gamma}{\gamma - 1}\left(\frac{\partial}{\partial t}\frac{p}{\rho^\gamma} + (\mathbf{v}\cdot\nabla)\frac{p}{\rho^\gamma}\right) = -\mathscr{L}, \tag{1.5}$$

where $\gamma = 5/3$ is the ratio of specific heats and $\mathscr{L}$ is called the energy loss (gain) function. Equation (1.5) is known as the entropy equation since $c_v \ln(p/\rho^\gamma)$ is the entropy, where c_v is the specific heat at constant volume. In an adiabatic medium (*i.e.* no exchange of energy among neighbouring small volumes), $\mathscr{L} = 0$.

In the solar corona, the energy loss function may be written as

$$\mathscr{L} = -\nabla\cdot(\kappa\nabla T) + \rho^2 Q(T) - H, \tag{1.6}$$

where the first term represents the heat flux due to thermal conduction, the second is the radiation loss function and the third is the total energy gained through heating.

In magnetised plasmas, the thermal conduction is given by

$$\nabla\cdot(\kappa\cdot\nabla T) = \nabla_\parallel\cdot(\kappa_\parallel\nabla_\parallel T) + \nabla_\perp\cdot(\kappa_\perp\nabla_\perp T), \tag{1.7}$$

where κ is the thermal conductivity tensor. Thermal conduction along the magnetic field is essentially by electrons with $\kappa_{\parallel} = \kappa_0 T^{5/2}$ $\mathrm{Wm^{-1}K^{-1}}$ and $\kappa_0 = 10^{-11}$. Thermal conduction across the magnetic field that is mainly by protons is very weak in strongly magnetised plasmas.

In the optically thin plasma approximation, where temperature is of order $\gtrsim 10^4$ K, the radiative loss function is approximated by a piecewise continuous function of the form

$$Q(T) = \chi T^{\alpha}, \tag{1.8}$$

where χ and α take different values in different temperature intervals. (Rosner et al., 1978; Priest, 2000)

1.3.2 The Propagation of MHD Waves

Here we focus on the structure of solar atmosphere by a straight magnetic field. In what follows, we shall present some analytical studies of the behaviour of MHD waves in the solar corona. Hence, we investigate the propagation of waves in a magnetic cylinder when the gravity is neglected (Edwin and Roberts, 1983).

First we start by introducing the ideal MHD equations and its linearised equations, and then identify properties of waves propagating in an unbounded homogeneous medium (Roberts, 1981a).

1.3.3 The Ideal MHD Equations

The ideal MHD equations consist of the equations of continuity, momentum, induction and energy as following:

$$\frac{\partial \rho}{\partial t} + \nabla \cdot (\rho \mathbf{v}) = 0, \tag{1.9}$$

$$\rho \frac{\partial \mathbf{v}}{\partial t} + \rho(\mathbf{v} \cdot \nabla)\mathbf{v} = -\nabla p + \frac{1}{\mu_0}(\nabla \times \mathbf{B}) \times \mathbf{B}, \tag{1.10}$$

$$\frac{\partial \mathbf{B}}{\partial t} = \nabla \times (\mathbf{v} \times \mathbf{B}), \tag{1.11}$$

$$\frac{\partial p}{\partial t} + \mathbf{v} \cdot \nabla p = -\gamma p \nabla \cdot \mathbf{v}, \tag{1.12}$$

$$\nabla \cdot \mathbf{B} = 0, \tag{1.13}$$

where μ_0 is the magnetic permeability of free space.

1.3.4 The Linearised MHD Equations

The linearised MHD equations will be obtained by writing all dependent variables in the from

$$f(x, y, z, t) = f_0(x, y, z) + f_1(x, y, z, t), \tag{1.14}$$

and neglecting terms nonlinear with respect to variables given in Equations (1.9)–(1.13). Then the linear MHD equations are

$$\frac{\partial \rho_1}{\partial t} + \nabla \cdot (\rho_0 \mathbf{v}_1) = 0, \tag{1.15}$$

$$\rho_0 \frac{\partial \mathbf{v}_1}{\partial t} = -\nabla(p_1 + \frac{1}{\mu_0}\mathbf{B}_0 \cdot \mathbf{B}_1) + \frac{1}{\mu_0}\ (\mathbf{B}_0 \cdot \nabla)\mathbf{B}_1 + \frac{1}{\mu_0}(\mathbf{B}_1 \cdot \nabla)\mathbf{B}_0, \tag{1.16}$$

$$\frac{\partial \mathbf{B}_1}{\partial t} = \nabla \times (\mathbf{v}_1 \times \mathbf{B}_0), \tag{1.17}$$

$$\frac{\partial p_1}{\partial t} + \mathbf{v}_1 \cdot \nabla p_0 = -\rho_0 c_0^2 \nabla \cdot \mathbf{v}_1, \tag{1.18}$$

$$\nabla \cdot \mathbf{B}_1 = 0, \tag{1.19}$$

where $c_0^2 = \gamma p_0/\rho_0$ is the square of the sound speed and the background state is assumed to be static and stationary ($\mathbf{v}_0 = 0$).

1.3.5 MHD Waves in an Unbounded Homogeneous Medium

Consider an unbounded homogeneous medium with a uniform magnetic field $\mathbf{B}_0 = B_0\hat{\mathbf{z}}$. The basic equilibrium state is characterised by the values ρ_0 and p_0 for the plasma density and pressure, respectively. Thus, Equations (1.15) and (1.18) are given in the form

$$\frac{\partial \rho_1}{\partial t} + \rho_0 \nabla \cdot \mathbf{v}_1 = 0, \tag{1.20}$$

$$\frac{\partial p_1}{\partial t} = -\rho_0 c_0^2 \nabla \cdot \mathbf{v}_1. \tag{1.21}$$

Since $\mathbf{v}_1 = (v_{1x}, v_{1y}, v_{1z})$ and $\mathbf{B}_1 = (B_{1x}, B_{1y}, B_{1z})$ so the induction equation (1.17) can be written as

$$\frac{\partial B_{1x}}{\partial t} = B_0 \frac{\partial v_{1x}}{\partial z}, \qquad \frac{\partial B_{1y}}{\partial t} = B_0 \frac{\partial v_{1y}}{\partial z}, \qquad \frac{\partial B_{1z}}{\partial t} = B_0(\Gamma - \Delta). \tag{1.22}$$

Here $\Delta = \nabla \cdot \mathbf{v}_1$ and $\Gamma = \partial v_{1z}/\partial z$.

Now, differentiating Equation (1.16) with respect to time and using Equations (1.21) and (1.22), we obtain

$$\frac{\partial^2 \mathbf{v}_1}{\partial t^2} = c_0^2 \nabla\Delta - v_A^2 \nabla(\Gamma - \Delta) + v_A^2 \frac{\partial^2 \mathbf{v}_1}{\partial z^2} - v_A^2 \frac{\partial \Delta}{\partial z}\hat{\mathbf{z}}, \tag{1.23}$$

where $v_A = B_0/(\mu_0\rho_0)^{1/2}$ is the Alfvén speed. Equation (1.23), by applying the operator ∇, becomes

$$\frac{\partial^2 \Delta}{\partial t^2} = (c_0^2 + v_A^2)\nabla^2\Delta - v_A^2 \nabla^2\Gamma. \tag{1.24}$$

Taking the z component of Equation (1.23) gives

$$\frac{\partial^2 v_{1z}}{\partial t^2} = c_0^2 \frac{\partial \Delta}{\partial z}. \tag{1.25}$$

Eventually, the combination of Equations (1.24) and (1.25) yields

$$\frac{\partial^4 \Delta}{\partial t^4} - (c_0^2 + v_A^2)\frac{\partial^2}{\partial t^2}\nabla^2\Delta + c_0^2 v_A^2 \frac{\partial^2}{\partial z^2}\nabla^2\Delta = 0, \tag{1.26}$$

which represents the governing equation of propagating waves in an unbounded homogeneous medium.

Obviously, Equation (1.26) has a trivial solution when $\Delta = 0$ for which $v_{1z} = 0$ where there are no pressure changes. This constitutes the Alfvén mode which has the dispersion relation

$$\omega^2 - k^2 v_A^2 = 0, \tag{1.27}$$

representing transverse oscillations driven by the tension in the magnetic field.

For non-trivial solution, we use Fourier-analysis for Δ by writing

$$\Delta = \hat{\Delta}(x) e^{i(\omega t + ly + kz)}, \tag{1.28}$$

where ω is the frequency, and l and k are the wavenumbers. Then substituting (1.28) into (1.26) gives

$$\frac{\mathrm{d}^2\hat{\Delta}}{\mathrm{d}x^2} - (l^2 + m_0^2)\hat{\Delta}(x) = 0, \tag{1.29}$$

where

$$m_0^2 = \frac{(k^2c_0^2 - \omega^2)(k^2v_A^2 - \omega^2)}{(c_0^2 + v_A^2)(k^2c_T^2 - \omega^2)}, \qquad c_T^2 = \frac{c_0^2v_A^2}{c_0^2 + v_A^2}.$$

If we take the Fourier-analysis for the x-dependence in $\hat{\Delta}$, i.e. ($\hat{\Delta} \sim e^{inx}$) then we have from (1.29)

$$n^2 + l^2 + m_0^2 = 0, \tag{1.30}$$

which is

$$\omega^4 - \mathbf{K}^2(c_0^2 + v_A^2)\omega^2 + \mathbf{K}^2k^2c_0^2v_A^2 = 0, \tag{1.31}$$

with the wavevector $\mathbf{K} = (n,\ l,\ k)$.

Then, the total form of dispersion relation for equation (1.26) is

$$(\omega^2 - k^2v_A^2)(\omega^4 - \mathbf{K}^2(c_0^2 + v_A^2)\omega^2 + \mathbf{K}^2k^2c_0^2v_A^2) = 0, \tag{1.32}$$

which is the dispersion relation for the Alfvén wave, and the fast and slow magneto-acoustic waves.

The dispersion relation (1.32) describes the propagation of waves through obtaining the phase speed c_{ph} that relates the wave frequency ω to the wavevector $\mathbf{K}$. The solution to the dispersion relation (1.32) gives the phase speeds

$$c_{ph}^2 = v_A^2\cos^2(\phi), \qquad \text{and} \qquad c_{ph}^2 = \frac{1}{2}c_{ms}^2\left[1 \pm \left(1 - 4\frac{c_t^2}{c_{ms}^2}\cos^2(\phi)\right)^{1/2}\right], \tag{1.33}$$

where ϕ is the angle of propagation between the wavenumber k (or the wavevector $\mathbf{K}$) and the magnetic field B_0, with $k = |\mathbf{K}|\cos(\phi)$ and

$$c_{ms}^2 = c_0^2 + v_A^2, \qquad c_t^{-2} = c_0^{-2} + v_A^{-2}.$$

The speed c_{ms} is defined as the magnetosonic speed (or the fast speed) and c_t is identified as the tube speed (or the slow speed). The first part of Equation (1.33)

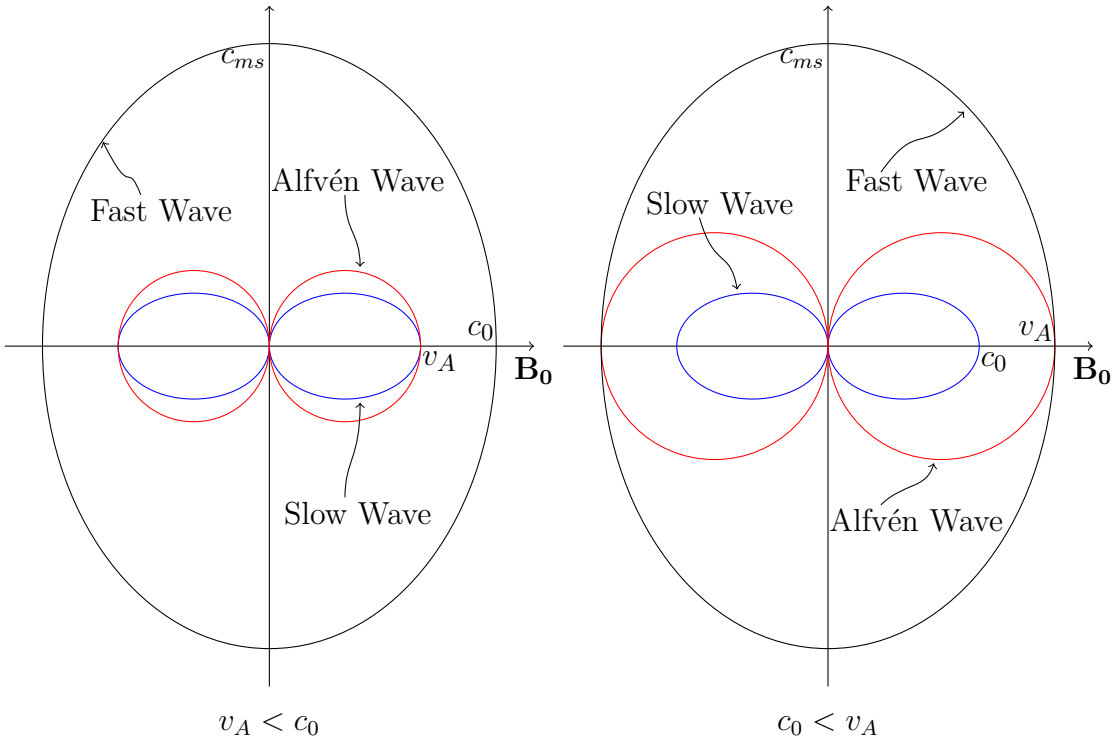

Figure 1.3: Phase speed diagram for magnetohydrodynamic waves.

represents the phase speed of Alfvén wave while the second gives the phase speed of the fast and slow magneto-acoustic waves. It is clear that when $\phi = 0$ this means that the propagation is along the magnetic field, so both Alfvén and slow waves can propagate only along the magnetic field with the phase speed $c_{ph} \leq v_A$ for the former and $c_{ph} \leq \min(c_0, v_A)$ for the later (see Figure 1.3). When $\phi = \pi/2$ the propagation is perpendicular to the magnetic field and the phase speed is $c_{ph} = c_{ms}$ which is the greatest speed can the fast wave propagates with as shown in Figure 1.3. The phase speed of the fast wave (at any other angle) occurs in the range $\max(c_0, v_A) \leq c_{ph} < c_{ms}$. However, the magneto-acoustic waves are compressive since $\Delta \neq 0$ whereas the Alfvén wave is incompressible because $\Delta = 0$.

1.3.6 MHD Waves in a Magnetic Cylinder

The model of a solar coronal loop is usually assumed to take a cylindrical shape as it appears monolithic in observation and since this loop is highly magnetized, it is called a magnetic cylinder. The propagation of magnetoacoustic waves in a magnetic cylinder has been studied by many researchers. In this section we closely follow the study by Edwin and Roberts (1983).

Consider a uniform cylinder of a radius a with magnetic field $B_0\hat{\mathbf{z}}$ embedded in external magnetic field $B_e\hat{\mathbf{z}}$. The equilibrium state is described by

$$\mathbf{B} = \begin{cases} B_0, & r < a \\ B_e, & r > a \end{cases}, \tag{1.34}$$

with the pressure balance being given by the relation

$$p_0 + \frac{B_0^2}{2\mu_0} = p_e + \frac{B_e^2}{2\mu_0}. \tag{1.35}$$

It follows from this equation that the ratio of densities outside and inside the cylinder is

$$\frac{\rho_e}{\rho_0} = \frac{2c_0^2 + \gamma v_A^2}{2c_e^2 + \gamma v_{Ae}^2}, \tag{1.36}$$

where p_0, ρ_0, $c_0 = (\gamma p_0/\rho_0)^{1/2}$ and $v_A = B_0/(\mu_0\rho_0)^{1/2}$ are the pressure, density, sound speed and Alfvén speed inside the cylinder, and p_e, ρ_e, $c_e = (\gamma p_e/\rho_e)^{1/2}$ and $v_{Ae} = B_e/(\mu_0\rho_e)^{1/2}$ are the same quantities outside the cylinder. As before,

γ is the ratio of specific heats.

The linearized MHD equations of this model in terms of cylindrical coordinates $(r,\ \theta,\ z)$ are given by

$$\frac{\partial^2}{\partial t^2}\left(\frac{\partial^2}{\partial t^2}-(c_0^2+v_A^2)\nabla^2\right)\Delta+c_0^2v_A^2\frac{\partial^2}{\partial z^2}\nabla^2\Delta=0, \tag{1.37}$$

$$\left(\frac{\partial^2}{\partial t^2}-v_A^2\frac{\partial^2}{\partial z^2}\right)\Gamma=0, \tag{1.38}$$

where in this case

$$\nabla^2\equiv\frac{\partial^2}{\partial r^2}+\frac{1}{r}\frac{\partial}{\partial r}+\frac{1}{r^2}\frac{\partial^2}{\partial\theta^2}+\frac{\partial^2}{\partial z^2},$$

and

$$\Delta=\nabla\cdot\mathbf{v},\qquad \Gamma=\hat{\mathbf{z}}\cdot\mathrm{curl}\mathbf{v}=\frac{1}{r}\frac{\partial}{\partial r}(rv_\theta)-\frac{1}{r}\frac{\partial v_r}{\partial\theta}.$$

If we take

$$\Delta=R(r)\exp i(\omega t+n\theta+kz), \tag{1.39}$$

then equations (1.37) and (1.38) lead to the Bessel equation for function $R(r)$:

$$\frac{\mathrm{d}^2R}{\mathrm{d}r^2}+\frac{1}{r}\frac{\mathrm{d}R}{\mathrm{d}r}-\left(m_0^2-\frac{n^2}{r^2}\right)R=0, \tag{1.40}$$

where

$$m_0^2=\frac{(k^2c_0^2-\omega^2)(k^2v_A^2-\omega^2)}{(c_0^2+v_A^2)(k^2c_T^2-\omega^2)},\qquad c_T^2=\frac{c_0^2v_A^2}{c_0^2+v_A^2}.$$

The wave motion outside the tube is described by the same equations with the only difference that m_e is substituted for m_0, where

$$m_e^2=\frac{(k^2c_e^2-\omega^2)(k^2v_{Ae}^2-\omega^2)}{(c_e^2+v_{Ae}^2)(k^2c_{Te}^2-\omega^2)},\qquad c_{Te}^2=\frac{c_e^2v_{Ae}^2}{c_e^2+v_{Ae}^2},$$

is taken to be positive.

For the solution bounded and regular on the axis $r=0$ of the cylinder, we have

$$R(r)=A_0\left\{\begin{array}{ll} I_n(m_0r), & m_0^2>0 \\ J_n(n_0r), & n_0^2=-m_0^2>0 \end{array}\right\}(r<a), \tag{1.41}$$

where A_0 is a constant and J_n is the Bessel functions of order n, and I_n is the

modified Bessel function of the first kind and order n.

Outside the cylinder ($r > a$), we take

$$R(r) = A_1 K_n(m_e r), \qquad r > a, \tag{1.42}$$

where A_1 is a constant and K_n is the modified Bessel function of the second kind and order n.

Now, matching the radial velocity and the total pressure at $r = a$ because of continuity across the cylindrical boundary, this leads to the dispersion relations for surface and body waves which propagate in a magnetic cylinder surrounded by magnetic region:

$$\rho_0(k^2 v_A^2 - \omega^2) m_e \frac{K_n'(m_e a)}{K_n(m_e a)} = \rho_e(k^2 v_{Ae}^2 - \omega^2) m_0 \frac{I_n'(m_0 a)}{I_n(m_0 a)}, \tag{1.43}$$

for surface waves ($m_0^2 > 0$), and

$$\rho_0(k^2 v_A^2 - \omega^2) m_e \frac{K_n'(m_e a)}{K_n(m_e a)} = \rho_e(k^2 v_{Ae}^2 - \omega^2) m_0 \frac{J_n'(n_0 a)}{J_n(n_0 a)}, \tag{1.44}$$

for body waves ($m_0^2 = -n_0^2 < 0$).

These dispersion relations give the well-known sausage mode (symmetric) when $n = 0$ whereas when $n = 1$ they give the kink mode (asymmetric). In the case $n > 1$, this gives the so-called flute modes.

Under coronal conditions, *i.e.* $B_0 \approx B_e$, v_A, $v_{Ae} > c_0$, c_e and $\rho_0 > \rho_e$, only fast and slow body waves can emerge while there is no presence of surface waves.

In the incompressible limit ($\gamma \to \infty$), meaning $c_0, c_e \to \infty$, m_0 and m_e tend to $|k|$. Hence, Equation (1.43) becomes

$$\rho_0 \left(k^2 v_A^2 - \omega^2\right) \phi_n = \rho_e \left(k^2 v_{Ae}^2 - \omega^2\right), \quad \phi_n = \frac{I_n(|k|a) K_n'(|k|a)}{I_n'(|k|a) K_n(|k|a)}. \tag{1.45}$$

As before, the sausage and kink modes are given by $n = 0$ and $n = 1$, respectively. In the slender tube limit ($|k|a \ll 1$), Equation (1.45) gives a phase speed of the sausage mode as

$$\frac{\omega}{k} = v_A \left[1 - \frac{\rho_e}{\rho_0}\left(1 - \frac{v_{Ae}^2}{v_A^2}\right) \frac{k^2 a^2}{4} K_0(|k|a)\right]. \tag{1.46}$$

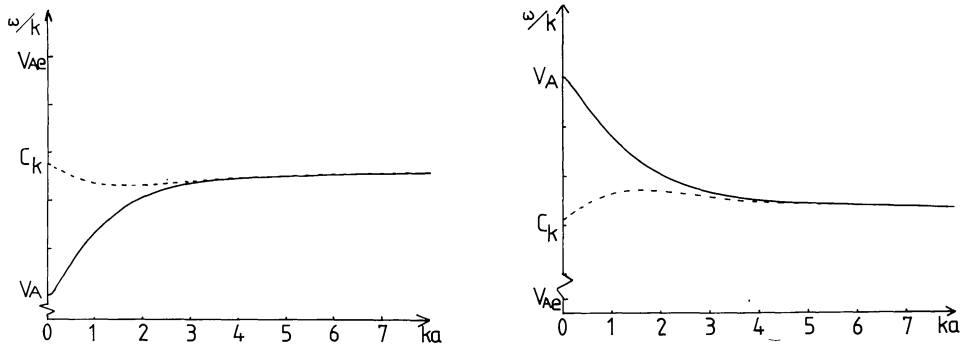

(a) (b)

Figure 1.4: The phase speed of the sausage (solid line) and kink (dashed line) modes in the incompressible medium for (a) $v_{Ae} > v_A$ and (b) $v_{Ae} < v_A$. (Edwin and Roberts, 1983)

1.4 The Influence of the Cooling of the Background Plasma on Coronal Loop Oscillations

One feature that should be taken into account when studying the nature of coronal oscillations is the temperature evolution of the coronal plasma. There has been a plethora of observations which show a number of different temperature evolution scenarios (see, *e.g.* Winebarger et al., 2003; Nagata et al., 2003; López Fuentes et al., 2007). Nagata et al. (2003) observed that there are at least two categories of temperature evolution. Hot loops, which are heated to temperatures $T > 2.5$ MK, are seen by the X-ray imagers, *e.g.* *Yohkoh's* Soft X-ray Telescope (SXT) and *Hinode's* X-ray Telescope (XRT). Hot loops are short lived and are seen to undergo relatively fast cooling down to EUV temperatures (the temperature affecting EUV absorption lines), appearing in EUV imagers. The other category are cool loops, which are observed with temperatures in the range $0.4 - 1.3$ MK in EUV images and have relatively long lifetimes. Often the temperature change is on a slow scale when compared to the lifetime of perturbations. The physical process of the plasma cooling depends upon the loop temperature (*i.e.*, cool or hot). It has been found that radiation is the dominant mechanism for the cooling of the EUV loops ($T < 2.0$ MK) whereas thermal conduction is the

cooling mechanism for loops with $T > 2.0$ MK. A number of observed oscillating coronal loops are reported to undergo a temperature decrease. This decrease has an exponential profile with cooling times of $500 - 2000$ seconds (Aschwanden and Terradas, 2008; Ugarte-Urra et al., 2009).

Hot loops are thought to be heated by impulsive heating events, *e.g.* flares, micro-flares, nano-flares. The origin of these energisation mechanisms could be either waves or reconnection (Antolin et al., 2008a,b, 2009). There have been a number of simulations investigating the evolution of coronal loops after heating events (*e.g.* Jakimiec et al., 1992; Cargill, 1994; Mendoza-Briceño et al., 2004a; Aschwanden and Tsiklauri, 2009; Taroyan and Erdélyi, 2009; Taroyan and Erdélyi, 2010; Taroyan et al., 2011). Impulsive heating events only last for a relatively short time, and if the plasma reaches a hot enough temperature by the end of the heating, thermal conduction dominates the cooling of the plasma. From calculations by, *e.g.* Cargill (1994), the decrease in temperature due to thermal conduction takes an almost exponential form.

In a recent review by De Moortel and Nakariakov (2012), it has been reported that cooling is likely to be a natural aspect in oscillating coronal loops where this feature is not taken into account in the earlier models. Landi et al. (2009) have studied the cooling of observed coronal loops in active region using the data of various instruments. It is found that the rapid cooling leads to forming loop condensations which finally settle in prominence layer. These condensations have been observed many times in the past but diagnosing plasma properties of cooling loops were prevented due to the limitations of instruments. The scenario of condensing loops was consistent with the theoretical models of loop condensations developed by Karpen and Antiochos (2008).

In a recent theoretical work by Morton et al. (2010), the effect of radiative-cooling of the background plasma state on the propagation of magneto–acoustic waves in a uniformly magnetized plasma was investigated. Although the approximation of unbounded uniformity of the plasma may seem to be a severe simplification, this step was necessary in order to give insight into the underlying physics. The radiation mechanism was assumed to be the mechanism for the cooling of the plasma and the plasma cooled exponentially in time, which captures well the key features of the observational data. As a result, they found that

the slow and fast modes are damped due to cooling. The radiative cooling was shown to damp the slow mode by up to 60% within characteristic lifetimes. This effect is much stronger than the contribution predicted by De Moortel and Hood (2004). Bradshaw and Cargill (2010) examined the influence of cooling plasma on impulsively heated coronal loops due to radiative-enthalpy mechanism. The dominant mechanism of cooling is specified by measuring the scaling between coronal temperature and density, $T \propto n^{\delta}$, where δ is determined by the relative importance of the coronal radiative losses to the enthalpy flux to the transition region. It is found that radiation is the dominant mechanism of cooling with a relatively small coronal mass loss when δ has larger values whereas enthalpy is responsible for cooling with a relatively large coronal mass loss once δ has smaller values.

Transverse oscillations of coronal loops with slowly changing density have been studied by Ruderman (2011). In the case of a homogeneous density along the loop, the cooling is found to cause a reduction to the density and a growth to the amplitude with time whereas in the case of a stratified loop with the same temperature inside and outside, the oscillation frequency increases with time and the cooling amplifies the kink oscillations. The latter case with constant temperature of external plasma is studied and the obtained results are qualitatively the same in both cases. Wang (2011) found that the plasma in hot loop oscillation experiences a gradual cooling according to the observed intensity evolution in Fe XIX, Fe XVII and Ca XIII. Despite of the plasma cooling, the rapid damping of oscillation amplitude in Fe XIX line is found to be real but not dominated by the cooling effect.

1.4.1 Cooling by Radiation Mechanism

We have mentioned that the cooling of the background plasma could be due to radiation mechanism for EUV loops ($T < 2.0$ MK). Observationally, the cooling of coronal loops has been found to have an exponential profile of the form

$$T = T_0 \exp\left(-\frac{t}{\tau_{cool}}\right), \tag{1.47}$$

where T_0 is the initial temperature and τ_{cool} is the cooling time scale (Aschwanden and Terradas, 2008; Morton and Erdélyi, 2010).

Recently, Morton et al. (2010) have considered a simple model to investigate the influence of a radiatively cooling background plasma on the propagating MHD waves in a homogenous coronal plasma. The model is as follows. The background temperature (pressure) is decreasing with time. The magnetic field is uniform and along the z direction, *i.e.* $\mathbf{B}_0 = B_0\hat{\mathbf{z}}$. The equilibrium plasma density is constant. A special form of radiative function is assumed to make certain that the analytically obtained temperature evolution of the background plasma cooled by radiation is identical with the observed cooling profile of coronal loops.

The energy equation in this model is given as

$$\frac{\rho^\gamma}{\gamma - 1}\left(\frac{\partial}{\partial t}\frac{p}{\rho^\gamma} + (\mathbf{v}\cdot\nabla)\frac{p}{\rho^\gamma}\right) = -\rho^2 Q(T) + H, \tag{1.48}$$

where $\rho^2 Q(T)$ is the optically thin radiative loss function and H is the coronal heating term.

The equilibrium in this model is radiatively unstable owing to the absence of thermal conduction. The reduction in the coronal heating term means that the plasma will undergo a cooling. Then, the cooling of the background plasma will continue in a runway manner. In order to model this process to be consistent with the observations (Aschwanden and Terradas, 2008), it is assumed that the loss/heat terms have the form of Newtonian cooling. Therefore, a simple function of the form δp representing the loss and heat terms is assumed to reach the observed exponential cooling of the background plasma. Thus, the energy equation for the background state when there is no background flow, *i.e.* $v_0 = 0$, reduces to

$$p_0(t) = p_i \exp(-\delta t), \tag{1.49}$$

where the '0' index denotes background quantity, p_i is the pressure value at $t = 0$ and δ is a small quantity. It is clear that the background pressure decreases with time and perfect pressure balance is not kept, however the equilibrium nearly holds because of low-beta plasma, $\beta \ll 1$. Comparing the numerical evaluation of the pressure evolution with Equation (1.49) it is found that $\delta = 1/\tau_{cool}$. The observed cooling times are $500\,\mathrm{s} < \tau_{cool} < 2000\,\mathrm{s}$. Thus, $1/2000\,\mathrm{s}^{-1} < \delta < 1/500\,\mathrm{s}^{-1}$. Subsequently, the cooling profile of the background plasma given in Equation (1.47) and Equation (1.49) is identical since $T \propto p_0$.

Overall, in spite of the simplicity of the suggested model, the analytically obtained solutions exhibit considerable results about the behaviour of MHD waves in a cooling coronal plasma that give us a step along to model coronal loops. The cooling of the plasma causes a significant change in the properties of the modes where the frequency of the magneto-acoustic modes decreases with time. Further to this, the damping by radiation is found to affect the slow mode more than the fast mode where the slow mode suffers a strong damping within typical lifetimes of oscillations observed in coronal loops. For more details, see Morton et al. (2010).

1.4.2 Cooling by Thermal Conduction

Thermal conduction is the dominant mechanism of the plasma cooling in hot coronal loops, $T > 6$ MK, (see, Mendoza-Briceño et al., 2004b; Aschwanden and Tsiklauri, 2009). The cooling of coronal loops heated by small flares (nano-flares) investigated by Cargill (1994). He estimated the characteristic time which is taken by the plasma to cool by radiation, τ_r, and thermal conduction, τ_c. The dominant method responsible for cooling can be specified by evaluating the ratio of conductive and radiative cooling times. It is accepted that thermal conduction is the dominant cooling process when $\tau_c < \tau_r$ while radiation dominates the cooling once $\tau_c > \tau_r$. Further to this, the temperature of regions that undergo conductive cooling decreases roughly in an exponential form with time.

Aschwanden and Tsiklauri (2009) studied the hydrodynamic evolution of the electron temperature and electron density for impulsively heated coronal loops using analytical approximations. They found a function of an exponential profile for the temperature evolution describing heating process. However, the region of high temperature ($T \gtrsim 10$ MK) is found to cooled by thermal conduction and the cooling is represented by a function with an exponent of $-2/5$ as follows

$$T_{cond}(t) = T_p \left[1 + \frac{(t - t_p)}{\tau_{cond}}\right]^{-2/5}, \qquad \tau_{cond} = \frac{21}{5}\frac{n_p k_B L^2}{\kappa T_p^{5/2}},$$

where τ_{cond} is the conduction timescale, t_p is the density peak time (the time at which the density has a peak value), T_p is the temperature at the density peak time, n_p is the density peak value, L is the loop half-length, k_B is the Boltzmann

constant, κ is the Spitzer thermal conductivity coefficient.

A general function describing the time evolution of the temperature $T(t)$ in the cooling phase for the regions of temperature ($T \gtrsim 1$ MK) cooled by the radiative and conductive cooling has the following quadratic formula

$$T(t) = T_p \left[1 - \frac{(t - t_p)}{n_{cool}\ \tau_{cool}}\right]^2, \qquad \frac{1}{\tau_{cool}} = \frac{1}{\tau_{rad}} + \frac{1}{\tau_{cond}}, \qquad \text{for } t_p \leq t \leq t_e,$$

where τ_{rad} is the radiative cooling time, n_{cool} is the cooling times (this factor corrects for the time variation of the conductive and radiative cooling timescales). The temperature according to this function decreases monotonically until the end time $t_e = t_p + n_{cool}\ \tau_{cool}$. The two phases of dominant conductive cooling and radiative cooling are combined by the previous relation of the cooling time, τ_{cool}, which approaches the value of the conductive cooling timescale if $\tau_{cond} \ll \tau_{rad}$, and the value of the radiative cooling timescale when $\tau_{rad} \ll \tau_{cond}$.

To sum up, despite the fact that the effort made to understand the cooling mechanism of the solar corona and an almost exponential form of the numerically calculated suggested general functions of cooling process, there are still no observations for hot oscillating loops that cool exponentially according to our knowledge.

1.5 Boundary Conditions

The careful choice of the boundary conditions in a model of coronal loop may lead to obtain important consequences. However, there are finite number of boundary conditions which can be physically accepted. Antiochos et al. (1985) studied the influence of boundary conditions on thermal stability of static coronal loops. They concluded that the perturbed quantities such as temperature, density or pressure, at the loop footpoints vanish. In addition to this, the appropriate choice of conditions is found to indicate that the stability is not affected by the amount of quantities at the boundary (loop base). Furthermore, Mok and Van Hoven (1995) studied the effect of chromospheric boundary conditions on coronal magnetic loops using numerical simulations. It is summarised that the rigid-wall boundary at the chromosphere and the line-tied condition are not realistic. This is because

of dynamic plasma in the transition region.

In a static 1D isothermal medium, De Moortel and Hood (2003) studied the properties of slow MHD waves propagation in solar coronal magnetic fields for various boundary conditions. According to observations shown by De Moortel et al. (2002a,b), they assumed that the initial conditions for all perturbed quantities vanish while the boundary conditions for both perturbed velocity and pressure gradient are functions of time or zero at the loop footpoints. The results show that the introduced boundary conditions lead to the formation of the thermal and the slow mode where the former is found to be oscillatory and decaying, and the latter suffers strong damping due to thermal conduction.

1.6 Outline of the Thesis

In this chapter, we have given a brief introduction about the structure of the Sun. As mentioned before, coronal-loop structures are highly magnetised and can support a wide range of MHD waves and oscillations. Coronal observations indicate that waves and oscillations are ubiquitous in the solar atmosphere and many of them are seen to be strongly damped. In this thesis, we focus only on the damping of longitudinal slow (propagating and standing) oscillations due to cooling background plasma. The cooling of the coronal loop is assumed an exponential profile. The following chapters will be organised as follows.

Firstly, we investigate the propagating slow MHD wave in a uniform magnetised plasma under the influence of a cooling background state. In a weakly stratified atmosphere, thermal conduction is the dominant mechanism for the cooling background plasma in hot coronal loops. The governing equation in a 1D form for the slow modes is derived by using dimensionless quantities. The WKB theory is applied to obtain the dispersion relation which describes the properties of the longitudinal acoustic mode. The analytic solution of the time-dependent amplitude is derived by exploiting the method of characteristics. We display the results in a system with a variable background calculated by using standard solar coronal values and compare them to the observed oscillations.

Next, we examine the effect of dynamic background plasma on longitudinal standing modes oscillating in a hot coronal loop. The background plasma

is assumed to be decaying exponentially, with characteristic cooling times typical for coronal loops, because of a physically unspecified thermodynamic source. The damping of coronal loop oscillations is dominated by *weak* thermal conduction which appears in perturbations and disappear in the background plasma. Similarly, the governing equation is solved by the WKB approximation and the temporally evolving amplitude is derived with the aid of the properties of Sturm-Liouville problem. We exhibit the obtained results numerically to give further insight into the behaviour of the MHD waves.

Finally, the work in this chapter complements the previous project and generalises the results found there. The influence of the plasma cooling on longitudinal standing MHD waves that are damping due to *strong* thermal conduction will be investigated. We intend to widen the scope of our investigation into the competition between the influence of cooling and damping on the amplitude of hot oscillating loops. We have used numerical evaluations to analyse the variation of time-dependent amplitude and compare it with the previous study.

Chapter 2

Damping of Longitudinal Magneto–Acoustic Oscillations in Slowly Varying Coronal Plasma

In this chapter, we concentrate on the behaviour of propagating longitudinal MHD waves in a cooling background plasma. We closely follow Erdélyi et al. (2011). In most earlier studies, a time-independent equilibrium was considered. Here we relax this restriction and allow the equilibrium to evolve in time. In weakly stratified atmosphere, thermal conduction is assumed to be the dominant mechanism of the background plasma cooling which is assumed to occur on a time scale greater than the characteristic travel times of the perturbations, thus is applicable to oscillations in hot loops. Solutions to the background plasma equations show that the cooling profile of the plasma is exponential in time, in qualitative agreement with observations. The dispersion relation which describes the slow modes and their properties is derived using the WKB theory. An analytic expression for the time-dependent amplitude of the waves is also derived, and the method of characteristics is used to find an approximate analytical solution. The analytically obtained solutions are evaluated numerically to give further insight in the behaviour of the MHD waves in a system with a time-dependent background. The results show that thermal conduction has a dominant effect on the slow modes, causing their amplitude to damp strongly. The rate of damping is quantified in the model and is found to be dependent upon the amount of stratification in the plasma and the initial temperature of the background.

The damping is also shown to be weakly dependent upon position in the slowly varying equilibrium.

2.1 Introduction

Propagating slow magneto-acoustic waves have been a subject of many observational and theoretical studies. Coronal oscillations interpreted as propagating slow MHD waves are seen to be strongly damped. Among various proposed mechanisms it is found that thermal conduction is the most efficient dissipative mechanism for oscillations in the hot corona. However, the thermal conduction alone cannot account for the observed damping. For example, De Moortel and Hood (2003) studied the propagation of MHD slow waves in a *static* 1D, isothermal medium where thermal conduction and compressive viscosity were considered as damping mechanisms for perturbations. They found that a mechanism complimentary to thermal conduction is needed to cause the observed damping.

In this chapter, we study further the propagation of longitudinal MHD waves in a magnetised plasma in a weakly stratified atmosphere representing hot coronal loops. The plasma cools due to thermal conduction. The chapter is organised as follows. In the next section we describe the model of dynamic background plasma and write down the linearised system of governing equations. In Section 2.3 we use the WKB theory to obtain the analytical solution for the oscillation amplitude. In Section 2.4 we present a numerical evaluation of the analytical solution. Finally, the summary of the results is given in Section 2.5.

2.2 Governing Equations

Consider a magnetised plasma where the background temperature is changing with time due to thermal conduction, while density is independent of time. The magnetic field is uniform and stationary, and it is in the z-direction, *i.e.* $\mathbf{B}_0 = B_0\hat{\mathbf{z}}$. We use the low-beta plasma approximation applicable to solar coronal conditions. The rigid tube approximation that is applicable to longitudinal wave is used. This enables us to neglect the magnetic field perturbation. As a result, a longitudinal slow MHD wave is a superposition of two sound waves

propagating along the magnetic field in the opposite directions. The governing MHD equations for the plasma take the form

$$\frac{\partial \rho}{\partial t} + \nabla \cdot (\rho \mathbf{v}) = 0, \tag{2.1}$$

$$\rho \frac{\partial \mathbf{v}}{\partial t} + \rho(\mathbf{v} \cdot \nabla)\mathbf{v} = -\nabla p + \frac{1}{\mu_0}(\nabla \times \mathbf{B}) \times \mathbf{B} + \rho \mathbf{g}, \tag{2.2}$$

$$\frac{R}{\tilde{\mu}} \frac{\rho^{\gamma}}{(\gamma - 1)} \left[\frac{\partial}{\partial t} \frac{T}{\rho^{\gamma - 1}} + (\mathbf{v} \cdot \nabla) \frac{T}{\rho^{\gamma - 1}} \right] = \kappa \nabla^2 T, \tag{2.3}$$

$$\frac{\partial \mathbf{B}}{\partial t} = \nabla \times (\mathbf{v} \times \mathbf{B}), \tag{2.4}$$

$$p = \frac{R}{\tilde{\mu}} \rho T, \tag{2.5}$$

where $\mathbf{v}$ is the flow velocity, $\mathbf{B}$ the magnetic field, g the gravity acceleration, μ_0 the magnetic permeability of free space, γ the ratio of specific heats, R the gas constant, $\tilde{\mu}$ the mean molecular weight, T the temperature, $\kappa \nabla^2 T$ thermal conduction term where $\kappa = \kappa_0 T^{5/2}$, and ρ and p are the plasma density and pressure, respectively.

The medium is assumed to be cooling due to thermal conduction with no temporal change in density, and it is also assumed that there is no background flow (*i.e.* $\mathbf{v}_0 = 0$). Hence, for the background state, Equations (2.1) – (2.5) reduce to

$$\mathbf{v}_0 = 0, \qquad \frac{\partial \rho_0}{\partial t} = 0, \tag{2.6}$$

$$\frac{\mathrm{d}p_0}{\mathrm{d}z} = -\rho_0 g, \tag{2.7}$$

$$\rho_0 = \rho_0(z), \tag{2.8}$$

$$p_0 = \frac{R}{\tilde{\mu}} \rho_0 T_0, \tag{2.9}$$

$$\frac{R\,\rho_0}{\tilde{\mu}(\gamma - 1)} \frac{\partial T_0}{\partial t} = \kappa \nabla^2 T_0, \tag{2.10}$$

where the index '0' denotes a background quantity.

Equation (2.7) can be written as

$$\frac{1}{p_0}\mathrm{d}p_0 = \frac{l}{H}\mathrm{d}\tilde{z}, \tag{2.11}$$

where $z = l\tilde{z}$ (here l is the characteristic length scale of perturbations) and $H = p_0/\rho_0 g$. Here we are interested in a weakly stratified atmosphere where the characteristic length scale is much smaller than the scale height H, *i.e.* $l/H \ll 1$, consequently we arrive at

$$\frac{\mathrm{d}p_0}{\mathrm{d}z} \approx 0. \tag{2.12}$$

The solution to Equation (2.10) by separation of variables, using Equations (2.9) and (2.12), gives the temperature:

$$T_0(z,t) = T_i \exp\left(\frac{-(\gamma-1)\lambda\tilde{\mu}\kappa t}{R\rho_i}\right)[-c_2 z^2 + c_3 z + c_4], \tag{2.13}$$

and the density:

$$\rho_0(z) = \frac{\rho_i}{-c_2 z^2 + c_3 z + c_4}, \tag{2.14}$$

which is physically valid when $c_2, c_3 \ll 1$ and $c_3 > c_2$. In Equation (2.13) λ is the separation constant, $c_2 = \lambda/2$, c_3 and c_4 are constants, T_i is the initial temperature at $z = 0$, and ρ_i is the density at $z = 0$.

Note that the background temperature decreases exponentially with time. It has been shown for radiative-cooling loops that an exponential profile provides a good fit for the observed cooling (Aschwanden and Terradas, 2008; Morton and Erdélyi, 2009*b*, 2010). To the best of our knowledge, there are no such observations for hot loops cooling due to thermal conduction.

The form of the density profile in Equation (2.14) is consistent with a weakly stratified atmosphere. For a gravitationally stratified atmosphere the density profile is given by

$$\rho_0 = \rho_i \exp\left(-\frac{z}{H}\right). \tag{2.15}$$

The hydrostatic scale height H is given by $H = RT/\tilde{\mu}g$, hence for hot loops H is in the range $94 - 282$ Mm. In the case of weak stratification, *i.e.* $l/H \ll 1$, the

density can be approximated as

$$\rho_0 \approx \rho_i \left(1 - \frac{z}{H} + \frac{1}{2}\left(\frac{z}{H}\right)^2\right). \tag{2.16}$$

Equation (2.14) can be written

$$\rho_0 = \frac{\rho_i}{1+y} \approx \rho_i(1-y) \approx \rho_i \left[1 - (-c_2 z^2 + c_3 z + c_4 - 1)\right],$$

upon the assumption that y is small. Comparing to Equation (2.16), the values for the constants are $c_4 = 1$, $c_3 = H^{-1}$ and $c_2 = \lambda/2 = H^{-2}/2$ and hence y is small when $z \ll H$. This means that λ represents the effect of stratification.

Perturbing the background equations, the linearized MHD equations can be found by writing all variables in the form of Equation (1.14).

Since thermal conduction is known to have a strong effect on slow modes, we will concentrate our analysis on the properties of these modes. It has been shown by a number of authors (*e.g.* Roberts, 2006 and Luna-Cardozo et al., 2012) that slow modes can be isolated by assuming $v_{1x} = v_{1y} = 0$. Therefore the linear, dissipative, MHD equations for slow modes in the presence of thermal conduction reduce to a 1D system given by

$$\frac{\partial \rho_1}{\partial t} + \rho_0 \frac{\partial v_1}{\partial z} + v_1 \frac{\partial \rho_0}{\partial z} = 0, \tag{2.17}$$

$$\rho_0 \frac{\partial v_1}{\partial t} = -\frac{\partial p_1}{\partial z}, \tag{2.18}$$

$$\frac{R}{\tilde{\mu}}\left[\frac{\rho_1}{\gamma-1}\frac{\partial T_0}{\partial t} + \frac{\rho_0}{\gamma-1}\frac{\partial T_1}{\partial t} + \rho_0 T_0 \frac{\partial v_1}{\partial z} - \frac{T_0}{\gamma-1} v_1 \frac{\partial \rho_0}{\partial z}\right] = \kappa \nabla^2 T_1, \tag{2.19}$$

$$p_1 = \frac{R}{\tilde{\mu}}\left[\rho_0 T_1 + \rho_1 T_0\right]. \tag{2.20}$$

Here $v_1 \equiv v_{1z}$ and the subscript '1' indicates the perturbations. Although there are now no terms relating to the magnetic field, slow waves are still guided by the magnetic field. Dimensionless variables can now be introduced to simplify

the equations, where the following dimensionless quantities are defined:

$$\tilde{\rho}_1 = \frac{\rho_1}{\rho_i}, \qquad \tilde{\rho}_0 = \frac{\rho_0}{\rho_i}, \qquad \tilde{p}_1 = \frac{p_1}{p_i}, \qquad \tilde{T}_1 = \frac{T_1}{T_i}, \qquad \tilde{T}_0 = \frac{T_0}{T_i}, \qquad \tilde{\mathbf{v}}_1 = \frac{\mathbf{v}_1}{c_{si}},$$

$$c_{si} = \frac{l}{\tau}, \qquad c_{si}^2 = \frac{\gamma p_i}{\rho_i}, \qquad \tilde{t} = \frac{t}{\tau}, \qquad \tilde{z} = \frac{z}{l}, \qquad \tilde{\lambda} = \left(\frac{l}{H}\right)^2, \qquad \tilde{c_2} = lc_2,$$

$$\tilde{c_3} = lc_3.$$

Here c_{si} is the initial sound speed, l is the characteristic wavelength of the oscillations, and τ is the characteristic period of oscillations. Thus, the equation of energy conservation in terms of dimensionless variables, will be

$$\rho_1 \frac{\partial T_0}{\partial t} + \rho_0 \frac{\partial T_1}{\partial t} + (\gamma - 1)\rho_0 T_0 \nabla . \mathbf{v}_1 \ - T_0 v_1 \frac{\partial \rho_0}{\partial z} = \sigma \frac{\partial^2 T_1}{\partial z^2}, \tag{2.21}$$

where

$$\sigma = \frac{(\gamma - 1)\kappa\, \rho_i T_i}{\gamma\, p_i^2\, \tau}.$$

When deriving Equation (2.21) we have dropped the tilde. Using coronal values (*e.g.* De Moortel and Hood, 2003), we find σ that is a small quantity, where the standard solar coronal values of all variables

$$\begin{cases} T_0 = 1 - 6 \text{ MK}, \\ \rho_0 = 1.67 \times 10^{-12} \text{ kg m}^{-3}, \\ \kappa = 10^{-11}\, T_0^{5/2} \text{ W m}^{-1} \text{ K}^{-1}, \\ \tilde{\mu} = 0.6, \\ R = 8.3 \times 10^3 \text{ m}^2 \text{ s}^{-2} \text{ deg}^{-1}, \\ \gamma = 5/3, \\ \tau = 300 \text{ s}, \end{cases} \tag{2.22}$$

give a value of $\sigma = 0.04$ for $T = 1$ MK and $\sigma = 0.61$ for $T = 6$ MK.

After the linearisation, the ideal-gas law equation is

$$p_1 = \rho_0 T_1 + \rho_1 T_0, \tag{2.23}$$

and the continuity equation is

$$\frac{\partial \rho_1}{\partial t} + \rho_0 \frac{\partial v_1}{\partial z} + v_1 \frac{\partial \rho_0}{\partial z} = 0, \tag{2.24}$$

while the energy equation takes the form

$$\frac{\partial p_1}{\partial t} + \gamma \rho_0 T_0 \frac{\partial v_1}{\partial z} = \sigma \frac{\partial^2 T_1}{\partial z^2}. \tag{2.25}$$

Differentiating Equation (2.25) with respect to z and using Equation (2.18), we arrive at

$$\frac{\partial^2 v_1}{\partial t^2} - T_0 \frac{\partial^2 v_1}{\partial z^2} = -\frac{\sigma}{\gamma \rho_0} \frac{\partial^3 T_1}{\partial z^3}. \tag{2.26}$$

To solve the equation of energy, we start from the continuity equation and use the gas law equation to find an equation in terms of velocity variable. Substituting Equation (2.23) into Equation (2.24), we obtain

$$\frac{1}{T_0}\frac{\partial p_1}{\partial t} - \frac{p_1}{T_0^2}\frac{\partial T_0}{\partial t} - \frac{\rho_0}{T_0}\frac{\partial T_1}{\partial t} + \frac{\rho_0 T_1}{T_0^2}\frac{\partial T_0}{\partial t} + \rho_0 \frac{\partial v_1}{\partial z} + v_1 \frac{\partial \rho_0}{\partial z} = 0. \tag{2.27}$$

The dimensionless background temperature is given by (after removing tilde)

$$T_0(z,\, t) = \frac{\exp(-\lambda \sigma t)}{\rho_0(z)},$$

thus

$$\frac{\partial T_0}{\partial t} = \delta T_0, \quad \text{where} \quad \delta = -\lambda \sigma. \tag{2.28}$$

Then, after substituting Equation (2.28) and multiplying by T_0, Equation (2.27) reduces to

$$\frac{\partial p_1}{\partial t} - \delta p_1 - \rho_0 \frac{\partial T_1}{\partial t} + \delta \rho_0 T_1 + \rho_0 T_0 \frac{\partial v_1}{\partial z} + T_0 v_1 \frac{\partial \rho_0}{\partial z} = 0. \tag{2.29}$$

Substituting this equation into Equation (2.25), we obtain the following equation

$$(\gamma - 1)\rho_0 T_0 \frac{\partial^2 v_1}{\partial t \partial z} - \delta \rho_0 T_0 \frac{\partial v_1}{\partial z} - \frac{\partial}{\partial t}(T_0 v_1)\frac{\partial \rho_0}{\partial z} = \sigma \frac{\partial^3 T_1}{\partial t \partial z^2} - \rho_0 \frac{\partial^2 T_1}{\partial t^2} + \delta \rho_0 \frac{\partial T_1}{\partial t}, \tag{2.30}$$

which represents another relation between the perturbed temperature and perturbed velocity in addition to Equation (2.26). Now, we aim to derive the governing equation for the velocity perturbation. Differentiating Equation (2.29) once

with respect to t and three times with respect to z, and using Equations (2.25) and (2.26), after some algebra, we arrive at

$$\gamma\frac{\rho_0}{\sigma}\frac{\partial^4 v_1}{\partial t^4} - \gamma\left[\frac{\rho_0\delta}{\sigma} + \frac{3}{\rho_0^2}\left(\frac{\partial\rho_0}{\partial z}\right)^2 - \frac{2}{\rho_0}\frac{\partial^2\rho_0}{\partial z^2} - \frac{1}{\rho_0}\frac{\partial\rho_0}{\partial z}\frac{\partial}{\partial z} + \frac{\partial^2}{\partial z^2}\right]\frac{\partial^3 v_1}{\partial t^3}$$
$$+\gamma\left[\frac{3\delta}{\rho_0^2}\left(\frac{\partial\rho_0}{\partial z}\right)^2 - \frac{2\delta}{\rho_0}\frac{\partial^2\rho_0}{\partial z^2} - \frac{\delta}{\rho_0}\frac{\partial\rho_0}{\partial z}\frac{\partial}{\partial z} + \left(\delta - \frac{\rho_0 T_0}{\sigma}\right)\frac{\partial^2}{\partial z^2}\right]\frac{\partial^2 v_1}{\partial t^2}$$
$$-\left[\frac{\gamma\delta\rho_0 T_0}{\sigma}\frac{\partial^2}{\partial z^2} - 2\frac{\partial T_0}{\partial z}\frac{\partial^3}{\partial z^3} - T_0\frac{\partial^4}{\partial z^4}\right]\frac{\partial v_1}{\partial t} + \left[2\delta\frac{\partial T_0}{\partial z}\frac{\partial^3}{\partial z^3} + \delta T_0\frac{\partial^4}{\partial z^4}\right]v_1 = 0. \quad (2.31)$$

To simplify Equation (2.31) we neglect all terms of order $\sigma\delta$ and higher powers in σ or δ as σ and δ are small parameters. Then, after multiplying Equation (2.31) by σ, and rearranging we obtain the governing equation in the form

$$\begin{aligned}\gamma\rho_0\frac{\partial^4 v_1}{\partial t^4} &- \gamma\rho_0 T_0\frac{\partial^2}{\partial z^2}\frac{\partial^2 v_1}{\partial t^2} \\ &= \gamma\left[\rho_0\delta + \frac{3\sigma}{\rho_0^2}\left(\frac{\partial\rho_0}{\partial z}\right)^2 - \frac{2\sigma}{\rho_0}\frac{\partial^2\rho_0}{\partial z^2} - \frac{\sigma}{\rho_0}\frac{\partial\rho_0}{\partial z}\frac{\partial}{\partial z} + \sigma\frac{\partial^2}{\partial z^2}\right]\frac{\partial^3 v_1}{\partial t^3} \\ &\quad + \left[\gamma\delta\rho_0 T_0\frac{\partial^2}{\partial z^2} - 2\sigma\frac{\partial T_0}{\partial z}\frac{\partial^3}{\partial z^3} - \sigma T_0\frac{\partial^4}{\partial z^4}\right]\frac{\partial v_1}{\partial t}. \quad (2.32)\end{aligned}$$

After some algebra and eliminating the small terms under the assumption that the background quantities are slowly varying when compared to the perturbed quantities, the governing equation becomes

$$\frac{\partial}{\partial t}\left[\frac{\partial^2 v_1}{\partial t^2} - T_0\frac{\partial^2 v_1}{\partial z^2}\right] = \delta\left[\frac{\partial^2 v_1}{\partial t^2} - T_0\frac{\partial^2 v_1}{\partial z^2}\right] + \frac{\sigma}{\rho_0}\frac{\partial^2}{\partial z^2}\left[\frac{\partial^2 v_1}{\partial t^2} - \frac{T_0}{\gamma}\frac{\partial^2 v_1}{\partial z^2}\right]. \quad (2.33)$$

In the absence of thermal conduction, Equation (2.33) reduces to the wave equation that represents (longitudinal) acoustic mode propagating in a flux tube and has the form

$$\frac{\partial^2 v_1}{\partial t^2} - T_0\frac{\partial^2 v_1}{\partial z^2} = 0, \quad (2.34)$$

while in the case of unstratified atmosphere, *i.e.* no change in the background plasma quantities with height, Equation (2.33) reduces to the model governing

equation found by De Moortel and Hood (2003):

$$\frac{\partial}{\partial t}\left[\frac{\partial^2 v_1}{\partial t^2} - T_0\frac{\partial^2 v_1}{\partial z^2}\right] = \frac{\sigma}{\rho_0}\frac{\partial^2}{\partial z^2}\left[\frac{\partial^2 v_1}{\partial t^2} - \frac{T_0}{\gamma}\frac{\partial^2 v_1}{\partial z^2}\right]. \tag{2.35}$$

Assuming the background quantities are constant, one can Fourier analyse all perturbations as $\exp(\mathrm{i}(\omega t - kz))$. After that, Equation (2.33) reduces to the dispersion relation

$$\omega^3 - \mathrm{i}\sigma\,\omega^2 k^2 - \omega k^2 + \mathrm{i}\frac{\sigma}{\gamma}k^4 = 0, \tag{2.36}$$

where ω is the frequency and k is the wavenumber. This dispersion relation was obtained first by Field (1965). We see that Equation (2.33) is consistent with earlier studies (*e.g.* Field, 1965 and De Moortel and Hood, 2003).

2.3 Analytical Solutions

We now seek an analytic solution to the governing Equation (2.33). Unlike previous models which include thermal conduction, there is now a temporal dependence due to the temporally changing background temperature. This means that we cannot Fourier-analyse in time. Instead, since the right hand side of Equation (2.33) has derivatives multiplied by a small factor σ, the WKB approximation (*e.g.* Bender and Ország, 1978) can be used. The accuracy of the WKB approximation increases when σ decreases. Since the variables in Equation (2.33) depend on time t and space z, we introduce the "slow" variable $t_1 = \sigma t$ and the "local" variable $\zeta = \sigma z$ to solve this equation. The slow timescale physically means that the conductive-cooling timescale is longer than the period of the oscillations. The "local" lengthscale means that any significant changes in quantities in the z-direction occur on length scales longer than the wavelength of the oscillation. Now, in accordance with the WKB method, we write the velocity perturbation in the form

$$v_1(\zeta, t_1) = Q(\zeta, t_1)\exp\left(\frac{\mathrm{i}}{\sigma}\Theta(\zeta, t_1)\right), \tag{2.37}$$

where $Q(\zeta, t_1)$ and $\Theta(\zeta, t_1)$ are functions to be determined.

Substituting Equation (2.37) into Equation (2.33) and taking the largest-order

terms in σ, which are terms proportional to σ^{-5}, we obtain

$$\left(\frac{\partial\Theta}{\partial t_1}\right)^2 - c_s^2(\zeta,\, t_1)\left(\frac{\partial\Theta}{\partial\zeta}\right)^2 = 0, \qquad c_s(\zeta,\, t_1) = \sqrt{T_0}. \tag{2.38}$$

If we assume $\partial\Theta/\partial t_1 = \omega(\zeta, t_1)$ and $\partial\Theta/\partial\zeta = k(\zeta, t_1)$, where $\omega(\zeta, t_1)$ is the frequency and $k(\zeta, t_1)$ is the wavenumber, then Equation (2.38) is, in fact, a temporally and spatially dependent dispersion relation for the longitudinal (acoustic) mode.

The next largest-order terms in σ (of order σ^{-4}) give the equation for the amplitude:

$$-\frac{1}{c_s}\frac{\partial Q}{\partial t_1} + \frac{\partial Q}{\partial\zeta} + \left[\frac{\lambda}{4c_s} - \frac{1}{2c_s}\frac{\partial c_s}{\partial\zeta} - \frac{(\gamma-1)}{2\gamma\rho_0 c_s}\left(\frac{\partial\Theta}{\partial\zeta}\right)^2\right] Q = 0. \tag{2.39}$$

Equations (2.38) and (2.39) will be solved by using the method of characteristics, thus we need to derive boundary conditions at $z = 0$.

To achieve this, we study a thin layer around $z = 0$ where we may assume the spatial gradients of both T_0 and ρ_0 are very small, so they can be considered constant in space in this region. This enables the use of Fourier analysis $v_1 \sim \exp(\mathrm{i}kz)$. Equation (2.33) reduces to

$$\frac{\mathrm{d}^3 v_1}{\mathrm{d}t^3} + [\sigma\lambda + \sigma k^2]\frac{\mathrm{d}^2 v_1}{\mathrm{d}t^2} + T_0 k^2 \frac{\mathrm{d}v_1}{\mathrm{d}t} + \frac{\sigma\, T_0 k^4}{\gamma} v_1 = 0. \tag{2.40}$$

Next, we apply the WKB method to this equation by assuming that the perturbation in terms of the variable t_1, has the form

$$v_1(t_1) = Q_1(t_1)\exp\left(\frac{\mathrm{i}}{\sigma}\Theta_1(t_1)\right). \tag{2.41}$$

Substituting into Equation (2.40), the highest-order equation in σ gives

$$\frac{\mathrm{d}\Theta_1}{\mathrm{d}t_1} = c_s(t_1)k, \tag{2.42}$$

where $c_s(t_1) = \sqrt{T_0(t_1)} = \exp(-\lambda t_1/2)$. Equation (2.42), after integrating over

the interval $[0, t_1]$, has the solution

$$\Theta_1(t_1) = \frac{2k}{\lambda}[1 - c_s(t_1)]. \tag{2.43}$$

The next-order equation in σ is

$$\frac{\mathrm{d}Q_1}{\mathrm{d}t_1} - \left(\frac{\lambda}{4} - \frac{(\gamma-1)}{\gamma}\frac{k^2}{2}\right) Q_1 = 0, \tag{2.44}$$

which has the solution

$$Q_1(t_1) = \exp\left[\left(\frac{\lambda}{4} - \frac{(\gamma-1)}{\gamma}\frac{k^2}{2}\right) t_1\right], \tag{2.45}$$

where k is the wavenumber at $z = 0$.

We now have the necessary boundary conditions at $z = 0$ to proceed with the solution of Equations (2.38) and (2.39) using the method of characteristics.

We introduce the variables r and s to parameterise Equations (2.38) and (2.39). The characteristic equations of Equation (2.38) are given by

$$\frac{\partial t_1}{\partial s} = -\frac{1}{c_s}, \qquad \frac{\partial \zeta}{\partial s} = 1, \qquad \frac{\partial \Theta}{\partial s} = 0,$$

with boundary conditions for the characteristics curves

$$t_1(r, 0) = r, \qquad \zeta(r, 0) = 0, \qquad \Theta(r, 0) = \Theta_1(r),$$

where $\Theta_1(r)$ is given by Equation (2.43) and $(r, 0, \Theta_1)$ is a point on the curve $(t_1(r, s), \zeta(r, s), \Theta(r, s))$ which lies in the surface $\{(t_1, \zeta, \Theta(\zeta, t_1))\}$ that represents the graph of the function $\Theta(\zeta, t_1)$. The solutions of the characteristic equations are

$$s(\zeta, t_1) = \zeta, \tag{2.46}$$

$$\begin{aligned} r(\zeta, t_1) \;=\; & -\frac{2}{\lambda}\ln\left[\exp\left(\frac{-\lambda t_1}{2}\right)\right. \\ & \left. - \frac{\lambda\sigma}{2\sqrt{c_2}}\arctan\left(\frac{c_3\sqrt{F(\zeta)} + 2c_2(\zeta - \frac{c_3\sigma}{2c_2})}{2\sqrt{c_2}\sqrt{F(\zeta)} - c_3\sqrt{c_2}(\zeta - \frac{c_3\sigma}{2c_2})}\right)\right], \end{aligned} \tag{2.47}$$

$$\Theta(\zeta,t_1) = -\frac{2k}{\lambda}\left[\exp\left(\frac{-\lambda t_1}{2}\right) - \frac{\lambda\sigma}{2\sqrt{c_2}}\arctan\left(\frac{c_3\sqrt{F(\zeta)}+2c_2(\zeta-\frac{c_3\sigma}{2c_2})}{2\sqrt{c_2}\sqrt{F(\zeta)}-c_3\sqrt{c_2}(\zeta-\frac{c_3\sigma}{2c_2})}\right)-1\right]. \quad (2.48)$$

Similarly, the characteristic equations of Equation (2.39) are

$$\frac{\partial t_1}{\partial s} = -\frac{1}{c_s}, \qquad \frac{\partial \zeta}{\partial s} = 1, \qquad \frac{\partial Q}{\partial s} = \left(\frac{\lambda}{4c_s} - \frac{1}{2c_s}\frac{\partial c_s}{\partial \zeta} - \frac{(\gamma-1)}{2\gamma\rho_0 c_s}\left(\frac{\partial \Theta}{\partial \zeta}\right)^2\right)Q,$$

with boundary conditions

$$t_1(r,0) = r, \qquad \zeta(r,0) = 0, \qquad Q(r,0) = Q_1(r),$$

where $Q_1(r)$ is given by Equation (2.45) and $(r,0,Q_1)$ is a point on the curve $(t_1(r,s),\zeta(r,s),Q(r,s))$ which lies in the surface $\{(t_1,\zeta,Q(\zeta,t_1))\}$ that represents the graph of the function $Q(\zeta,t_1)$. The solutions of the characteristic equations are Equations (2.46), (2.47) and

$$Q(\zeta,t_1) = \exp\left[\left(\frac{\lambda}{4}-\frac{\gamma-1}{\gamma}\frac{k^2}{2}\right)\left\{r+\frac{\sigma}{\sqrt{c_2}}\exp\left(\frac{\lambda t_1}{2}\right)\right.\right. \times \left.\left.\arctan\left(\frac{c_3\sqrt{F(\zeta)}+2c_2(\zeta-\frac{c_3\sigma}{2c_2})}{2\sqrt{c_2}\sqrt{F(\zeta)}-c_3\sqrt{c_2}(\zeta-\frac{c_3\sigma}{2c_2})}\right)\right\} + \frac{1}{4}\ln\left(\frac{\sigma^2}{F(\zeta)}\right)\right], \quad (2.49)$$

where

$$F(\zeta) = -c_2\zeta^2 + c_3\sigma\zeta + \sigma^2 = \frac{\sigma^2}{\rho_0(\zeta)}. \quad (2.50)$$

Taking the Taylor expansion of the amplitude and ignoring the small terms under the assumption of slowly varying background coronal plasma and weakly stratified atmosphere, we arrive at

$$Q(\zeta,t_1) = 1 - \left(\frac{\gamma-1}{\gamma}\frac{k^2}{2} - \frac{\lambda}{4}\right)t_1 + \frac{1}{4}\sqrt{\lambda}\,\zeta. \quad (2.51)$$

Equation (2.37), combined with Equations (2.47) – (2.50), provides a full solution

to Equation (2.33). All other perturbed quantities can now be calculated using Equations (2.17) − (2.20). The equations may not reveal much information yet as they are complicated in nature. We examine a limiting case for the amplitude to reveal some properties. Assume that $\lambda = 0$ (unstratified atmosphere), then the system of Equations (2.47), (2.49), and (2.50) reduces to

$$Q(t) = \exp\left[\left(-\frac{(\gamma-1)}{\gamma}\frac{k^2}{2}\right)\sigma t\right]. \tag{2.52}$$

This limit is in good agreement with its counterpart in De Moortel and Hood (2003). The amplitude of the wave is damped and the damping is dependent upon the value of σ and k.

2.4 Numerical Evaluations

It has been shown by Morton et al. (2010) that the WKB estimates provide good approximations to the frequency and amplitude variations in time and space when the plasma is cooling due to radiation. We see no reasons why this should be any different here, where thermal dissipation in the form of thermal conduction is considered. Numerical calculations are now used to demonstrate how the analytic solutions of the MHD waves behave in a system with a variable background.

The amplitude of the slow wave is computed using characteristic solar coronal values. In Figure 2.1 we plot the amplitude of the longitudinal (acoustic) wave, given in Equation (2.49), for different values of λ (which is the separation constant and is related to the squared reciprocal of scale height) and the value of thermal ratio σ at $z = 0$. It is found that the amplitude decays rapidly in time for all values of λ and σ, over typical observed timescales of oscillations. In particular, Figure 2.1(a) depicts that the oscillation amplitude declines dramatically under the coronal values of temperature 1 MK. Figure 2.1(b) illustrates a faster decay of the wave amplitude for a temperature 3 MK, *i.e.* for even hotter loops. The decay of the amplitude is enhanced even further for very hot (SXT/XRT) loops, *i.e.* $T = 6$ MK as shown in Figure 2.1(c). In each plot shown in Figure 2.1, it is also clearly seen that increasing the stratification of the plasma, *i.e.* increasing λ, decreases the rate of the damping. Because the magnitude of λ is directly related to the rate of cooling of the background plasma, the new and important result

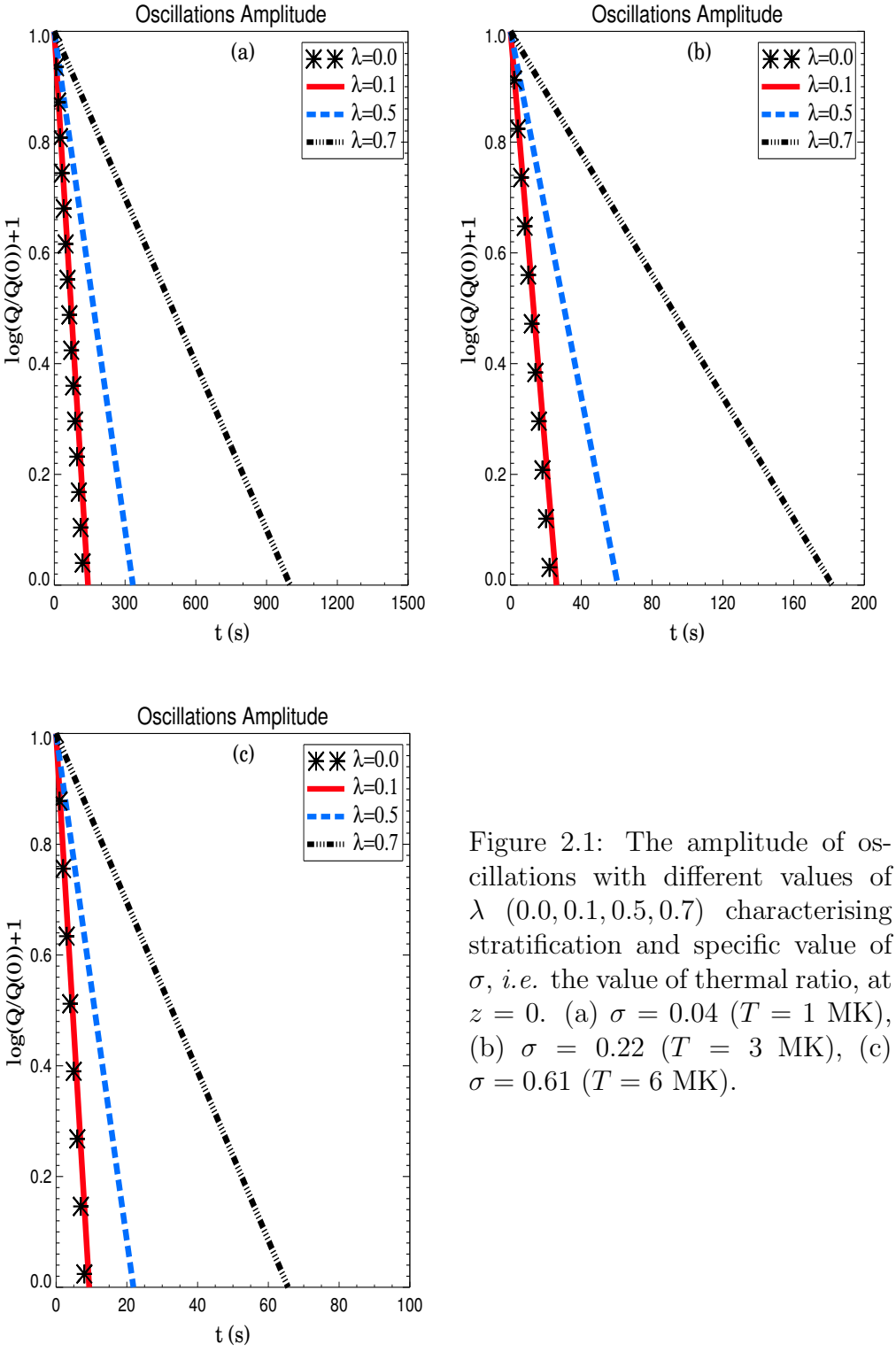

Figure 2.1: The amplitude of oscillations with different values of λ $(0.0, 0.1, 0.5, 0.7)$ characterising stratification and specific value of σ, *i.e.* the value of thermal ratio, at $z = 0$. (a) $\sigma = 0.04$ ($T = 1$ MK), (b) $\sigma = 0.22$ ($T = 3$ MK), (c) $\sigma = 0.61$ ($T = 6$ MK).

here is that the strength of the damping of the oscillations is reduced due to the introduction of the cooling background plasma compared to that predicted by De Moortel and Hood (2003) (see, Figure 2.1 for comparison). This is clearly seen in Equation (2.51), where the background cooling term $[\lambda t_1]$, is in competition with the wave damping term, which is $\propto k$. We can also see in Equation (2.51) that stratification decreases the rate of damping of the slow mode due to thermal conduction, this is consistent with the finding of De Moortel and Hood (2004).

A note of caution is needed when interpreting these results. The temperature of the plasma drops rapidly due to the cooling. As $T \rightarrow 2$ MK, radiation will start to become the dominant damping mechanism. Thus as T reaches 2 MK, the damping of the longitudinal mode may not look as shown here. A full numerical simulation incorporating the variable background and the variable value of σ will need to undertaken that is well beyond the scope of the present study and may require a full numerical approach even for an initial insight because of the complex nature of the mathematical modelling (*e.g.* generating background flows, *etc.*).

In Figure 2.2 we show how the magnitude of the thermal-conduction coefficient, $[\kappa]$, affects the rate of damping of the longitudinal (acoustic) mode. Altering the value of κ by an order of magnitude leads to large changes in the rate of damping, *i.e* the amplitude of longitudinal (acoustic) wave decreases more rapidly with an increasing value of κ.

Next, Figure 2.3 shows how the decay of the amplitude varies for different values of $z = (0.0, 0.1, 0.5)$. Two values of the thermal ratio $\sigma = (0.04, 0.22)$ are taken to illustrate the influence of thermal conduction on cool and hot corona, T=(1 MK, 3 MK), and the characteristic value of $\lambda = 0.1$. This plot shows that the strength of the damping due to thermal conduction will be the same along a loop.

What is of interest is how the results presented here compare to observations. We provide a quantitative comparison between reported properties of slow modes and the theory. First, we consider slow modes in relatively cool coronal loops ($T \approx 1$ MK) observed in EUV imagers, *e.g.* TRACE (De Moortel, 2009). Slow modes are observed as small intensity oscillations which have amplitudes greater than 2% of the background intensity with an average of 4%. Hence, the slow modes are not observed once the amplitude of the oscillation has decreased by

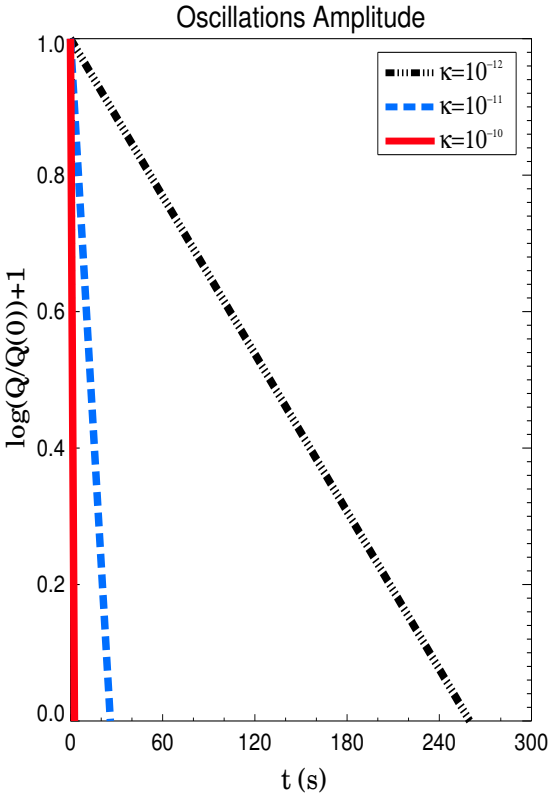

Figure 2.2: The amplitude of oscillations with different values of the thermal-conduction coefficient, $\kappa_0 = (10^{-10}, 10^{-11}, 10^{-12})$ $\mathrm{m^2\,s^{-1}\,K^{-5/2}}$ at $z = 0$ and $\lambda = 0.1$ where $T = 3$ MK.

say, about 50%. The average distance traveled by the slow waves is 9 Mm with an average phase speeds of $\approx 100 - 120$ km $\mathrm{s^{-1}}$, hence they last for ≈ 100 seconds. Comparing this to Figure 2.1(a) we find that this is possible in the loops with the larger values of stratification. Moreover, decay times for the slow waves in Doppler-shift oscillations are in the range $5.7 - 36.8$ minutes (Wang et al., 2003a).

However, the wavenumber, $[k]$, is small for the observed oscillations ($k \approx 10^{-8}$) and it can be seen from Equations (2.49) and (2.51) that for small values of k the damping due to thermal conduction is negligible. Hence, if thermal conduction is the dominant method of cooling in the corona, then we would expect to see amplification of the observed slow modes.

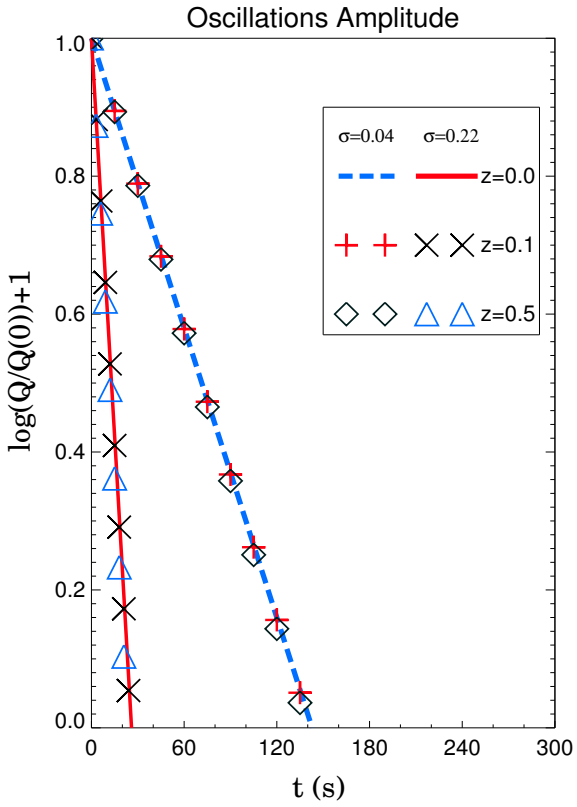

Figure 2.3: The amplitude of oscillations as function of time at different positions along the coronal magnetic field lines, *e.g.* $z = (0.0, 0.1, 0.5)$ and $\lambda = 0.1$, and with different values of $\sigma = (0.04, 0.22)$.

2.5 Discussion and Conclusion

The influence of variable background on the longitudinal (field-aligned) MHD wave propagating in a magnetised plasma in a weakly stratified atmosphere has been investigated. The background plasma is assumed to be cooling as the magneto–acoustic wave propagates. Thermal conduction is the dominant mechanism causing the plasma cooling and change of pressure as a function of time. The magnetic field was assumed to be constant and directed along the z-direction. A governing equation is derived under the assumption that the background plasma is cooling on a time scale greater than or comparable to the characteristic period of the perturbations. A temporally and spatially dependent dispersion relation that describes the propagation of the longitudinal magneto–acoustic mode is ob-

tained and an analytic equation for the time-dependent amplitude is also derived. The effect of the cooling background due to thermal conduction on the amplitude of hot-loop oscillations was then studied.

The governing equation is solved by using the WKB theory. Leading- and first-order equations for the dispersion relation and wave amplitude, respectively, are obtained and solved analytically. An approximate solution that represents the properties of the field-aligned acoustic wave is found with the aid of the method of characteristics. Numerical evaluation illustrates the behaviour of the analytic solutions. A comparison of wave behaviours for a range of initial temperatures is studied.

Although the efficiency of damping is reduced by the cooling background plasma, the amplitude of longitudinal (acoustic) waves was found to decay rapidly due to the influence of thermal conduction. The rate of damping of the oscillations was found to depend on the initial temperature of the plasma and the amount of stratification. It was previously shown that thermal conduction leads to the damping of slow-mode oscillations. For example, the amplitude of slow modes in this study was found to undergo damping, whereas in De Moortel and Hood (2003) the amplitude was found to experience a stronger damping. It should be noted that Morton et al. (2010) reported a strong damping of the slow mode due to the cooling of the background plasma by another dissipation mechanism, namely by radiation. Consequently, we conclude that the magneto–acoustic oscillations of the hot corona can experience strong damping because of cooling by thermal conduction, while radiation is the dominant method for damping cool coronal oscillations.

Overall, the presented results of the damping of coronal oscillations imply that both radiation and thermal-conduction mechanisms should be taken into account. This is due to the inclusion of a cooling background plasma having an efficient and dominating influence on the properties and lifetimes of MHD oscillations in the cool and hot corona, respectively. The main finding is that these dissipative processes introduce a dynamic plasma background. Such a background is often reported in observations. The MHD wave theory of dynamic plasma is in its early stage of development and we argue that, for an adequate model of solar coronal processes, consideration of a dynamic plasma background in the

modelling is essential. The temporal evolution of the background plasma has an extremely important effect on the properties of waves in flaring and post-flare loops and needs to be incorporated into future models. This is especially necessary if deriving plasma parameters from magneto-seismological methods, *e.g.* in applications to the solar corona.

Chapter 3

The Effect of Variable Background on Oscillating Coronal Loop

This chapter deals with the effect of a variable, *i.e.* time-dependent, background on the standing acoustic (*i.e.* longitudinal) modes generated in a hot coronal loop. We closely follow Al-Ghafri and Erdélyi (2012). A theoretical model of 1D geometry describing the coronal loop is applied. The background temperature is allowed to change as a function of time and undergoes an exponential decay with characteristic cooling times typical for coronal loops. The magnetic field is assumed to be uniform. Thermal conduction is assumed to be the dominant mechanism for damping hot coronal oscillations in the presence of a physically unspecified thermodynamic source that maintains the initial equilibrium. The coefficient of thermal conductivity is presumed to be varying as a function of time to examine how the variation of thermal conduction affects the properties of standing slow-mode waves.

The influence of the rapidly cooling background plasma on the behaviour of standing acoustic (longitudinal) waves is investigated analytically. The temporally evolving dispersion relation and wave amplitude are derived by using the WKB theory. An analytic solution for the time-dependent amplitude that describes the influence of thermal conduction on the standing longitudinal (acoustic) wave is obtained by exploiting the properties of Sturm-Liouville problem. Next, numerical evaluations further illustrate the behaviour of the standing acoustic

waves in a system with variable, time dependent background. The results are applied to a number of detected loop oscillations. We find a remarkable agreement between the theoretical predictions and the observations. Despite the emergence of the cooling background plasma in the medium, thermal conduction is found to cause a strong damping for the slow standing magneto-acoustic waves in hot coronal loops in general. Further to this, the increase in the value of thermal conductivity leads to a strong decay in the amplitude of the longitudinal standing slow MHD waves.

3.1 Introduction

The highly magnetised solar corona has been detected to support strongly evolving MHD oscillations in hot ($T \geq 6$ MK) active-region loops (Wang et al., 2002, 2003b; Taroyan et al., 2007). These oscillations are suggested to be standing-slow mode MHD waves. The evolution of longitudinal slow MHD waves is found to be influenced by dissipation. The observational and theoretical studies argued that the mechanism for the rapid damping of standing oscillations is essentially caused by thermal conduction with weak contribution from other mechanisms such as viscosity, for example (see Ofman and Wang, 2002).

In this chapter, we intend to investigate the effect of a temporally evolving temperature on the longitudinal standing MHD oscillations of hot coronal loops. The background plasma is allowed to cool due to the presence of a physically unspecified thermodynamic source. The chapter is organised as follows. In Section 3.2 we present the model of a straight coronal loop and derive the linear governing equation for the longitudinal standing magneto-acoustic mode. In Section 3.3 we derive the analytical solution of oscillation amplitude using the WKB method. Then, the evolution of oscillation amplitude is evaluated numerically in Section 3.4. In the last section we present the conclusions of the work discussed in this chapter.

3.2 The Model and Governing Equations

Consider a uniformly magnetised plasma in which the temperature is changing as function of time due to a physically unspecified thermodynamic source and the

density is a constant. The magnetic field is assumed to be uniform and aligned with the z-axis, *i.e.* $\mathbf{B}_0 = B_0\hat{\mathbf{z}}$. Therefore, the background state can be described as follows:

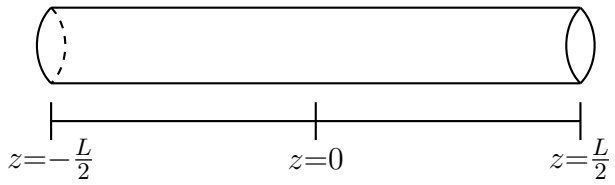

Figure 3.1: Coronal loop.

$$T_0 = T_0(t), \tag{3.1}$$

$$p_0 = p_0(t), \tag{3.2}$$

$$\rho_0 = \text{const.}, \tag{3.3}$$

$$B_0 = \text{const.}, \tag{3.4}$$

$$\epsilon = \frac{P}{\tau_c} \ll 1. \tag{3.5}$$

Here T_0, p_0, ρ_0 and B_0 are the background quantities identifying the temperature, pressure, density and magnetic field, respectively; P is the characteristic period of the loop's slow oscillation, and τ_c is the cooling time scale.

The governing MHD equations for the plasma motion take the following form

$$\frac{\partial \rho}{\partial t} + \nabla.(\rho \mathbf{v}) = 0, \tag{3.6}$$

$$\rho\frac{\partial \mathbf{v}}{\partial t} + \rho(\mathbf{v}.\nabla)\mathbf{v} = -\nabla p + \frac{1}{\mu_0}(\nabla \times \mathbf{B}) \times \mathbf{B}, \tag{3.7}$$

$$\frac{R}{\tilde{\mu}}\rho^{\gamma}\left[\frac{\partial}{\partial t}\frac{T}{\rho^{\gamma-1}} + (\mathbf{v}.\nabla)\frac{T}{\rho^{\gamma-1}}\right] = (\gamma-1)\nabla(\kappa_{\parallel}\nabla T) + \mathcal{L}, \tag{3.8}$$

$$p = \frac{R}{\tilde{\mu}}\rho T, \tag{3.9}$$

$$\frac{\partial \mathbf{B}}{\partial t} = \nabla \times (\mathbf{v} \times \mathbf{B}), \tag{3.10}$$

where $\mathbf{v}$ is the velocity, $\mathbf{B}$ is the magnetic field, μ_0 is the magnetic permeability of free space, γ is the ratio of specific heats, R is the gas constant, $\tilde{\mu}$ is the mean molecular weight, T is the temperature, $\nabla(\kappa_{\parallel}\nabla T)$ is the thermal conduction term where $\kappa_{\parallel} = \kappa_0 T^{5/2}$, $\mathcal{L}$ is a physically unspecified thermodynamic source term, ρ and p are the plasma density and pressure, respectively.

Assuming that there is no background flow and the background density is

constant, the previous equations determining the background plasma state reduce to

$$v_0 = 0, \quad \rho_0 = \text{const.}, \tag{3.11}$$

$$\nabla p_0 = 0, \tag{3.12}$$

$$p_0 = \frac{R}{\tilde{\mu}} \rho_0 T_0, \qquad i.e.\ p_0 \sim T_0, \tag{3.13}$$

$$\frac{R}{\tilde{\mu}} \rho_0 \frac{\mathrm{d}T_0}{\mathrm{d}t} = \mathcal{L}, \tag{3.14}$$

where the '0' index denotes background quantity. The observed cooling of coronal loops has been shown to be well-approximated by exponential profile for radiative-cooling loops (Aschwanden and Terradas, 2008; Morton and Erdélyi, 2009*b*, 2010). More recently, Erdélyi et al. (2011) found that the temperature decreases exponentially in time due to thermal conduction in hot coronal loops. As a result, we will assume here that the cooling temperature profile of coronal loops has the form

$$T_0 = T_{0i} \exp\left(-\frac{t}{\tau_c}\right), \tag{3.15}$$

where T_{0i} is the initial temperature at $t = 0$.

Let us perturb the background state, where all variables can be written in the form

$$f(z,t) = f_0(t) + f_1(z,t),$$

where the subscript '1' indicates perturbed quantities. In this study we consider longitudinal motions only, *i.e.* $\mathbf{v} = v\hat{\mathbf{z}}$, so the linearised perturbed MHD equations in a 1D system are

$$\frac{\partial \rho_1}{\partial t} + \rho_0 \frac{\partial v_1}{\partial z} = 0, \tag{3.16}$$

$$\rho_0 \frac{\partial v_1}{\partial t} = -\frac{\partial p_1}{\partial z}, \tag{3.17}$$

$$\frac{R}{\tilde{\mu}} \left[\rho_1 \frac{\mathrm{d}T_0}{\mathrm{d}t} + \rho_0 \frac{\partial T_1}{\partial t} + (\gamma - 1)\rho_0 T_0 \frac{\partial v_1}{\partial z} \right] = (\gamma - 1)\kappa_0 T_0^{5/2} \frac{\partial^2 T_1}{\partial z^2}, \tag{3.18}$$

$$p_1 = \frac{R}{\tilde{\mu}} \left\{ \rho_0 T_1 + T_0 \rho_1 \right\}. \tag{3.19}$$

Here $v_1 \equiv v_{1z}$ is the longitudinal velocity perturbation. It is clear that there are no terms exhibiting the magnetic field but the standing waves are still guided by the magnetic field. Non-dimensionalisation will be used to simplify the 1D governing Equations (3.16) – (3.19). The dimensionless quantities are introduced as

$$\begin{aligned} \tilde{t} &= \frac{t}{P}, \quad \tilde{z} = \frac{z}{L}, \quad c_{si} = \frac{L}{P}, \quad \tilde{p}_0 = \frac{p_0}{p_{0i}}, \quad \tilde{T}_0 = \frac{T_0}{T_{0i}}, \\ c_{si}^2 &= \frac{\gamma p_{0i}}{\rho_0}, \quad \tilde{\rho}_1 = \frac{\rho_1}{\rho_0}, \quad \tilde{p}_1 = \frac{p_1}{p_{0i}}, \quad \tilde{T}_1 = \frac{T_1}{T_{0i}}, \quad \tilde{v}_1 = \frac{v_1}{c_{si}}, \end{aligned} \tag{3.20}$$

where the subscript i represents the value of the quantity at $t = 0$, L is the loop length, and c_{si} is the initial sound speed.

Now, we aim to find the governing equation for the perturbed velocity, which reveals the behaviour of the standing magneto–acoustic mode subject to initial conditions generated in a hot solar coronal loop. Using the continuity and ideal gas law equations, Equation (3.18) in terms of dimensionless variables, removing the tilde for the sake of simplicity, takes the form

$$\frac{\partial^2 v_1}{\partial t^2} - T_0 \frac{\partial^2 v_1}{\partial z^2} = -\frac{\sigma}{\gamma} T_0^{5/2} \frac{\partial^3 T_1}{\partial z^3}, \qquad \sigma = \frac{(\gamma - 1)\tilde{\mu}\kappa_0 T_{0i}^{5/2}}{RL\sqrt{\gamma\, p_{0i}\, \rho_0}}, \tag{3.21}$$

where σ is defined as thermal ratio and found to be a small quantity under typical solar coronal conditions (see, *e.g.* De Moortel and Hood, 2003) quoted in Equation (2.22) with $L = 10^8$ m, giving characteristic values of $\sigma \in [0.0068, 0.48]$ for $T \in [0.6 \times 10^6, 5 \times 10^6$ K].

Equation (3.21) with the aid of Equations (3.13) and (3.19) can be rewritten as

$$\frac{1}{T_0^{7/2}} \left(\frac{\partial^2 v_1}{\partial t^2} - T_0 \frac{\partial^2 v_1}{\partial z^2} \right) = -\frac{\sigma}{\gamma} \frac{\partial^3}{\partial z^3} \left[\frac{p_1}{T_0} - \rho_1 \right]. \tag{3.22}$$

Differentiating with respect to time, and using Equations (3.16) and (3.17), we obtain

$$\frac{\partial}{\partial t} \left[\frac{1}{T_0^{7/2}} \left(\frac{\partial^2 v_1}{\partial t^2} - T_0 \frac{\partial^2 v_1}{\partial z^2} \right) \right] = \frac{\sigma}{\gamma} \left[\frac{\gamma}{T_0} \frac{\partial^4 v_1}{\partial t^2 \partial z^2} + \gamma \frac{\mathrm{d}}{\mathrm{d}t} \left(\frac{1}{T_0} \right) \frac{\partial^3 v_1}{\partial t \partial z^2} - \frac{\partial^4 v_1}{\partial z^4} \right], \tag{3.23}$$

which is the governing equation and can be recast to a convenient form for further analysis as

$$\frac{\partial}{\partial t}\left(\frac{\partial^2 v_1}{\partial t^2}-T_0\frac{\partial^2 v_1}{\partial z^2}\right)=\frac{7}{2}\frac{1}{T_0}\frac{\mathrm{d}T_0}{\mathrm{d}t}\left(\frac{\partial^2 v_1}{\partial t^2}-T_0\frac{\partial^2 v_1}{\partial z^2}\right)-\sigma T_0^{3/2}\frac{\mathrm{d}T_0}{\mathrm{d}t}\frac{\partial^3 v_1}{\partial t\partial z^2}$$
$$+\sigma T_0^{5/2}\frac{\partial^2}{\partial z^2}\left(\frac{\partial^2 v_1}{\partial t^2}-\frac{T_0}{\gamma}\frac{\partial^2 v_1}{\partial z^2}\right). \quad (3.24)$$

There are three different cases of interest for the present context one can recover from Equation (3.24):

Case I. In the absence of the thermal conduction [σ] and the physically unspecified thermodynamic source in the energy equation [$\mathcal{L}\propto \mathrm{d}T_0/\mathrm{d}t$] the governing equation (3.22) reduces to

$$\frac{\partial^2 v_1}{\partial t^2}-c_s^2\frac{\partial^2 v_1}{\partial z^2}=0, \qquad c_s=\sqrt{T_0}=\text{const.}, \quad (3.25)$$

which has the solution

$$v_1(z,t)=\alpha\cos(\pi z)\cos(\pi c_s t). \quad (3.26)$$

This is subject to the initial and boundary conditions representing a line-tied flux tube perturbed as the fundamental mode

$$v_1(\pm 1/2,t)=0, \quad v_1(z,0)=\alpha\cos(\pi z), \quad \frac{\partial v_1}{\partial t}(z,0)=0, \quad (3.27)$$

where α is the initial amplitude of the standing wave at $t=0$. A more general, *e.g.* broad-band, perturbation would, of course, give the solution in the mathematical form of a Fourier series.

Case II. In the case of no thermal conduction, *i.e.* $\sigma=0$, the effect of cooling of the background plasma on the system will be found by solving the following equation

$$\frac{\partial^2 v_1}{\partial t^2}-c_s^2\frac{\partial^2 v_1}{\partial z^2}=0, \qquad c_s(t)=\sqrt{T_0(t)}\neq\text{const.}, \quad (3.28)$$

which is *formally* exactly Equation (3.25) but with variable background temperature, $T_0=T_0(t)$. In spite of the absence of σ, the coefficient of the bracket in the first term in the right-hand-side of Equation (3.24) is originally derived from the

time derivative of thermal conduction term as seen in Equation (3.22). Therefore, this term is not added to Equation (3.28).

Case III. The effect of thermal conduction on the behaviour of the standing acoustic waves in the presence of a physically unspecified thermodynamic source will be investigated by solving Equation (3.24).

3.3 Analytical Solutions

Our goal now is to find an analytic solution to the governing Equation (3.28) first in case II and next to Equation (3.24) in case III. Let us point out that Equations (3.24) and (3.28) have derivatives multiplied by small factors σ and ϵ. This enables the use of the WKB theory to obtain an approximate solution. The WKB estimates give good approximations when the smaller value of factor used.

3.3.1 The Effect of Cooling

Case II. Let us first start to solve Equation (3.28) to establish the behaviour of standing magneto–acoustic waves under the influence of cooling of the background plasma. Assuming that $t_1 = \epsilon t$ which is defined as a slow timescale, meaning the cooling timescale is (much) longer than the period of the oscillations, Equation (3.28) will reduce to

$$\frac{\partial^2 v_1}{\partial t_1^2} - \frac{c_s^2}{\epsilon^2}\frac{\partial^2 v_1}{\partial z^2} = 0. \tag{3.29}$$

In line with applying the WKB estimates, let the perturbed velocity variable have the form

$$v_1(z, t_1) = Q(z, t_1) \exp\left(\frac{\mathrm{i}}{\epsilon}\Theta(t_1)\right). \tag{3.30}$$

The amplitude Q can be expanded in the power series as follows

$$Q(z, t_1) = Q_0 + \epsilon\, Q_1 + \cdots . \tag{3.31}$$

Substituting Equations (3.30) and (3.31) into Equation (3.29), and taking terms of order ϵ^{-3} we obtain to leading order

$$\frac{\partial^2 Q_0}{\partial z^2} + \frac{\omega^2}{c_s^2} Q_0 = 0, \tag{3.32}$$

where $\omega = \mathrm{d}\Theta/\mathrm{d}t_1$. The boundary conditions (3.27) applicable to the function Q_0 is

$$Q_0 = 0 \qquad \text{at} \quad z = \pm\frac{1}{2}. \tag{3.33}$$

Equations (3.32) and (3.33) represent a boundary-value problem that determines the frequency of the standing longitudinal (acoustic) mode in a cooling plasma with a varying temperature as function of time. The general solution physically acceptable to this boundary value problem has the form

$$Q_0(z,t_1) = \sum_{n=0}^{\infty} A_n(t_1)\cos\left((2n+1)\pi z\right), \qquad \omega_n(t_1) = (2n+1)\pi c_s(t_1), \tag{3.34}$$

where $n = 0, 1, 2, \cdots$. Then, collecting terms of order ϵ^{-2}, we obtain the equation determining the amplitude

$$\frac{\partial^2 Q_1}{\partial z^2} + \frac{\omega^2}{c_s^2}Q_1 = \frac{\mathrm{i}}{c_s^2}\left[\frac{\mathrm{d}\omega}{\mathrm{d}t_1}Q_0 + 2\omega\frac{\partial Q_0}{\partial t_1}\right]. \tag{3.35}$$

It follows from Equation (3.27) that Q_1 satisfies the boundary conditions

$$Q_1 = 0 \qquad \text{at} \quad z = \pm\frac{1}{2}. \tag{3.36}$$

The boundary-value problem, Equations (3.35) and (3.36), determining Q_1 has a solution only when the right-hand-side of Equation (3.35) satisfies the compatibility condition, which is the condition that it is orthogonal to Q_0 (see, Ruderman, 2011). This condition can be obtained by multiplying Equation (3.35) by Q_0, integrating with respect to z from $-1/2$ to $1/2$ and using the boundary conditions (3.36). The compatibility condition is eventually written as

$$\int_{-1/2}^{1/2}\frac{\mathrm{i}}{c_s^2}\left[\frac{\mathrm{d}\omega}{\mathrm{d}t_1}Q_0^2 + 2\omega Q_0\frac{\partial Q_0}{\partial t_1}\right]\mathrm{d}z = 0, \tag{3.37}$$

which gives the amplitude of the standing wave in the following form

$$A_n(t_1) = A_n(0)\exp\left(\frac{t_1}{4}\right) = A_n(0)\sqrt{\frac{c_s(0)}{c_s(t_1)}}. \tag{3.38}$$

The value of constant $A_n(0)$ can be found from Equation (3.34) at $t_1 = 0$, which is in the form of Fourier cosine series, using the boundary condition (3.27). Then, the solution (3.38), in scaled (*i.e.* physical) variables, takes the form

$$A_n(t) = \alpha \sqrt{\frac{c_s(0)}{c_s(t)}}. \tag{3.39}$$

This result describes the variation of a time-dependent amplitude of longitudinal standing waves in a dynamically cooling magnetic flux tube. Apparently, Equation (3.39) indicates that the cooling (or heating) leads to an amplification (decrease) of loop oscillation.

Indeed, it can be seen from this result that the physical complexity of the cooling background is embodied implicitly in the sound speed, *i.e.* the phase speed of the wave propagation. Although the governing equations in Case I and Case II have mathematically similar form, the difference between them occurs in the variability of the phase speed, where the sound speed is constant in Case I and variable in Case II.

3.3.2 The Effect of Weak Thermal Conduction

Case III. the behaviour of the standing wave in a system dominated by thermal conduction will be obtained by solving the governing Equation (3.24). Similarly, the WKB theory will be used to find the solution of Equation (3.24).

Let us now introduce the slow time $t_1 = \epsilon t$ and a scaled variable $\sigma = \epsilon\tilde{\sigma}$ representing the effect of *weak* thermal conduction, so that Equation (3.24) becomes

$$\frac{\partial^3 v_1}{\partial t_1^3} + \frac{7}{2}\frac{\partial^2 v_1}{\partial t_1^2} - \frac{c_s^2}{\epsilon^2}\frac{\partial^3 v_1}{\partial t_1 \partial z^2} - \tilde{\sigma} c_s^5 \frac{\partial^3 v_1}{\partial t_1 \partial z^2} - \tilde{\sigma} c_s^5 \frac{\partial^4 v_1}{\partial t_1^2 \partial z^2} - \frac{5}{2}\frac{c_s^2}{\epsilon^2}\frac{\partial^2 v_1}{\partial z^2} + \frac{\tilde{\sigma}}{\epsilon^2}\frac{c_s^7}{\gamma}\frac{\partial^4 v_1}{\partial z^4} = 0, \tag{3.40}$$

and the perturbed velocity by the new scaled variables and the WKB approximation is given by Equation (3.30). Substituting Equations (3.30) and (3.31) into Equation (3.40), and taking the highest-order terms in ϵ, which is again ϵ^{-3}, we obtain

$$\frac{\partial^2 Q_0}{\partial z^2} + \frac{\omega^2}{c_s^2} Q_0 = 0, \tag{3.41}$$

with the boundary conditions

$$Q_0 = 0 \qquad \text{at} \quad z = \pm\frac{1}{2}. \tag{3.42}$$

The solution to this boundary-value problem is given by

$$Q_0(z,t_1) = \sum_{n=0}^{\infty} B_n(t_1)\cos\left((2n+1)\pi z\right), \qquad \omega_n(t_1) = (2n+1)\pi c_s(t_1), \tag{3.43}$$

where $n = 0, 1, 2, \cdots$, and $B_n(t_1)$ stands for the amplitude of the longitudinal standing modes, and it will be found by taking the second-highest-order terms in ϵ for Equation (3.40) as follows.

The next-largest-order terms in ϵ, of order ϵ^{-2}, result in

$$\frac{\partial^2 Q_1}{\partial z^2} + \frac{\omega^2}{c_s^2}Q_1 = \frac{\mathrm{i}}{\omega c_s^2}\left[\left(\frac{7}{2}\omega^2 + 3\omega\frac{\mathrm{d}\omega}{\mathrm{d}t_1}\right)Q_0 + 3\omega^2\frac{\partial Q_0}{\partial t_1} + c_s^2\frac{\partial^3 Q_0}{\partial t_1 \partial z^2} + \left(\frac{5}{2}c_s^2 - \tilde{\sigma}\omega^2 c_s^5\right)\frac{\partial^2 Q_0}{\partial z^2} - \tilde{\sigma}\frac{c_s^7}{\gamma}\frac{\partial^4 Q_0}{\partial z^4}\right]. \tag{3.44}$$

It results from Equation (3.27) that Q_1 satisfies the boundary conditions

$$Q_1 = 0 \qquad \text{at} \quad z = \pm\frac{1}{2}. \tag{3.45}$$

Analogous to Equations (3.35) and (3.36), this boundary-value problem has a solution only when the right-hand side of Equation (3.44) satisfies the compatibility condition. Consequently,

$$\int_{-1/2}^{1/2}\frac{\mathrm{i}}{\omega c_s^2}\left[\left(\frac{7}{2}\omega^2 + 3\omega\frac{\mathrm{d}\omega}{\mathrm{d}t_1}\right)Q_0^2 + 3\omega^2 Q_0\frac{\partial Q_0}{\partial t_1} + c_s^2 Q_0\frac{\partial^3 Q_0}{\partial t_1 \partial z^2} + \left(\frac{5}{2}c_s^2 - \tilde{\sigma}\omega^2 c_s^5\right)Q_0\frac{\partial^2 Q_0}{\partial z^2} - \tilde{\sigma}\frac{c_s^7}{\gamma}Q_0\frac{\partial^4 Q_0}{\partial z^4}\right]\mathrm{d}z = 0. \tag{3.46}$$

Substituting (3.43) into (3.46), we obtain the amplitude of the n-th harmonic standing wave

$$B_n(t_1) = B_n(0)\exp\left[\frac{1}{4}t_1 + \frac{\tilde{\sigma}}{5}\left(\frac{\gamma-1}{\gamma}\right)(2n+1)^2\pi^2\left(c_s^5(t_1) - 1\right)\right], \tag{3.47}$$

which can be re-written as

$$B_n(t) = B_n(0)\exp\left[\frac{\epsilon}{4}t + \frac{\sigma}{5\epsilon}\left(\frac{\gamma-1}{\gamma}\right)(2n+1)^2\pi^2\left(c_s^5(t)-1\right)\right], \tag{3.48}$$

where $c_s^5(t) = \left(\sqrt{T_0(t)}\right)^5 = \exp(-5\epsilon\, t/2)$. Now, Equation (3.43) with the initial conditions (3.27) is applied to obtain the value of constants $B_n(0)$. Hence, the solution (3.48) is

$$B_n(t) = \alpha\exp\left[\frac{\epsilon}{4}t + \frac{\sigma}{5\epsilon}\left(\frac{\gamma-1}{\gamma}\right)(2n+1)^2\pi^2\left(c_s^5(t)-1\right)\right], \tag{3.49}$$

which reveals the temporal evolution of longitudinal standing-mode amplitude due to thermal conduction in a temporally variable (cooling or heating) background plasma.

Note that, in the limit $\sigma \to 0$, *i.e.* if there is no thermal conduction, Equation (3.49) reduces to Equation (3.39), which represents the amplitude variation of standing waves generated in a model of merely cooling plasma without non-ideal effects as, *e.g.*, thermal conduction. Moreover, in the absence of thermal conduction, Equations (3.44) and (3.46) are converted into Equations (3.35) and (3.37), respectively; but this procedure is not straightforward because the coefficient of thermal conduction $[\kappa_\parallel]$ is a function of time and composed of both σ and $T_0^{5/2}$ as such seen in Equation (21). Hence, we need to deal with all terms of Equations (3.44) and (3.46) to recapture Equations (3.35) and (3.37) so all steps are demonstrated as follows.

Eliminating all terms that include $\tilde{\sigma}$, Equation (3.44) becomes

$$\frac{\partial^2 Q_1}{\partial z^2} + \frac{\omega^2}{c_s^2}Q_1 = \frac{\mathrm{i}}{\omega c_s^2}\left[\left(\frac{7}{2}\omega^2 + 3\omega\frac{\mathrm{d}\omega}{\mathrm{d}t_1}\right)Q_0 + 3\omega^2\frac{\partial Q_0}{\partial t_1} + c_s^2\frac{\partial^3 Q_0}{\partial t_1 \partial z^2} + \frac{5}{2}c_s^2\frac{\partial^2 Q_0}{\partial z^2}\right]. \tag{3.50}$$

The second term on the right hand side of Equation (3.50) can be written as

$$3\omega\frac{\mathrm{d}\omega}{\mathrm{d}t_1}Q_0 = (2{+}1)\omega\frac{\mathrm{d}\omega}{\mathrm{d}t_1}Q_0 = \left(-\omega^2 + \omega\frac{\mathrm{d}\omega}{\mathrm{d}t_1}\right)Q_0, \qquad \text{where} \quad \frac{\mathrm{d}\omega}{\mathrm{d}t_1} = -\frac{\omega}{2}, \tag{3.51}$$

and the fourth term, after using Equation (3.41), has the form

$$c_s^2\frac{\partial^3 Q_0}{\partial t_1 \partial z^2} = -\omega^2\frac{\partial Q_0}{\partial t_1}. \tag{3.52}$$

Then, substituting Equations (3.51) and (3.52), Equation (3.50) reduces to

$$\frac{\partial^2 Q_1}{\partial z^2} + \frac{\omega^2}{c_s^2} Q_1 = \frac{\mathrm{i}}{\omega c_s^2} \left[\left(\frac{5}{2}\omega^2 + \omega \frac{\mathrm{d}\omega}{\mathrm{d}t_1} \right) Q_0 + 2\omega^2 \frac{\partial Q_0}{\partial t_1} + \frac{5}{2} c_s^2 \frac{\partial^2 Q_0}{\partial z^2} \right]. \tag{3.53}$$

The first term and the last term on the right hand side of Equation (3.53) can be combined together to give

$$\frac{5}{2}\omega^2 Q_0 + \frac{5}{2} c_s^2 \frac{\partial^2 Q_0}{\partial z^2} = \frac{5}{2} c_s^2 \left[\frac{\omega^2}{c_s^2} Q_0 + \frac{\partial^2 Q_0}{\partial z^2} \right] = 0. \tag{3.54}$$

Eventually, by employing Equation (3.54), Equation (3.53) reduces to

$$\frac{\partial^2 Q_1}{\partial z^2} + \frac{\omega^2}{c_s^2} Q_1 = \frac{\mathrm{i}}{\omega c_s^2} \left[\omega \frac{\mathrm{d}\omega}{\mathrm{d}t_1} Q_0 + 2\omega^2 \frac{\partial Q_0}{\partial t_1} \right], \tag{3.55}$$

which is exactly Equation (3.35) after taking ω as a common factor from the bracket. Similarly, we can recover Equation (3.37) from Equation (3.46) by using the same steps.

Now, expanding the sound speed by Taylor expansion and neglecting small terms of order ϵ^2 and higher, Equation (3.49) becomes

$$B_n(t) = \alpha \exp \left[\frac{\epsilon}{4} t - \frac{\sigma}{2} \left(\frac{\gamma - 1}{\gamma} \right) (2n+1)^2 \pi^2 \left(t - \frac{5}{4} \epsilon\, t^2 \right) \right]. \tag{3.56}$$

Subsequently, we can reveal some properties of the oscillation amplitude by examining various limits. For instance, assuming that $\epsilon = 0$, which means that there is no cooling in the model, Equation (3.56) is reduced to

$$B_n(t) = \alpha \exp \left[-\frac{\sigma}{2} \left(\frac{\gamma - 1}{\gamma} \right) (2n+1)^2 \pi^2\, t \right], \tag{3.57}$$

which is identical with its counterpart in De Moortel and Hood (2003). It is clear from Equation (3.57) that the wave amplitude is subject to a damping and the rate of damping depends on the value of σ.

3.4 Numerical Evaluations

Morton et al. (2010) and Erdélyi et al. (2011) have shown that the WKB ap-

proximation estimates accurately the solutions to the frequency and amplitude variations in time and space for waves supported by oscillating magnetic loops due to plasma cooling by radiation and/or thermal conduction, respectively. The obtained approximate solutions by the WKB theory can be motivated using numerical evaluations to demonstrate a clear view of the behaviour of MHD waves which is analytically found.

The amplitude of the longitudinal (acoustic) standing waves, that is given by Equation (3.38), is calculated using standard solar coronal values for the background quantities. Figure 3.2 shows the dependence of the amplitude on time for various values of ϵ. This figure shows that cooling causes the wave amplification, the faster cooling the stronger the amplification. It should be mentioned that this result is in agreement with that obtained by Erdélyi et al. (2011) who found that the efficiency of damping is reduced by the background plasma cooling. Recall that Figure 3.2 displays the amplitude evolution in the case when there is no damping.

Figure 3.3 shows the time dependence of the amplitude of standing longitudinal (acoustic) waves, which is given by Equation (3.48), for a range of values of ϵ and various values of σ corresponding to various initial temperatures. It is found that the variation of ϵ leads to a considerable change in the rate of damping of both cool and hot loops. Figure 3.3(a) shows the evolution of the oscillation amplitude in the EUV (cool) loops with the initial temperature. The wave damping is becoming stronger when the initial temperature increases as we can see in Figure 3.3(b) and 3.3(c). Cooling decreases the damping rate.

Figure 3.4 illustrates the effect of varying the magnitude of thermal conduction coefficient, κ, on the rate of damping of the standing acoustic wave using Equation (3.48). Typical values for the coefficient of the thermal conductivity $\kappa = \kappa_0 T_0^{5/2} = [10^{-10}, 10^{-11}, 10^{-12}]T_0^{5/2}$ are taken to shed light on the effect of thermal conduction in hot coronal loops, $T_0 = 3$ MK, and $\epsilon = 0.1$ is assumed (see, Priest, 2000). It is found that the rate of damping is changing rather rapidly when κ is increased by an order of magnitude.

It is instructive to compare the obtained results with observations. We only present here a quantitative comparison with the properties of hot loop oscillations

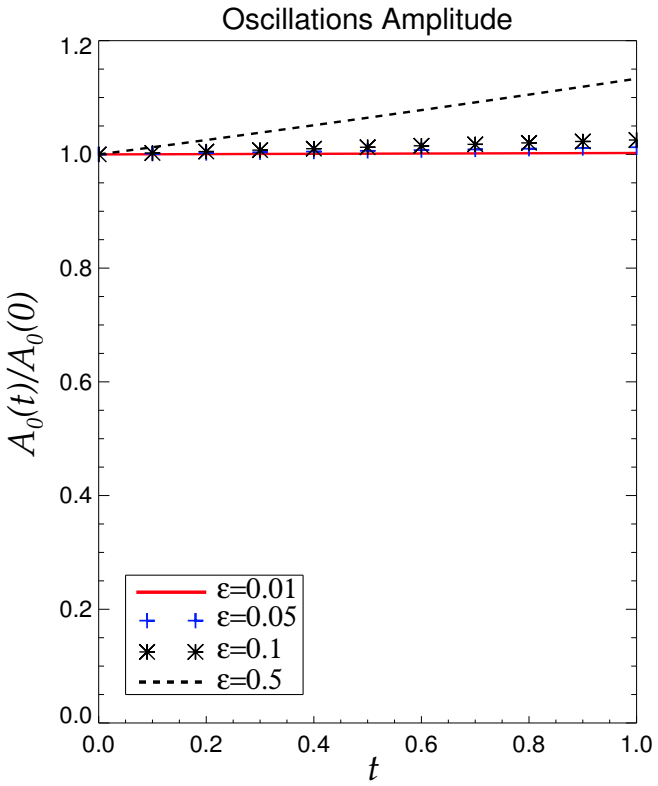

Figure 3.2: The amplitude of the standing wave with various values of ϵ. The time is measured in units of L/c_{si}.

observed by SUMER (see, Wang et al., 2003a), where the standing slow-mode waves are detected only in the region of temperature $\geq$ 6 MK. The periods of oscillations are $7-31$ minutes. The slow standing wave was observed to be strongly damped with characteristic decay times $5.7-36.8$ minutes mainly likely due to thermal conduction. The typical length of coronal loops is around 230 Mm.

In our work, we found that hot loop oscillations experience a strong damping due to thermal conduction when the value of ϵ is small enough as shown in Figure 3.3(c). Further to this, Figure 3.4 exhibits that the large value of thermal conduction coefficient leads to a rapid damping. However, the observed damping of standing acoustic modes was in a region of temperature $\gtrsim$ 6 MK as discussed by Ofman and Wang (2002) and Mendoza-Briceño et al. (2004a) which is not applicable for the present results.

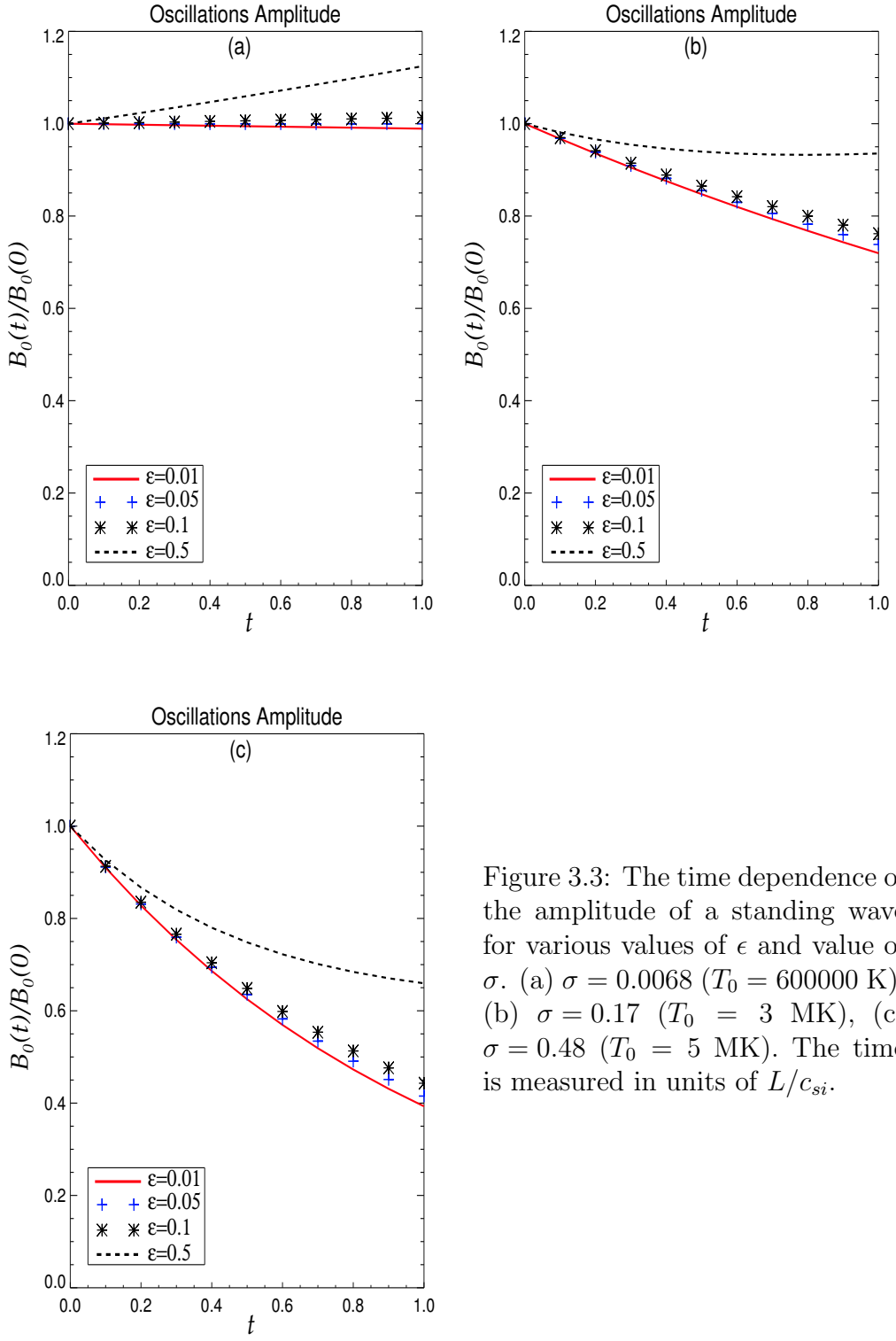

Figure 3.3: The time dependence of the amplitude of a standing wave for various values of ϵ and value of σ. (a) $\sigma = 0.0068$ ($T_0 = 600000$ K), (b) $\sigma = 0.17$ ($T_0 = 3$ MK), (c) $\sigma = 0.48$ ($T_0 = 5$ MK). The time is measured in units of L/c_{si}.

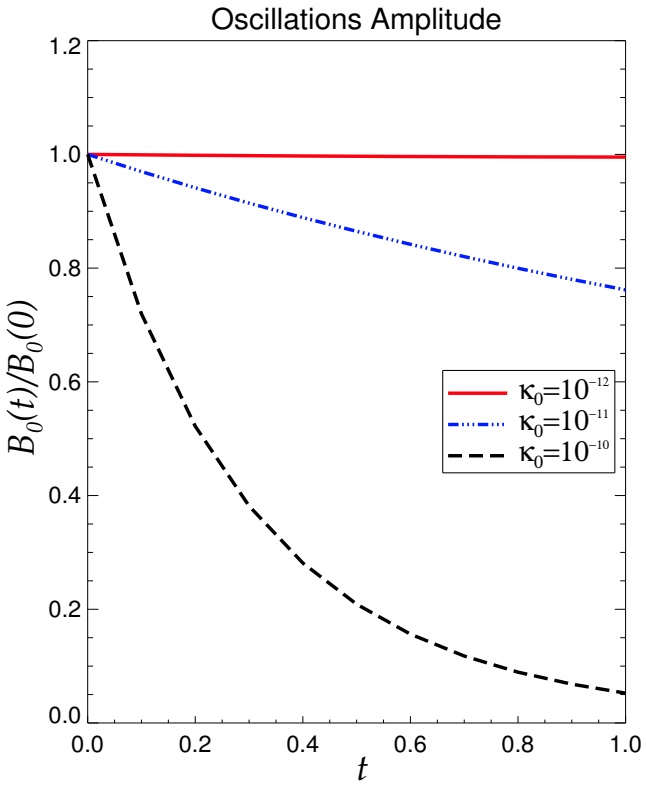

Figure 3.4: The amplitude of the standing wave with different values of the thermal-conduction coefficient, κ_0=$(10^{-10}, 10^{-11}, 10^{-12})$ $\mathrm{m^2\,s^{-1}\,K^{-5/2}}$ and specific value of the ratio of period to the cooling time, $\epsilon = 0.1$ where $T_0 = 3$ MK. The time is measured in units of L/c_{si}.

3.5 Discussion and Conclusion

In this work, we have investigated the influence of a cooling background on the standing longitudinal magneto-acoustic waves generated in a uniformly magnetised plasma. Thermal conduction is assumed to be the dominant mechanism for damping of oscillations in hot coronal loops. The background temperature is allowed to change as a function of time and to decay exponentially with characteristic cooling times typical for coronal loops. The magnetic field is assumed to be constant and in the z direction, which may be a suitable model for loops with large aspect ratio. A time-dependent equation governing the plasma perturbation is derived. It is assumed that the characteristic time of the background quan-

tities variation is much larger that the characteristic oscillation period. Three cases have been considered: (I) absence of thermal conduction σ and physically unspecified cooling or heating mechanism $\mathcal{L}$, (II) presence of physically unknown thermodynamic source $\mathcal{L}$ only, *i.e.* $\sigma = 0$, (III) the influence of thermal conduction σ combined with the physically unknown mechanism $\mathcal{L}$.

The WKB theory is used to find the analytical solution of the governing equation in cases II and III, while the governing equation in case I is solved directly and gives the undamped standing wave with constant sound speed. An approximate solution that describes a time-dependant amplitude of the standing acoustic mode is obtained with the aid of the properties of a Sturm-Liouville problem. The analytically derived solutions are illustrated numerically.

In the second case, the individual influence of cooling background plasma on hot-loop oscillation is found to cause an amplification to the amplitude of the longitudinal standing wave. It is noted that the rate of amplification increases with the increase of the ratio of the oscillatory period to the cooling time, ϵ.

In the third case, which is the most interesting, the temporally evolving amplitude is found to undergo a strong damping due to thermal conduction in the hot corona. Further to this, we note that the presence of cooling in a model of a hot coronal loop leads to a reduction in the efficiency of damping. The variation of the ratio of the period of oscillation to the cooling time scale, ϵ, plays an effective role on changing the rate of damping of oscillating hot coronal loops, causing a fast decline in the decay rate of oscillation amplitude, for $\epsilon \ll 1$.

The obtained results are in agreement with the previous studies (Morton and Erdélyi, 2009*b*, 2010; Morton et al., 2010; Erdélyi et al., 2011) and demonstrate that the temporal evolution of coronal plasma due to dissipative process, *i.e.* the cooling of the background plasma due to radiation/thermal conduction, has a great influence on the coronal oscillations. In the modelling of solar coronal loop, the temporally and spatially dependent dynamic background plasma must be considered to understand the properties of observed MHD waves.

Chapter 4

Longitudinal MHD Waves in Strongly Dissipative Time-Dependent Plasma

The present Chapter extends the study by Al-Ghafri and Erdélyi [2012, Solar Phys., in press] outlined in the previous chapter, on the effect of cooling on standing slow magnetosonic waves in coronal magnetic loops. The results presented here are submitted for publication (Al-Ghafri et al., 2012). Thermal conduction is assumed as the damping mechanism, so it is applicable for dissipation of oscillations in coronal loops. In contrast to the previous chapter, the coefficient of thermal conduction is taken to be arbitrary so that the damping time can be comparable to the oscillation period. The use of low-beta plasma approximation enables us to ignore the magnetic field perturbation when studying longitudinal waves. Therefore, the governing MHD equations reduce to a 1D system describing the behaviour of standing sound waves. The background equilibrium plasma temperature is assumed to be decaying exponentially in time with the characteristic cooling time much larger than the oscillation period. Then, the WKB theory is used to investigate the properties of longitudinal standing oscillation. An analytic expression for the oscillation amplitude is derived. The analytically obtained solution for the oscillation frequency and amplitude are evaluated numerically. The results show that the oscillation period increases with time due to the effect of plasma cooling. Further to this, the presence of plasma cooling also amplifies the amplitude of oscillations in relatively cool coronal loops whereas for

very hot coronal loop oscillations the rate of damping is enhanced by the cooling. These theoretical results may serve as impetus for developing the tools of solar magneto-seismology in dynamic plasmas.

4.1 Introduction

Coronal observations indicate that standing slow MHD waves are commonly detected in hot coronal loops with temperatures of the order or larger than 6 MK. Many studies have been scoped into the damping mechanisms to interpret the observed fast damping of oscillations. Several mechanisms have been proposed. In most of these studies, it is found that the dominant mechanism for damping of oscillations in hot coronal loops is thermal conduction. The plasma in hot coronal loop oscillation is found to experience a gradual cooling (Wang, 2011). However, Wang (2011) found that the rapid damping of oscillation amplitude is not caused by the cooling.

In this chapter we aim to study the effect of plasma cooling on the damping rate of slow standing MHD waves in coronal loops for *arbitrary* (in strength) thermal conduction coefficient. The Chapter is organised as follows. In the next Section we formulate the problem, and present the governing equations and boundary conditions. In Section 4.3 we carry out the analytical study of the problem using the WKB method. In Section 4.4 the analytical solution is examined numerically and the properties of oscillations are depicted using typical solar coronal values. Section 4.5 contains the summary and discussion of the results and our conclusions.

4.2 The Model and Governing Equations

We consider standing slow MHD waves in hot coronal magnetic loops. We model a magnetic loop as a straight homogeneous magnetic flux tube of length L with the constant magnetic field magnitude equal to B_0 (see Figure 3.1). We assume that the homogeneous plasma density, ρ_0, does not vary with time. On the other hand, both the plasma temperature, T_0, and pressure, p_0, are functions of time, the temperature dependence on time being given by Equation (3.15).

In our model the coefficient of thermal conduction along the magnetic field is given by $\kappa_{\parallel} = \kappa_0 T_0^{5/2}$, where κ_0 is a constant. The strength of thermal conduction is determined by the inverse Peclet number, σ, which is presented in Equation (3.21). If we take $L = 100$ Mm and $T_0 = 0.6 \div 6$ MK as typical solar coronal values then we obtain $0.007 \lesssim \sigma \lesssim 0.7$.

The dimensionless variables are used to solve the governing MHD equations and introduced as in Equation (3.20) with $\tilde{c}_s = \sqrt{\tilde{T}_0}$ referring to the dimensionless sound speed, and we put $P = L/c_{si}$. In what follows we drop the tilde.

Al-Ghafri and Erdélyi (2012) have shown that the linearised system of governing equations can be reduced to one equation for v_1,

$$\frac{\partial^3 v_1}{\partial t^3} + \frac{7}{2}\epsilon\frac{\partial^2 v_1}{\partial t^2} - \frac{5}{2}\epsilon c_s^2\frac{\partial^2 v_1}{\partial z^2} - c_s^2\frac{\partial^3 v_1}{\partial t \partial z^2} - \epsilon\sigma c_s^5\frac{\partial^3 v_1}{\partial t \partial z^2} - \sigma c_s^5\frac{\partial^4 v_1}{\partial t^2 \partial z^2} + \frac{\sigma}{\gamma}c_s^7\frac{\partial^4 v_1}{\partial z^4} = 0. \tag{4.1}$$

Next, in order to set appropriate boundary conditions, we also need the relation between the velocity and temperature perturbation:

$$\frac{\partial^2 v_1}{\partial t^2} - \frac{c_s^2}{\gamma}\frac{\partial^2 v_1}{\partial z^2} + \epsilon\frac{\partial v_1}{\partial t} = -\frac{1}{\gamma}\left(\frac{\partial^2 T_1}{\partial t \partial z} + \epsilon\frac{\partial T_1}{\partial t}\right). \tag{4.2}$$

To study the damping of standing waves we need to impose the boundary conditions at $z = \pm 1/2$. Since the loop ends are bounded by the dense photospheric plasma, we assume that the perturbation velocity vanishes at these ends,

$$v_1 = 0 \quad \text{at} \quad z = \pm 1/2. \tag{4.3}$$

The thermal conduction drops dramatically at the photosphere. Hence, it is viable to assume that the loop is thermally insulated,

$$\frac{\partial T_1}{\partial z} = 0 \quad \text{at} \quad z = \pm 1/2. \tag{4.4}$$

Using Equation (4.2) we rewrite this boundary condition in terms of v_1,

$$\frac{\partial^2 v_1}{\partial t^2} - \frac{c_s^2}{\gamma}\frac{\partial^2 v_1}{\partial z^2} + \epsilon\frac{\partial v_1}{\partial t} = 0 \quad \text{at} \quad z = \pm 1/2. \tag{4.5}$$

Equations (4.1) and (4.2), and the boundary conditions (4.3) and (4.5) are used in

the next section to study the damping of standing slow waves in cooling coronal loops.

4.3 Analytical Solution

Let us introduce the 'slow time' $t_1 = \epsilon t$, meaning the cooling timescale is (much) longer than the period of the oscillations. Now, we rewrite Equation (4.1) and the boundary condition (4.5) in terms of slow time,

$$\epsilon^3\frac{\partial^3 v_1}{\partial t_1^3}+\frac{7\epsilon^3}{2}\frac{\partial^2 v_1}{\partial t_1^2}-\frac{5\epsilon c_s^2}{2}\frac{\partial^2 v_1}{\partial z^2}-\epsilon c_s^2\frac{\partial^3 v_1}{\partial t_1 \partial z^2}-\epsilon^2\sigma c_s^5\frac{\partial^3 v_1}{\partial t_1 \partial z^2}-\epsilon^2\sigma c_s^5\frac{\partial^4 v_1}{\partial t_1^2 \partial z^2}+\frac{\sigma c_s^7}{\gamma}\frac{\partial^4 v_1}{\partial z^4}=0, \tag{4.6}$$

$$\epsilon^2\frac{\partial^2 v_1}{\partial t_1^2}-\frac{c_s^2}{\gamma}\frac{\partial^2 v_1}{\partial z^2}+\epsilon^2\frac{\partial v_1}{\partial t_1}=0 \quad \text{at} \quad z=\pm 1/2. \tag{4.7}$$

Then, we use the WKB method and look for the solution to Equation (4.6) with the boundary conditions (4.3) and (4.7) in the form

$$v_1(z,t_1)=Q(z,t_1)\exp\left(\mathrm{i}\epsilon^{-1}\Theta(t_1)\right). \tag{4.8}$$

Function Q is expanded in the power series with respect to ϵ, i.e.,

$$Q=Q_0+\epsilon Q_1+\ldots. \tag{4.9}$$

4.3.1 Approximation of Geometrical Optics

Substituting Equations (4.8) and (4.9) into Equation (4.6) and the boundary conditions (4.3) and (4.7), we obtain in the leading-order approximation, often called the approximation of geometrical optics (e.g. Bender and Ország, 1978),

$$\frac{\partial^4 Q_0}{\partial z^4}+\frac{\gamma\omega}{c_s^2}\left(\omega-\frac{\mathrm{i}}{\sigma c_s^3}\right)\frac{\partial^2 Q_0}{\partial z^2}-\frac{\mathrm{i}\gamma\omega^3}{\sigma c_s^7}Q_0=0, \tag{4.10}$$

$$Q_0=0, \quad \frac{\partial^2 Q_0}{\partial z^2}=0 \quad \text{at} \quad z=\pm 1/2, \tag{4.11}$$

where $\omega = \mathrm{d}\Theta/\mathrm{d}t_1$. The characteristic equation for Equation (4.10) is

$$\lambda^4+\alpha\lambda^2-\beta=0, \tag{4.12}$$

where

$$\alpha = \gamma\frac{\omega^2}{c_s^2} - \mathrm{i}\frac{\gamma\omega}{\sigma c_s^5}, \qquad \beta = \mathrm{i}\frac{\gamma\omega^3}{\sigma c_s^7}. \tag{4.13}$$

The four roots of the bi-quadratic Equation (4.12) are $\lambda = \pm \mathrm{i}k_\pm$, where $k_\pm$ are given by

$$k_\pm = \sqrt{\frac{\alpha \mp \sqrt{\alpha^2 + 4\beta}}{2}}. \tag{4.14}$$

For the definitness we assume that $\Re(k_\pm) > 0$, where $\Re$ denotes the real part of a quantity.

Then, the general solution to Equation (4.10) is

$$Q_0(z, t_1) = A_1 \cos(k_+ z) + A_2 \sin(k_+ z) + A_3 \cos(k_- z) + A_4 \sin(k_- z), \tag{4.15}$$

where $A_i(t_1)$, $i = 1, \ldots, 4$, are functions of time to be determined. Substituting Equation (4.15) in the boundary conditions (4.11) we obtain two systems of linear homogeneous algebraic equations,

$$\begin{aligned} A_1 \cos(k_+/2) + A_3 \cos(k_-/2) &= 0, \\ A_1\, k_+^2 \cos(k_+/2) + A_3\, k_-^2 \cos(k_-/2) &= 0, \end{aligned} \tag{4.16}$$

$$\begin{aligned} A_2 \sin(k_+/2) + A_4 \sin(k_-/2) &= 0, \\ A_2\, k_+^2 \sin(k_+/2) + A_4\, k_-^2 \sin(k_-/2) &= 0. \end{aligned} \tag{4.17}$$

The first system corresponds to symmetric and the second to antisymmetric eigenmodes. Each of the two systems has a non-trivial solution only when its determinant is equal to zero. This condition gives the dispersion equation. Hence, the dispersion equation for symmetric eigenmodes is

$$(k_+^2 - k_-^2)\cos(k_+/2)\cos(k_-/2) = 0, \tag{4.18}$$

while it is

$$(k_+^2 - k_-^2)\sin(k_+/2)\sin(k_-/2) = 0, \tag{4.19}$$

for antisymmetric eigenmodes. Since

$$(k_+^2 - k_-^2)^2 = \alpha^2 + 4\beta = \frac{\gamma^2\omega^2}{c_s^4}\left(\omega^2 - \frac{1}{\sigma^2 c_s^6} + 2\mathrm{i}\frac{(2-\gamma)\omega}{\gamma\sigma c_s^3}\right) \neq 0,$$

when $\omega \neq 0$, the dispersion equations for symmetric and antisymmetric eigenmodes reduce to $k_\pm = \pi(2n-1)$ and $k_\pm = 2\pi n$, respectively, where $n = 1, 2, \ldots$ However, there is no solution to the eigenvalue problem formed by Equation (4.10) and boundary conditions (4.11) that satisfies the condition $k_+ = k_-$.

Now, the two expressions of $k_\pm$ for symmetric and antisymmetric eigenmodes in the case $k_+ \neq k_-$ can be unified to $k_\pm = \pi n$, where now odd n corresponds to symmetric and even to antisymmetric eigenmodes. After simple algebra we can rewrite this equation in terms of ω,

$$\omega^3 - \mathrm{i}(\pi n)^2 \sigma c_s^5 \omega^2 - (\pi n)^2 c_s^2 \omega + \mathrm{i}\frac{\sigma c_s^7}{\gamma}(\pi n)^4 = 0, \tag{4.20}$$

where two roots of this equation represent slow modes (propagating in opposite directions) and one root refers to thermal mode (non-propagating). This dispersion equation is in agreement with that found by Field (1965), De Moortel and Hood (2003) and Erdélyi et al. (2011) in an appropriate limit. Note that, in the limit $\sigma \to 0$, i.e. if there is no thermal conduction, Equation (4.20) reduces to $\omega^2 = (\pi n c_s)^2$. In the case of very strong thermal conduction, i.e. when $\sigma \to \infty$, Equation (4.20) becomes $\omega^2 = (\pi n c_s)^2/\gamma$.

4.3.2 Approximation of Physical Optics

In what follows we are only interested in the fundamental longitudinal mode corresponding to $n = 1$. Hence, either $k_+ = \pi$ or $k_- = \pi$. In both cases Equation (4.15) reduces to

$$Q_0(z, t_1) = A(t_1)\cos(\pi z), \tag{4.21}$$

where $A = A_1$ in the first case and $A = A_3$ in the second case. Now, we need to determine the function $A(t_1)$. To do this we proceed to the next order approximation, often called the approximation of physical optics (e.g. Bender and Ország, 1978). Substituting Equations (4.8) and (4.9) into Equation (4.6) and the boundary conditions (4.3) and (4.7), and collecting terms of the order of ϵ we

obtain

$$\frac{\sigma}{\gamma}c_s^7\frac{\partial^4 Q_1}{\partial z^4} + \left(\sigma c_s^5\omega^2 - \mathrm{i}c_s^2\omega\right)\frac{\partial^2 Q_1}{\partial z^2} - \mathrm{i}\omega^3 Q_1 = \left(\frac{7}{2}\omega^2 + 3\omega\frac{\mathrm{d}\omega}{\mathrm{d}t_1}\right)Q_0 + 3\omega^2\frac{\partial Q_0}{\partial t_1} + \left(\frac{5}{2}c_s^2 + \mathrm{i}\sigma c_s^5\omega + \mathrm{i}\sigma c_s^5\frac{\mathrm{d}\omega}{\mathrm{d}t_1}\right)\frac{\partial^2 Q_0}{\partial z^2} + \left(c_s^2 + 2\mathrm{i}\sigma c_s^5\omega\right)\frac{\partial^3 Q_0}{\partial t_1 \partial z^2}, \quad (4.22)$$

$$Q_1 = 0, \quad \frac{\partial^2 Q_1}{\partial z^2} = 0 \quad \text{at} \quad z = \pm 1/2. \quad (4.23)$$

When deriving Equation (4.23) we have taken into account that $Q_0 = 0$ at $z = \pm 1/2$.

If we put the right-hand side of Equation (4.22) equal to zero, then we obtain the same eigenvalue problem as in the leading-order approximation. This problem has a non-trivial solution $Q_0 = A\cos(\pi z)$. This implies that boundary-value problem (4.22), (4.23) has a solution only when the right-hand side of Equation (4.22) satisfies the compatibility condition, which is the condition that it is orthogonal to Q_0. This condition can be obtained by multiplying Equation (4.22) by Q_0, integrating with respect to z from $-1/2$ to $1/2$, and using the integration by parts and the boundary conditions (4.23). As a result we obtain

$$\int_{-1/2}^{1/2}\left[\left(\frac{7}{2}\omega^2 + 3\omega\frac{\mathrm{d}\omega}{\mathrm{d}t_1}\right)Q_0^2 + 3\omega^2 Q_0\frac{\partial Q_0}{\partial t_1} + \left(\frac{5}{2}c_s^2 + \mathrm{i}\sigma c_s^5\omega + \mathrm{i}\sigma c_s^5\frac{\mathrm{d}\omega}{\mathrm{d}t_1}\right)Q_0\frac{\partial^2 Q_0}{\partial z^2} + \left(c_s^2 + 2\mathrm{i}\sigma c_s^5\omega\right)Q_0\frac{\partial^3 Q_0}{\partial t_1 \partial z^2}\right]\mathrm{d}z = 0, \quad (4.24)$$

which gives the following equation for the evolution of the oscillation amplitude A,

$$2f(\omega, t_1)\frac{\mathrm{d}A}{\mathrm{d}t_1} + \left[\frac{\partial f}{\partial \omega}\frac{\mathrm{d}\omega}{\mathrm{d}t_1} + h(\omega, t_1)\right]A = 0, \quad (4.25)$$

where

$$f(\omega, t_1) = 3\omega^2 - 2\mathrm{i}\pi^2\sigma c_s^5\omega - \pi^2 c_s^2, \quad (4.26)$$

$$h(\omega, t_1) = 7\omega^2 - 2\mathrm{i}\pi^2\sigma c_s^5\omega - 5\pi^2 c_s^2. \quad (4.27)$$

Now, we re-write the dispersion Equation (4.20) as

$$c_s^{-7}\omega^3 - \mathrm{i}\pi^2\sigma c_s^{-2}\omega^2 - \pi^2 c_s^{-5}\omega + \mathrm{i}\frac{\sigma}{\gamma}\pi^4 = 0.$$

Differentiating this equation with respect to t_1, then multiplying by $2c_s^7$, and taking into account that $c_s = e^{-t_1/2}$ yields

$$2f\frac{\mathrm{d}\omega}{\mathrm{d}t_1} = -\omega h. \tag{4.28}$$

Substituting this result in Equation (4.25) and using Equation (4.26) we obtain

$$2f^2\frac{\mathrm{d}A}{\mathrm{d}t_1} = \pi^2 c_s^2 h(1 + \mathrm{i}\sigma c_s^3\omega)A. \tag{4.29}$$

Integrating this equation we eventually arrive at

$$A(t_1) = A_0 \exp\left(\pi^2 \int_0^{t_1} \frac{c_s^2 h(1 + \mathrm{i}\sigma c_s^3\omega)}{2f^2}\, dt'\right), \tag{4.30}$$

where $A_0 = A(0)$. Finally, the wave amplitude $a(t_1)$ is given by

$$a(t_1) = |A(t_1)| \exp\left(-\epsilon^{-1} \int_0^{t_1} \Im(\omega)\, dt'\right), \tag{4.31}$$

where $\Im$ indicates the imaginary part of a quantity.

It is instructive to compare the results obtained in this section with those obtained by Al-Ghafri and Erdélyi (2012). These authors assumed that σ is small and took, as mentioned earlier, $\sigma = \mathcal{O}(\epsilon)$. For small σ we obtain from Equation (4.20)

$$\omega \approx \pi c_s + \mathrm{i}\frac{\sigma\pi^2 c_s^5(\gamma - 1)}{2\gamma}. \tag{4.32}$$

When calculating $A(t_1)$ we take $\omega \approx \pi c_s$ and neglect the term proportional to σ in the exponent and in the expressions for f and h. As a result we have

$$A(t_1) \approx A_0 e^{t_1/4}. \tag{4.33}$$

Substituting Equations (4.32) and (4.33) in Equation (4.31) we obtain

$$a(t) = A_0 \exp\left[\left(\frac{\epsilon}{4} - \frac{\sigma\pi^2(\gamma - 1)}{2\gamma}\right) t\right], \tag{4.34}$$

where we have also substituted $t_1 = \epsilon t$. This expression coincides with that given by Al-Ghafri and Erdélyi (2012) (see their Equation (51)) if we take $n = 0$ in the

latter, which corresponds to the fundamental mode, and neglect the small term proportional to ϵt^2 in the exponent.

In the next section we use Equation (4.31) to analyse the temporary evolution of the oscillation amplitude.

4.4 Numerical Results

In this section, we use the analytical results obtained in the previous section to study the evolution of the periods and amplitudes of standing slow waves in cooling dynamical coronal loops. Since the analytical expressions are quite complex, we calculate the periods and amplitudes for typical solar coronal conditions numerically and plot the results. The oscillation period is equal to $2\pi/\omega_r$ where ω_r is the real part of the frequency, ω. The frequency has been calculated using Equation (4.20).

Figure 4.1 displays the evolution of the oscillation period with time for various values of ϵ and the initial loop temperature. We see that the oscillation period increases with time due to cooling. This is an expected result because cooling decreases the phase speed. We can see that the effect is more pronounced in cooler loops.

The dependence of the oscillation amplitude on time for various values of ϵ and the initial loop temperature is displayed in Figure 4.2 by exploiting Equation (4.31).

We see that, in general, the oscillation amplitude decreases due to thermal conduction. When the loop temperature is not very high ($T \lesssim 5$ MK) cooling reduces the damping rate. This feature is especially clearly seen in Figure 4.2(a). We can observe in this figure that the damping of oscillation is very weak. This result is consistent with the general conclusion that, in cool EUV loops ($T \lesssim 1$ MK) the thermal condition is too weak to cause substantial damping of standing oscillations (e.g. Al-Ghafri and Erdélyi, 2012). As a consequence, the amplification of oscillations due to cooling dominates damping due to thermal conduction, and the oscillation amplitude in cooling loops increases.

For a loop with larger temperatures ($T \gtrsim 3$ MK) even strong cooling ($\epsilon = 0.5$)

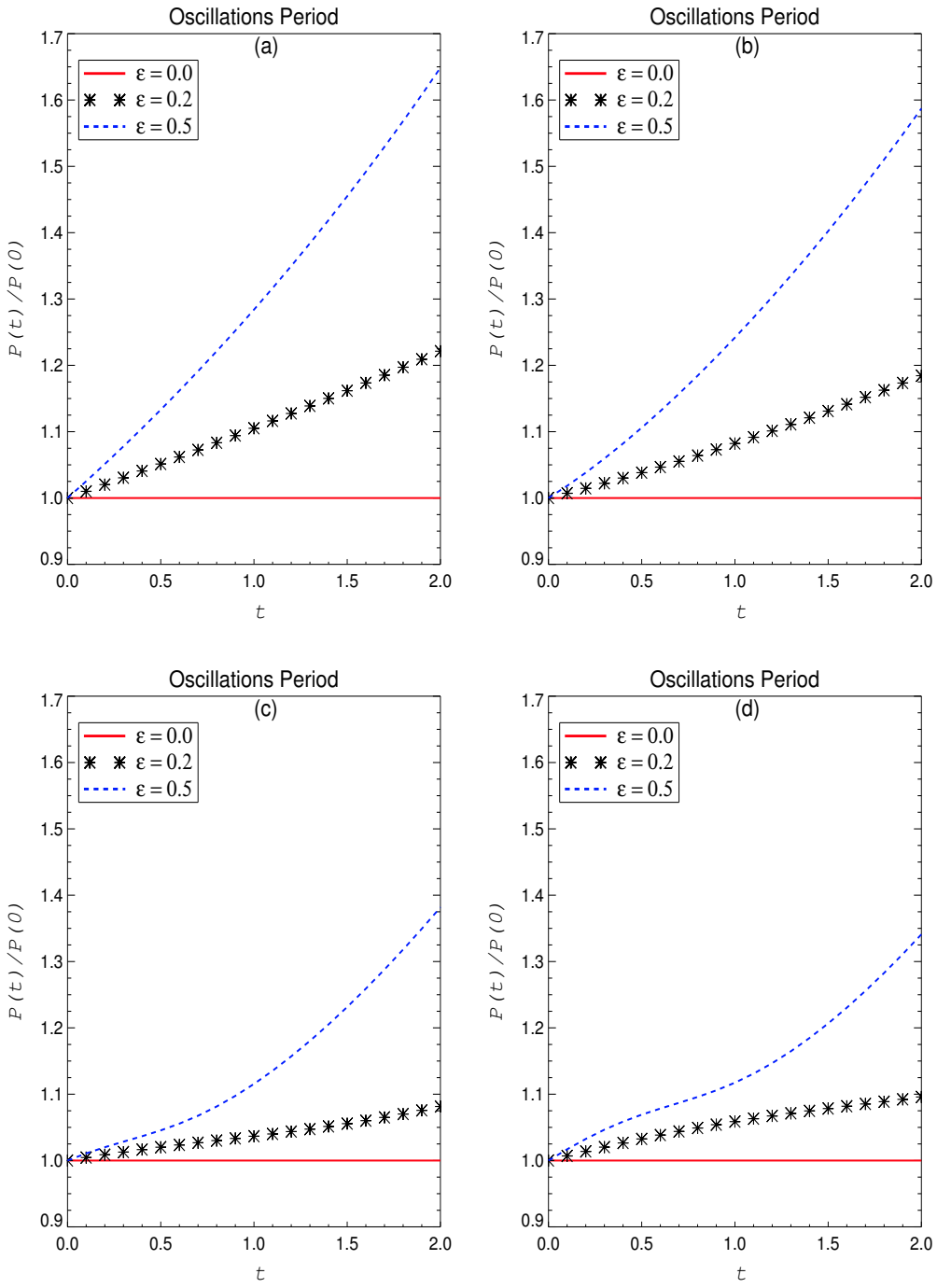

Figure 4.1: The dependence of the oscillation period on time for various values of ϵ and the loop temperature T. Recall that the time is measured in units of L/c_{si}. Panels (a), (b), (c) and (d) correspond to $T_{0i} = 0.6$ MK, $T_{0i} = 3$ MK, $T_{0i} = 5$ MK and $T_{0i} = 6$ MK respectively.

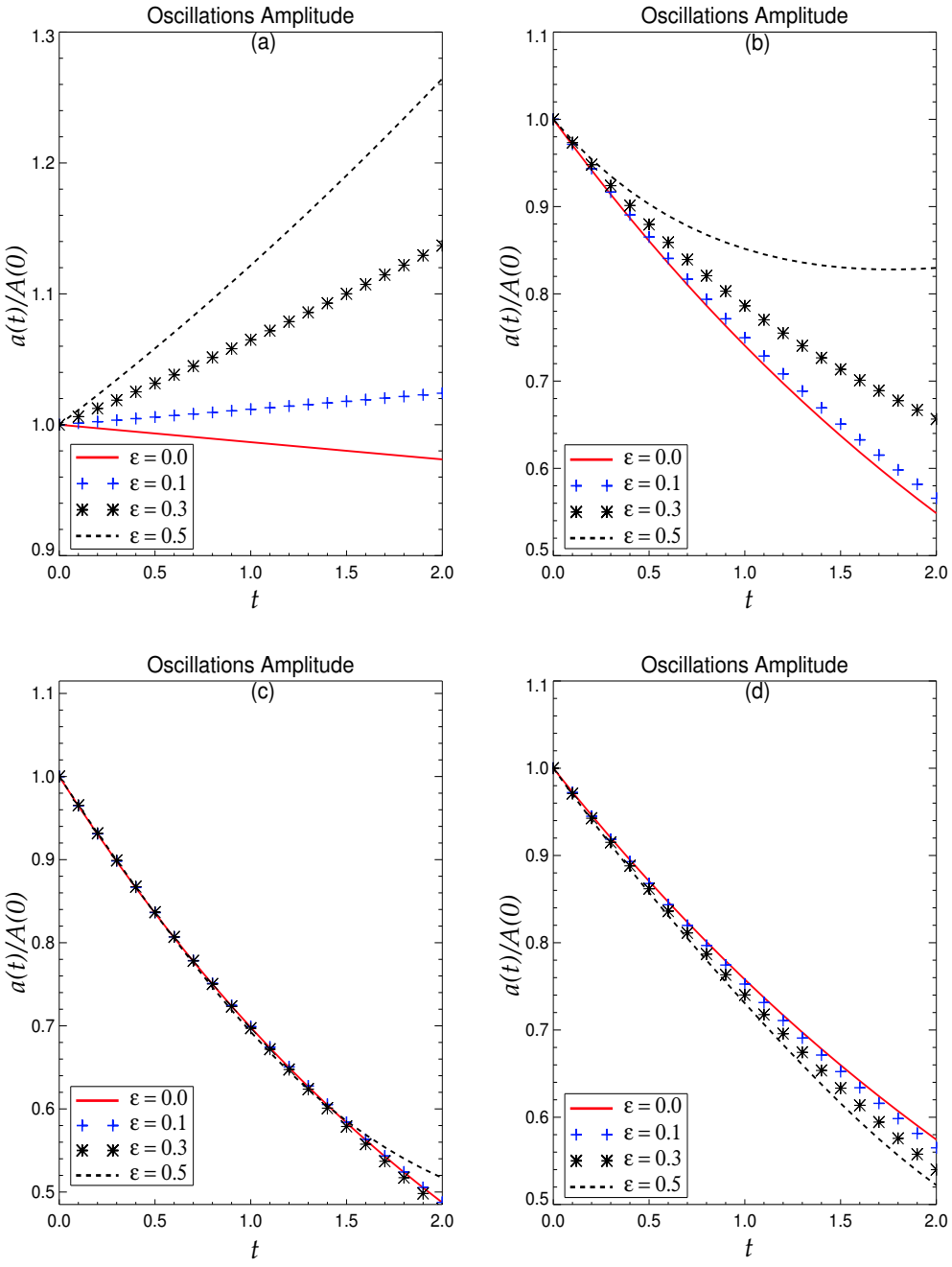

Figure 4.2: The dependence of the oscillation amplitude on time. Panels (a), (b), (c) and (d) correspond to $T_{0i} = 0.6$ MK ($\sigma = 0.0068$), $T_{0i} = 3$ MK ($\sigma = 0.17$), $T_{0i} = 5$ MK ($\sigma = 0.48$) and $T_{0i} = 6$ MK ($\sigma = 0.68$) respectively. The time is measured in units of L/c_{si}.

cannot counter-balance damping due to thermal conductions, thus it only can reduce the damping rate.

Figure 4.2(d) is especially interesting. We see in this figure that cooling enhances damping for oscillating hot coronal loops compared to relatively cool loops. The explanation of this effect is as follows. As we have already pointed out, the dependence of damping rate on the coefficient of thermal conduction and, consequently, on the loop temperature is not monotonic. It is clearly seen in Figure 4.2 that, in the absence of cooling, damping in a loop with $T = 6$ MK is weaker than that in a loop with $T = 5$ MK. This result is in the agreement with the observation by Sigalotti et al. (2007) that slow standing oscillations of relatively cool loops ($T \sim 5$ MK) damp faster than those in very hot loops with $T \sim 10$ MK. Cooling decreases the temperature of the loop and, as a result, damping in the loop with the initial temperature 6 MK is becoming stronger.

It is now instructive to compare the results obtained in this chapter with those obtained by Al-Ghafri and Erdélyi (2012). Figure 4.2(a) agrees very well with Figure 3(a) in Al-Ghafri and Erdélyi (2012). The agreement is fairly good for $T \lesssim 3$ MK. However, when the loop temperature increases further, the agreement is less clear. This discrepancy in not surprising because Al-Ghafri and Erdélyi (2012) assumed that damping is weak, which is less appropriate for sufficiently hot loops.

The results shown in Figure 4.2 are obtained for $\kappa_0 = 10^{-11}$. It is expedient to study the dependence of the damping rate on κ_0. Figure 4.3 shows the dependence of the oscillations amplitude on time for $\epsilon = 0.1$, $T_{0i} = 3$ MK, and various values of κ_0. This figure is plotted by applying Equations (4.31). As it can be expected, damping becomes stronger when κ_0 increases.

Figure 4.4 depicts the relation between the oscillation amplitude and the temperature for various values of ϵ at $t = 1$, where Equation (4.31) is applied to illustrate this relation. The damping rate of coronal oscillations increases gradually, takes its maximum at the temperature ~ 4 MK, and then decreases onwards.

It is worth studying what should be the cooling rate to *compensate* damping due to thermal condition and thus provide an undamped oscillation. In what follows we consider the oscillation as undamped if $a(2) = 1$, i.e. if the oscillation

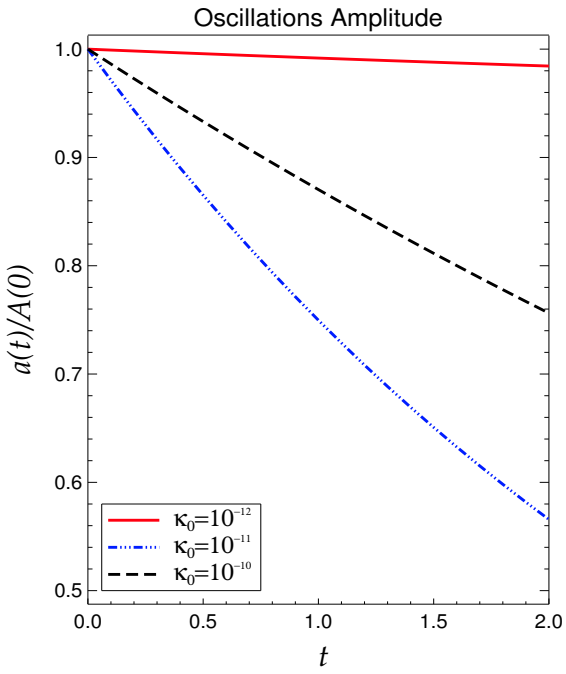

Figure 4.3: The dependence of the oscillation amplitude on time for $\epsilon = 0.1$, $T_{0i} = 3$ MK, and various values of κ_0. The time is measured in units of L/c_{si}.

amplitude at, say, $t = 2$ is the same as at the initial moment of time. Since the damping rate due to thermal conduction is a function of the initial temperature, so is the cooling rate needed to compensate the damping. The cooling rate is defined by the parameter ϵ. Let us calculate the dependence of the value of ϵ needed to compensate the damping on the inverse Peclet number σ analytically using Equation (4.34) valid for weak damping, and numerically using Equation (4.31). The results of this calculation are shown in Figure 4.5. As it can be expected, the analytical and numerical solutions are very close for small values of σ, but they are sufficiently different for larger values of σ.

4.5 Discussion and Conclusion

In this Chapter we have studied the effect of cooling of coronal loops on the damping of slow standing waves. We have used the low-beta plasma and rigid flux tube approximation, which enable us to disregard the magnetic field perturbation.

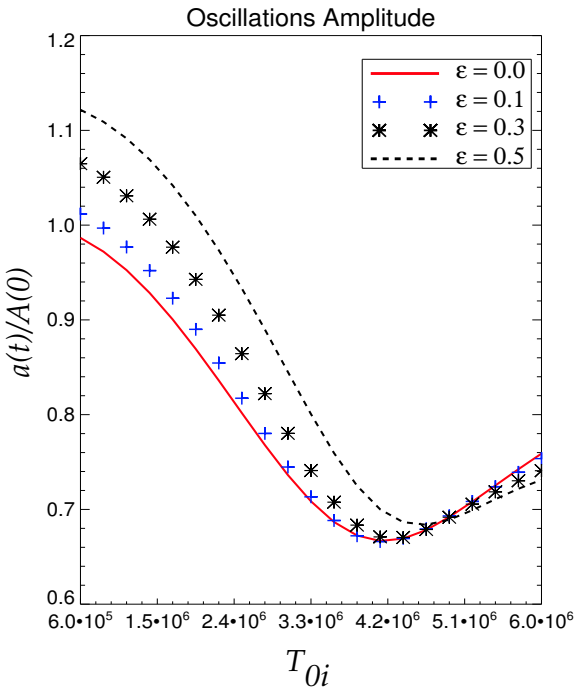

Figure 4.4: The dependence of the oscillation amplitude on temperature for $t = 1$, and various values of ϵ.

As a result we have reduced the problem to studying one-dimensional standing sound waves. We have assumed that, due to cooling, the temperature in the loop decreases exponentially with the characteristic time τ_c, which is much longer than the characteristic oscillation period P. The latter assumption has allowed us to use the WKB method with $\epsilon = P/\tau_c$ as a small parameter to model the damped oscillations. In the leading-order approximation of the WKB method, called the approximation of geometrical optics, we have derived the dispersion equation determining the instantaneous complex frequency of the loop oscillation. In the next order approximation, called the approximation of physical optics, we have obtained the equation determining the oscillation amplitude variation with time.

We have used the analytical results to calculate the dependence of the oscillation period and amplitude on time numerically. We have obtained that cooling results in the increase of the oscillation period. This is an expected result because cooling causes the decrease of the sound speed, and the oscillation period is equal to the double time of the travel of a signal from one loop footpoint to

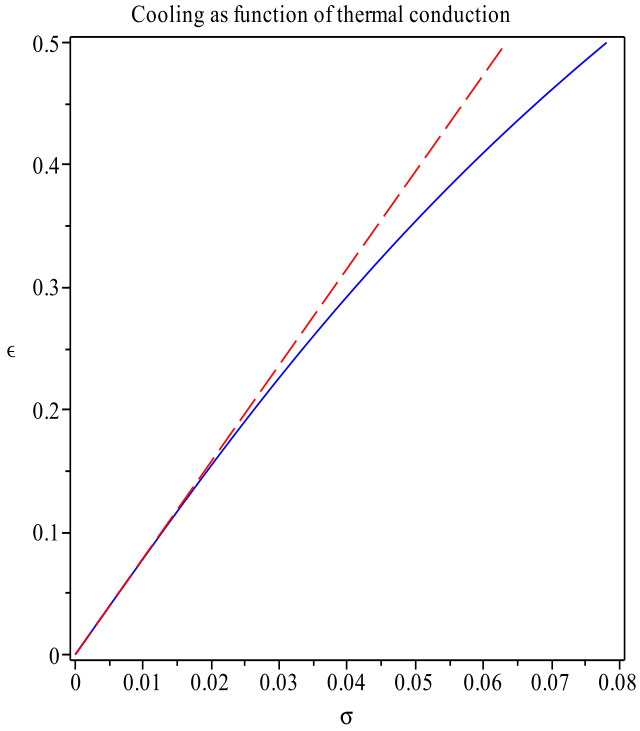

Figure 4.5: The dependence of the cooling on the thermal ratio (the inverse Peclet number) for $t = 2$, and $a(t) = 1$. The dashed and solid line correspond to the analytical and numerical calculations, respectively.

the other. In moderately hot loops (the temperature not exceeding $\sim$ 5 MK) cooling reduces the damping rate due to thermal conduction. In cold loops with the temperature below $\sim$ 1 MK the damping due to thermal conduction is very weak. As a result the effect of oscillation amplification dominates the damping and the oscillation amplitude increases with time. In hotter loops cooling cannot compete with damping and is able only to reduce the damping rate.

The damping rate is not a monotonic function of the temperature. While it increases with the temperature in relative cold loops, the temperature increase in very hot loops leads to the decrease of the damping rate. As a result, in very hot loop with the temperature about 6 MK and higher cooling causes the damping enhancement.

Chapter 5

Conclusion

5.1 Overview

In the beginning of our Thesis, we have given a brief description of the Sun structure. The solar corona, which is composed of different complex features such as coronal loops, open flux tubes, prominences, *etc.*, was the essential region of the solar structure for our attention in this study. Coronal loops are highly magnetised and can support various kinds of MHD waves which are natural carriers of energy. The aim of our study is to deal with the properties of waves and oscillations that are routinely observed in coronal loops. Many recent studies that presented the observations and damping of longitudinal oscillations were motivation for our study. In most theoretical studies, the analytically and numerically obtained results were found to agree well with the observations. The properties of MHD waves propagating in different types of uniform medium have been presented in detail. The cooling of coronal plasma by radiation and thermal conduction has been discussed.

In our study we have concentrated on the longitudinal slow (propagating and standing) MHD waves which are present in solar coronal loops with the temperatures ranging from less than 1 MK to more than 6 MK.

In contrast to previous studies, the longitudinal slow MHD waves have been assumed here to propagate in dynamic coronal plasma, meaning that the equilibrium is allowed to evolve with time. This is particularly relevant for flaring and post-flare loops. Thermal conduction was the main dissipative mechanism

responsible for cooling the background plasma in our work. In order to investigate the properties of longitudinal slow MHD waves, several analytical techniques have been used to treat the MHD equations such as linearisation, WKB theory, method of characteristic, the properties of Sturm-Liouville problems, *etc.* Finally, the analytically obtained solutions were examined using numerical evaluations. The body of the thesis was comprised of three chapters that can be summarised as follows.

5.2 Summary

Chapter 2 focused on the damping of propagating MHD waves in a weakly stratified atmosphere with the temperature decreasing due to cooling. Thermal conduction was assumed to be the dominant mechanism for the cooling of coronal loops. The cooling was assumed to occur on a time scale longer than the characteristic travel times of the perturbations. The effect of cooling background plasma on the properties of magneto-acoustic waves have been investigated. The temporally evolving dispersion relation that describes the properties of MHD waves was derived from the obtained governing equation for longitudinally propagating slow magneto-acoustic waves. The WKB theory has been used to find an analytic solution for the time-dependent amplitude of longitudinal slow waves. The analytically obtained solution has been evaluated numerically. The results show that the coronal loop oscillations experience strong damping. However, the presence of cooling and stratification gives rise to a reduction in the damping rate.

In Chapter 3, the longitudinal slow standing MHD waves generated in cooling coronal plasma were investigated. In accordance to previous observational and theoretical studies, the background temperature is assumed to decrease exponentially with time. The standing longitudinal (acoustic) wave is damped due to the presence of *weak* thermal conduction. Contrary to previous studies, the coefficient of thermal conductivity is assumed here to be a function of time. The behaviour of standing acoustic (longitudinal) waves has been analysed by deriving the time-dependent dispersion relation. The variation of amplitude, due to cooling, has been obtained by applying the properties of Sturm-Liouville problem. The analytical solution of the temporally evolving amplitude is shown numerically to give further insight into the behaviour of the MHD waves. The evaluation illustrates

that the increase of thermal conduction leads to a stronger decay in the amplitude of the longitudinal standing slow MHD waves. As in the case of propagating MHD waves, for the standing MHD waves it is also found that the cooling of the background coronal plasma causes reduction in the damping rate.

Chapter 4 completes the investigation into the effect of cooling on damping the longitudinal slow standing MHD waves. In this chapter we relaxed the condition that the damping is weak and allowed the thermal condition to be *arbitrary* in strength. The approximation of low-beta plasma and rigid flux tube enables us to ignore the magnetic field perturbation and reduce the problem to modelling 1D standing sound waves. We assumed that the temperature of the background plasma decays exponentially. Then, we used the WKB method to investigate the temporal evolution of the oscillation amplitude. The analytical expression for the amplitude has been derived. To illustrate the properties of MHD waves for typical solar coronal conditions, we evaluated the analytically obtained solution numerically. The results show that the influence of plasma cooling leads to an increase in the oscillation period. This is not surprising because the cooling deceases the phase speed. In addition to this, the oscillation amplitude of cooling coronal loops is amplified by cooling, which reduces the damping rate in coronal loops with moderate temperatures. In contrast, cooling enhances the damping rate of oscillations in very hot coronal loops.

5.3 Outlook

Overall, the Thesis has concentrated on the effect of cooling on the longitudinal slow magneto-acoustic waves generated in a dynamic coronal plasma. Thermal conduction was the only mechanism causing the damping for coronal oscillations. We have restricted our analysis to models where there is no background flow. The main reason for this is mathematical simplicity.

As forthcoming works, we can formulate the following problems:

- Investigating the properties of slow MHD waves with mixed boundary conditions, where the heat flux is proportional to the temperature.
- Studying the damping of oscillations due to the joint effect of thermal conduction and radiation.

- Studying the damping of oscillations due to the joint effect of thermal conduction and viscosity.

Bibliography

Al-Ghafri K S and Erdélyi R 2012 *Solar Phys.* **in press**.

Al-Ghafri K S, Ruderman M S and Erdélyi R 2012 *Astrophys. J.* **submitted**.

Andries J, Arregui I and Goossens M 2005 *Astrophys. J.* **624**, L57.

Antiochos S K, Shoub E C, An C H and Emslie A G 1985 *Astrophys. J.* **298**, 876.

Antolin P, Shibata K, Kudoh T, Shiota D and Brooks D 2008a *in* R Erdélyi and Mendoza-Briceño, C. A., eds, 'Waves and Oscillations in the Solar Atmosphere: Heating and Magneto-Seismology' Vol. 247 IAU Symposium p. 61.

Antolin P, Shibata K, Kudoh T, Shiota D and Brooks D 2008b *Astrophys. J.* **688**, 669.

Antolin P, Shibata K, Kudoh T, Shiota D and Brooks D 2009 *ASP* **415**, 247.

Asai A, Shimojo M, Isobe H, Morimoto T, Yokoyama T, Shibasaki K and Nakajima H 2001 *Astrophys. J. Lett.* **562**, L103.

Aschwanden M, Fletcher L, Schrijver C and Alexander D 1999 *Astrophys. J.* **520**, 880.

Aschwanden M J and Terradas J 2008 *Astrophys. J. Lett.* **686**, L127.

Aschwanden M J and Tsiklauri D 2009 *Astrophys. J.* **185**, 171.

Aschwanden M, Nightingale R, Andries J, Goossens M and Van Doorsselaere T 2003 *Astrophys. J.* **598**, 1375.

Ballai I, Jess D B and Douglas M 2011 *Astron. Astrophys.* **534**, A13.

Banerjee D, Erdélyi R, Oliver R and O'Shea E 2007 *Solar Phys.* **246**, 3.

Bender C M and Országh S A 1978 *Advanced Mathematical Methods for Scientists and Engineers* McGraw-Hill, Newyork.

Berghmans D and Clette F 1999 *Solar Phys.* **186**, 207.

Berghmans D, McKenzie D and Clette F 2001 *Astron. Astrophys.* **369**, 291.

Bogdan T, Carlsson M, Hansteen V, McMurry A, Rosenthal C, Johnson M, Petty-Powell S, Zita E, Stein R, McIntosh S and Nordlund A 2003 *Astrophys. J.* **599**, 626.

Bradshaw S J and Cargill P J 2010 *Astrophys. J.* **717**, 163.

Bradshaw S J and Erdélyi R 2008 *Astron. Astrophys.* **483**, 301.

Bray, Cram, Durrant and Loughhead 1991 *Plasma loops in the solar corona,* Cambridge University Press, Cambridge.

Cargill P J 1994 *Astrophys. J.* **422**, 381.

Cargill P J and Priest E R 1980 *Solar Phys.* **65**, 251.

Carter B K and Erdélyi R 2008 *Astron. Astrophys.* **481**, 239.

De Moortel I 2009 *Space Sci. Rev.* **149**, 65.

De Moortel I and Hood A W 2003 *Astron. Astrophys.* **408**, 755.

De Moortel I and Hood A W 2004 *Astron. Astrophys.* **415**, 705.

De Moortel I, Hood A W, Gerrard C L and Brooks S J 2004 *Astron. Astrophys.* **425**, 741.

De Moortel I, Ireland J, Hood A W and Walsh R W 2002b *Solar Phys.* **209**, 89.

De Moortel I, Ireland J, Hood A W and Walsh R W 2002c *Astron. Astrophys. Lett.* **387**, L13.

De Moortel I, Ireland J and Walsh R W 2000 *Astron. Astrophys. Lett.* **355**, L23.

De Moortel I, Ireland J, Walsh R W and Hood A W 2002a *Solar Phys.* **209**, 61.

De Moortel I and Nakariakov V M 2012 *Phil. Trans. R. Soc.* **370**, 3193.

De Pontieu B and Erdélyi R 2006 *Phil. Trans. Roy. Soc. London A* **364**, 383.

De Pontieu B, Erdélyi R and De Moortel I 2005 *Astrophys. J. Lett.* **624**, L61.

De Pontieu B, Erdélyi R and De Wijn A G 2003 *Astrophys. J. Lett.* **595**, L63.

De Pontieu B, Erdélyi R and James S P 2004 *Nature* **430**, 536.

De Pontieu B, McIntosh S W, Carlsson M, Hansteen V H, Tarbell T D, Schrijver C J, Title A M, Shine R A, Tsuneta S, Katsukawa Y, Ichimoto K, Suematsu Y, Shimizu T and Nagata S 2007 *Science* **318**, 1574.

DeForest C and Gurman J 1998 *Astrophys. J. Lett.* **501**, L217.

Dymova M V and Ruderman M S 2006 *Astron. Astrophys.* **459**, 241.

Edwin P and Roberts B 1983 *Solar Phys.* **88**, 179.

Erdélyi R 2006 *Phil. Trans. Roy. Soc. A*. **364**, 351.

Erdélyi R 2008 *in* B. N Dwivedi and U Narain, eds, 'Physics of the Sun and Its Atmosphere' (Princeton Series in Astrophysics) p. 61.

Erdélyi R, Al-Ghafri K S and Morton R J 2011 *Solar Phys.* **272**, 73.

Erdélyi R and Ballai I 2007 *Astro. Nachr.* **328**, 726.

Erdélyi R and Fedun V 2007a *Science* **318**, 1572.

Erdélyi R and Fedun V 2007b *Solar Phys.* **246**, 101.

Erdélyi R and Fedun V 2010 *Solar Phys.* **263**, 63.

Erdélyi R, Luna-Cardozo M and Mendoza-Briceño C 2008 *Solar Phys.* **252**, 305.

Erdélyi R and Taroyan Y 2008 *Astron. Astrophys. Lett.* **489**, L49.

Erdélyi R and Verth G 2007 *Astron. Astrophys.* **462**, 743.

Fan Y and Gibson S E 2003 *Astrophys. J. Lett.* **589**, L105.

Fedun V, Erdélyi R and Shelyag S 2009 *Solar Phys.* **258**, 219.

Fedun V, Shelyag S and Erdélyi R 2011 *Astrophys. J.* **727**, 17.

Field G 1965 *Astrophys. J.* **142**, 531.

Golub and Pasachoff 1997 *The Solar Corona,* Cambridge University Press, Cambridge.

Goossens M, Andries J and Aschwanden M J 2002 *Astron. Astrophys. Lett.* **394**, L39.

Goossens M, Erdélyi R and Ruderman M S 2011 *Space Sci. Rev.* **158**, 289.

Gruszecki M, Murawski K and Ofman L 2008 *Astron. Astrophys.* **488**, 757.

Ibáñez S M H and Escalona T O B 1993 *Astrophys. J.* **415**, 335.

Jakimiec J, Sylwester B, Sylwester J, Serio S, Peres G and Reale F 1992 *Astron. Astrophys.* **253**, 269.

Jess D B, Mathioudakis M, Erdélyi R, Crockett P J, Keenan F P and Christian D J 2009 *Science* **323**, 1582.

Karpen J T and Antiochos S K 2008 *Astrophys. J.* **676**, 658.

King D B, Nakariakov V M, Deluca E E, Golub L and McClements K G 2003 *Astron. Astrophys. Lett.* **404**, L1.

Kliem B, Dammasch I, Curdt W and Wilhelm K 2002 *Astrophys. J. Lett.* **568**, L61.

Lamb H 1932 *Hydrodynamics* Cambridge University Press, Cambridge: UK.

Landi E, Miralles M P, Curdt W and Hara H 2009 *Astrophys. J.* **695**, 221.

Linton M G, Dahlburg R B and Antiochos S K 2001 *Astrophys. J.* **553**, 905.

López Fuentes M, Klimchuk J and Mandrini C 2007 *Astrophys. J.* **657**, 1127.

Luna-Cardozo M, Verth G and Erdélyi R 2012 *Astrophys. J.* **748**, 110.

Luoni M L, Démoulin P, Mandrini C H and van Driel-Gesztelyi L 2011 *Solar Phys.* **270**, 45.

Mariska J T 2005 *Astrophys. J. Lett.* **620**, L67.

Mariska J T 2006 *Astrophys. J.* **639**, 484.

Marsh M S, De Moortel I and Walsh R W 2011 *Astrophys. J.* **734**, 81.

Marsh M S, Walsh R W and Plunkett S 2009 *Astrophys. J.* **697**, 1674.

Martínez González M J and Bellot Rubio L R 2009 *Astrophys. J.* **700**, 1391.

Martínez-Sykora J, Hansteen V and Carlsson M 2009 *Astrophys. J.* **702**, 129.

Mathioudakis M, Jess D and Erdélyi R 2013 *Space Sci. Rev.* **accepted**.

McEwan M P and De Moortel I 2006 *Astron. Astrophys.* **448**, 763.

McLaughlin J A, Hood A W and De Moortel I 2011 *Space Sci. Rev.* **158**, 205.

Mendoza-Briceño C, Erdélyi R and Sigalotti L 2002 *Astrophys. J. Lett.* **579**, L49.

Mendoza-Briceño C, Erdélyi R and Sigalotti L 2004a *Astrophys. J.* **605**, 493.

Mendoza-Briceño C, Sigalotti L and Añez-Parra N Y 2004b *Geofísica Internacional* **43**, 89.

Mok Y and Van Hoven G 1995 *Solar Phys.* **161**, 67.

Morton R and Erdélyi R 2009*a* *Astron. Astrophys.* **502**, 315.

Morton R and Erdélyi R 2009*b* *Astrophys. J.* **707**, 750.

Morton R and Erdélyi R 2010 *Astrophys. J.* **519**, A43.

Morton R, Hood A W and Erdélyi R 2010 *Astron. Astrophys.* **512**, A23.

Morton R J and Ruderman M S 2011 *Astron. Astrophys.* **527**, A53.

Nagata S, Hara H, Kano R, Kobayashi K, Sakao T, Shimizu T, Tsuneta S, Yoshida T and Gurman J B 2003 *Astrophys. J.* **590**, 1095.

Nakariakov V M, Verwichte E, Berghmans D and Robbrecht E 2000 *Astron. Astrophys.* **362**, 1151.

Nakariakov V, Ofman L, Deluca E, Roberts B and Davila J 1999 *Science* **285**, 862.

Nakariakov V and Verwichte E 2005 *Living Rev. Solar Phys.* **2**, 3.

Nightingale R, Aschwanden M and Hurlburt N 1999 *Solar Phys.* **190**, 249.

Ofman L and Aschwanden M 2002 *Astrophys. J. Lett.* **576**, L153.

Ofman L, Nakariakov V and DeForest C 1999 *Astrophys. J.* **514**, 441.

Ofman L, Nakariakov V and Seghal N 2000b *Astrophys. J.* **533**, 1071.

Ofman L, Romoli M, Poletto G, Noci C and Kohl J 1997 *Astrophys. J. Lett.* **491**, L111.

Ofman L, Romoli M, Poletto G, Noci C and Kohl J L 2000a *Astrophys. J.* **529**, 592.

Ofman L and Wang T 2002 *Astrophys. J. Lett.* **580**, L85.

Okamoto T, Tsuneta S, Berger T, Ichimoto K, Katsukawa Y, Lites B, Nagata S, Shibata K, Shimizu T, Shine R, Suematsu Y, Tarbell T and Title A 2007 *Science* **318**, 1577.

Orza B, Ballai I, Jain R and Murawski K 2012 *Astron. Astrophys.* **537**, A41.

Owen N, De Moortel I and Hood A 2009 *Astron. Astrophys.* **494**, 339.

Pandey V and Dwivedi B 2006 *Solar Phys.* **236**, 127.

Petrie G J D 2006 *Astrophys. J.* **649**, 1078.

Priest E R 2000 *Solar Magneto-hydrodynamics* Kluwer Dordrecht.

Robbrecht E, Verwichte E, Berghmans D, Hochedez J, Poedts S and Nakariakov V 2001 *Astron. Astrophys.* **370**, 591.

Roberts B 1981a *Solar Phys.* **69**, 27.

Roberts B 2006 *Phil. Trans. Roy. Soc. A.* **364**, 447.

Rosenthal C S, Bogdan T J, Carlsson M, Dorch S B F, Hansteen V, McIntosh S W, McMurry A, Nordlund Å and Stein R F 2002 *Astrophys. J.* **564**, 508.

Rosner R, Tucker W H and Vaiana G S 1978 *Astrophys. J.* **220**, 643.

Ruderman M S 2003 *Astron. Astrophys.* **409**, 287.

Ruderman M S 2007 *Solar Phys.* **246**, 119.

Ruderman M S 2010 *Solar Phys.* **267**, 377.

Ruderman M S 2011 *Solar Phys.* **271**, 41.

Ruderman M S and Roberts B 2002 *Astrophys. J.* **577**, 475.

Ruderman M S, Verth G and Erdélyi R 2008 *Astrophys. J.* **686**, 694.

Sakurai T, Goossens M and Hollweg J V 1991 *Solar Phys.* **133**, 227.

Schrijver C J, Title A, Berger T, Fletcher L, Hurlburt N, Nightingale R, Shine R, Tarbell T, Wolfson J, Golub L, Bookbinder J, DeLuca E, McMullen R, Warren H, Kankelborg C, Handy B and De Pontieu B 1999 *Solar Phys.* **187**, 261.

Sigalotti L D G, Mendoza-Briceño C A and Luna-Cardozo M 2007 *Solar Phys.* **246**, 187.

Taroyan Y 2008 *in* R Erdélyi and C. A Mendoza-Briceo, eds, 'Waves & Oscillations in the Solar Atmosphere: Heating and Magneto-Seismology' Vol. 247 IAU Symposium p. 184.

Taroyan Y and Erdélyi R 2009 *Space Sci. Rev.* **149**, 229.

Taroyan Y and Erdélyi R 2010 *in* S Hasan and R. J Rutten, eds, 'Magnetic Coupling between the Interior and Atmosphere of the Sun' Springer Berlin Heidelberg p. 287.

Taroyan Y, Erdélyi R and Bradshaw S J 2011 *Solar Phys.* **269**, 295.

Taroyan Y, Erdélyi R, Doyle J G and Bradshaw S J 2005 *Astron. Astrophys.* **438**, 713.

Taroyan Y, Erdélyi R, Wang T J and Bradshaw S J 2007 *Astrophys. J. Lett.* **659**, L173.

Terra-Homem M, Erdélyi R and Ballai I 2003 *Solar Phys.* **217**, 199.

Terradas J, Goossens M and Ballai I 2010 *Astron. Astrophys.* **515**, A46.

Tomczyk S, McIntosh S W, Keil S L, Judge P G, Schad T, Seeley D H and Edmondson J 2007 *Science* **317**, 1192.

Tsiklauri D and Nakariakov V M 2001 *Astron. Astrophys.* **379**, 1106.

Tsiropoula G, Tziotziou K, Wiegelmann T, Zachariadis T, Gontikakis C and Dara H 2007 *Solar Phys.* **240**, 37.

Ugarte-Urra I, Warren H P and Brooks D H 2009 *Astrophys. J.* **695**, 642.

Vaiana G, Krieger A and Timothy A 1973 *Solar Phys.* **32**, 81.

Van Doorsselaere T, Nakariakov V and Verwichte E 2008 *Astrophys. J. Lett.* **676**, L73.

Van Doorsselaere T, Verwichte E and Terradas J 2009 *Space Sci. Rev.* **149**, 299.

Verth G and Erdélyi R 2008 *Astrophys. J.* **486**, 1015.

Verwichte E, Haynes M, Arber T and Brady C S 2008 *Astrophys. J.* **685**, 1286.

Verwichte E, Marsh M, Foullon C, Van Doorsselaere T, De Moortel I, Hood A W and Nakariakov V M 2010 *Astrophys. J. Lett.* **724**, L194.

Vigeesh G, Fedun V, Hasan S S and Erdélyi R 2012 *Astrophys. J.* **755**, 18.

Wang T 2011 *Space Sci. Rev.* **158**, 397.

Wang T J, Solanki S K, Curdt W, Innes D E and Dammasch I E 2002 *Astrophys. J. Lett.* **574**, L101.

Wang T J, Solanki S K, Curdt W, Innes D E and Dammasch I E 2002a *in* A Wilson, ed., 'From Solar Minimum to Maximum' (ESA SP-508; Noordwijk: ESA) p. 465.

Wang T J, Solanki S K, Curdt W, Innes D E, Dammasch I E and Kliem B 2003a *Astron. Astrophys.* **406**, 1105.

Wang T J, Solanki S K, Innes D E and Curdt W 2005 *Astron. Astrophys.* **435**, 753.

Wang T J, Solanki S K, Innes D E, Curdt W and Marsch E 2003b *Astron. Astrophys. Lett.* **402**, L17.

Winebarger A R, Warren H P and Seaton D B 2003 *Astrophys. J.* **593**, 1164.

Zaqarashvili T and Erdélyi R 2009 *Space Sci. Rev.* **149**, 355.